

**Surface Interactions and Kinetics of TiO<sub>2</sub>  
Photocatalytic Oxidation of Organic Pollutants  
in Aqueous Solution**

Von der Naturwissenschaftlichen Fakultät der  
Gottfried Wilhelm Leibniz Universität Hannover

zur Erlangung des Grades  
**Doktor der Naturwissenschaften (Dr. rer. nat.)**

genehmigte Dissertation

von

**Mohamed Faycal Atitar, D.E.S.A. (Marokko)**

**2017**

Referent: Apl. Prof. Dr. rer. nat. habil. Detlef Bahnemann

Korreferent: Prof. Dr. rer. nat. Thomas Scheper

Tag der Promotion: 08.12.2017

**For My Family**



## Acknowledgments

First of all I would like to thank my PhD advisor Prof. Detlef Bahnemann, for his support, as well as for his comprehensive, stimulating discussions, and skilled supervision of this research. I thank him for introducing me the scientific research and giving me the possibility to contribute in various collaboration projects, and for the freedom to develop and realize my own ideas.

I would like to thank Dr. Ralf Dillert for the critical and productive discussions and also for sharing his enormous experience and knowledge for the completion of this work.

Many thanks go to all colleagues from Bahnemann's research group, and also from the institute of technical chemistry for the cooperation and support.

I would like to thank Dr. Juan Montoya and Dr. Elias Tauchert for their support in my research work at earlier stage and for their help in developing research ideas. I would also like to thank Prof. Adel Ismail for his cooperation and fruitful discussions.

My thanks also go to my Professors in Morocco, Pr. Mohamed El Azzouzi, Pr. Elhourch, and Pr. Kitane.

I also would like to express my gratitude to Prof. Alexey Emeline for giving me the opportunity to carry out part of the experimental work of this thesis at St. Petersburg State University, where I received invaluable technical assistance of the colleagues. In addition, I received enormous ideas from discussions with Pr. Alexey Emeline, Pr. Alexey Tsyganenko, E.S. Artemyeva, and D. Afanasev.

My parents Rabia Saidi and Thami Atitar, and sisters Ikram and Sara are always in my heart, and are one of my main reasons to succeed in achieving different goals throughout my life. I thank them for the long years of support and trust in me. My wife Maria deserves a special mention because she has been the essential partner of this adventure. Without her love, and support it would have been impossible to finish this task. Many thanks go to every person from my big family for the support during all these years.

My thanks also goes to: Brotherhood (Abdo, Choukri, Imad, Issam, Soufiane, Youssef, Yassine), my german and international friends (Ana, Anne, Ayad, Amer, Die Dreimanns, Die Wagners, Elias, Felipe, Irina, Ilyana, Jenny, Maryam, Mike,

Razan, Szmiti, Hamza, Tonya...), and friends in Morocco (Faissal, Reda, Ayoub, Nabil, Badr, Yousra...) for their constant encouragement in my research work.

Thanks also go to the German Academic Exchange Service (DAAD), for the scholarship in the Frame of a Sandwich-Program, and the Russian Foundation for Basic Research.

Thanks to everyone who supported me for the completion of this work

Faycal

## Kurzzusammenfassung

Für die Erhöhung der Effizienz von photokatalytischen Wasseraufbereitungsprozessen mit Hilfe metall-oxidischer Halbleiter ist es unumgänglich, die grundlegenden Mechanismen des photokatalytischen Abbaus zu verstehen. Im Rahmen dieser Arbeit wurden die Oberflächeninteraktionen, die Adsorptionskinetik, sowie die Kinetik des photokatalytischen Abbaus des Herbizids Imazapyr mittels des Photokatalysators Titandioxid ( $\text{TiO}_2$ ) untersucht.

Die Adsorption wurde mittels der abgeschwächte Totalreflexion – Fourier transformierte Infrarot (ATR-FTIR) Spektroskopie vermessen.  $\text{TiO}_2$  Filme wurden auf ZnSe Kristalle aufgebracht und die Oxid/Flüssigkeitsgrenzfläche wurde bei unterschiedlichen pH-Werten (z.B. 3, 5, 7 und 9) untersucht. Dabei konnte festgestellt werden, dass die Adsorption von Imazapyr auf der  $\text{TiO}_2$  Oberfläche pH-abhängig ist und bevorzugt bei pH Werten unterhalb des pHs des Ladungsnulldpunkts ( $\text{pH}_{\text{zpc}}$ ) abläuft. In dieser Arbeit wird gezeigt, dass bei der Adsorption die Carboxy-Gruppe von Imazapyr an die Ti(IV)-Zentren der Oberfläche bindet, hauptsächlich als überbrückender Ligand bei  $\text{pH} < \text{pH}_{\text{zpc}}$ . Steigt der pH-Wert so ist die Bindung von Imazapyr an die Oberfläche weniger begünstigt. Der Beitrag anderer Bindungsarten zur Interaktion zwischen Imazapyr und der  $\text{TiO}_2$  Oberfläche wird ebenfalls diskutiert.

Des Weiteren werden die Adsorptionsisothermen, die Adsorptionskinetik und die Kinetik des photokatalytischen Abbaus von Imazapyr hinsichtlich ihrer Rolle bei der Oberflächeninteraktion des Gesamtprozesses untersucht. Die Ergebnisse zeigen, dass die Adsorption von Imazapyr an die  $\text{TiO}_2$  Oberfläche eine Reaktion zweiter Ordnung ist und die Anforderungen des Monolayer-Langmuir-Modells erfüllt. Daher wurde die Kinetik des photokatalytischen Abbaus mittels des Langmuir-Hinshelwood Modells simuliert. Es konnte jedoch gezeigt werden, dass dieses Modell aufgrund der großen Differenz zwischen Adsorptionskonstanten (sowohl im Dunkeln als auch unter Lichteinfluss) nur unzureichend zutrifft. Um einige Aspekte der Kinetik und der ablaufenden Mechanismen besser abbilden zu können, wurden die Adsorptionsraten und die photokatalytischen Abbauraten normiert und diskutiert.

Dieser neuartige Ansatz, den photokatalytischen Abbau und die Adsorptionsphänomene unter Berücksichtigung des Gleichgewichts und der Kinetik in Verbindung zu bringen, führt zu der Schlussfolgerung, dass die Adsorption nicht

der hauptsächliche Faktor im photokatalytischen Prozess ist. Der Mechanismus des photokatalytischen Abbaus von Imazapyr beinhaltet eine Kombination aus beidem, sowohl dem direkten (komplette Oxidation) als auch dem indirekten (OH-Radikale) Mechanismus. Die normierten Raten der photokatalytischen Reaktion sind in etwa dreimal höher als die Adsorptionsraten. Daher überwiegt der indirekte Mechanismus beim TiO<sub>2</sub>-photokatalysierten Abbau von Imazapyr.

Die mesoporöse Struktur, die Morphologie, das Kristallwachstum, die Phasenumwandlung und die Oberfläche der Materialien beeinflussen den Mechanismus ebenso wie die Kinetik der photokatalytischen Reaktion. Die synthetisierten mesoporösen TiO<sub>2</sub> Photokatalysatoren sind photokatalytisch aktiv und weisen eine höhere Aktivität bei der Zersetzung von Imazapyr und Phenol im Vergleich zu kommerziell erhältlichem Aeroxid TiO<sub>2</sub> P-25 auf. Darüber hinaus ist die Anfangsabbaurate bei dem photokatalytischen Abbau von Imazapyr durch die neu synthetisierten TiO<sub>2</sub>-Materialien bis zu dreimal höher als die für TiO<sub>2</sub> P-25. Verschiedene Aspekte hinsichtlich der Rolle der beschriebenen Parameter der Aktivität der synthetisierten Materialien sind in dieser Arbeit dargelegt.

Diese Arbeit stellt fundamentale Betrachtungen des grundsätzlichen Mechanismus an, die sowohl in der Adsorption als auch in der photokatalytischen Oxidation von Imazapyr beteiligt sind. Außerdem wird die Rolle der kristallinen Phase, der Struktur, der Oberfläche und anderer Parameter, die für die Synthese von mesopösem TiO<sub>2</sub> wesentlich sind, in Betracht gezogen. Diese Erkenntnisse könnten die Grundlage für ein tieferes Verständnis und zukünftige Forschung bilden, die dazu beiträgt den Prozess der photokatalytischen Wasseraufbereitung weiterhin zu verbessern.

Keywords: Attenuated Total Reflection - Fourier Transform Infrarot (ATR-FTIR), Adsorption, Kristallphase, Kinetik, Langmuir-Hinshelwood, Mesoporöses TiO<sub>2</sub>, Oberflächeninteraktion.



## Abstract

In order to improve the efficiency of the photocatalytic water treatment process using metal-oxide semiconductors, an understanding of the fundamental mechanisms of photocatalytic processes is essential. In this thesis the surface interactions and the kinetics of the adsorption of the herbicide imazapyr on the catalyst surface, as well as the kinetics of the photocatalytic degradation of imazapyr have been investigated using titanium dioxide ( $\text{TiO}_2$ ) as photocatalyst.

The adsorption study was performed using films of  $\text{TiO}_2$  deposited on a ZnSe crystal with help of the attenuated total reflection – Fourier transformed infrared (ATR-FTIR) spectroscopy. The oxide/solution interface study was performed at different pH values, i.e., at pH 3, 5, 7, and 9. Our results show that the adsorption of imazapyr onto the  $\text{TiO}_2$  surface is pH dependent and favored at pH values below the point of zero charge ( $\text{pH}_{\text{zpc}}$ ) of  $\text{TiO}_2$ . This work also revealed that upon adsorption, the carboxylic acid group of imazapyr is bound at the surface Ti(IV) centers mainly as a bridging ligand at  $\text{pH} < \text{pH}_{\text{zpc}}$ . With increasing pH values, the binding of imazapyr to the surface becomes less favorable. The contribution of other binding modes in the interaction between imazapyr and the  $\text{TiO}_2$  surface is also discussed in the thesis.

Furthermore, investigations concerning the adsorption isotherms, the kinetics of adsorption, as well as the photocatalytic degradation of imazapyr revealed the role of the surface interactions for the overall process. The results of our study show that the adsorption of imazapyr onto the  $\text{TiO}_2$  surface is a second-order reaction and satisfies the criteria required by the monolayer Langmuir model. Consequently, the kinetics of the photocatalytic degradation of imazapyr have been modeled using the Langmuir-Hinshelwood model. It is demonstrated that this model cannot be sufficiently applied due to the huge difference between the adsorption constants obtained in the dark and under illumination. In order to reveal some aspects of the kinetics and the mechanism involved in the degradation of imazapyr, the rates of adsorption and of the photocatalytic degradation were normalized and discussed.

Based upon this new approach to correlate the photocatalytic degradation with the adsorption phenomena, taking both the equilibrium and the kinetics into consideration, it is concluded that the adsorption does not play a major role for the photocatalytic process. However, the mechanism of the photocatalytic degradation of imazapyr involves a combination of both, the direct (hole oxidation) and the indirect

(OH radical) mechanism. The normalized rates of the photocatalytic reaction are found to be approximately three times higher than the rates of adsorption. Thus, the indirect mechanism appears to be predominant for the TiO<sub>2</sub> photocatalyzed degradation of imazapyr.

Our investigations also revealed that the mesoporous structure, the morphology, the crystal growth, the phase transformation, and the surface area of the materials influence the mechanism as well as the kinetics of the photocatalytic reaction. Newly synthesized mesoporous TiO<sub>2</sub> photocatalysts were found to be photoactive and show a higher activity for the decomposition of imazapyr and phenol compared to the commercially available Aeroxide TiO<sub>2</sub> P-25. Moreover, the initial degradation rate using the newly synthesized TiO<sub>2</sub> materials is up to three times higher than that of P-25 for the photodegradation of imazapyr. The aspects concerning the role of different parameters on the activity of the thus synthesized materials have been discussed.

The work out-lined in this thesis highlights the fundamental understanding of the basic mechanisms involved in the adsorption as well as in the photocatalytic oxidation of imazapyr. Moreover, it draws attention to the role of the crystalline phase, the structure, the surface area, and other parameters that are intrinsic to the photocatalyst for the degradation of organic pollutants. These studies will be helpful for a deeper understanding and for future investigations regarding further improvement of the photocatalytic water treatment process.

Keywords: Attenuated total reflection - Fourier transformed infrared (ATR-FTIR), Adsorption, Crystal phase, Imazapyr herbicide, Kinetics, Langmuir-Hinshelwood, Mesoporous TiO<sub>2</sub>, Photodegradation, Surface interactions.

## Foreword

Worldwide drinking water is becoming increasingly scarce because of the high pollution caused by different organic pollutants such as surfactants, herbicides, and dyes. The number of investigations concerning water decontamination and purification is constantly growing. Advanced oxidation processes (AOPs) involving the *in situ* generation of highly reactive intermediate species (i.e.,  $\text{H}_2\text{O}_2$ ,  $\text{OH}^\bullet$ ,  $\text{O}_2^{\bullet-}$ ) are considered to be promising methods for water treatment due to their effectiveness and safety in comparison with other traditional methods. As a result, intensive research activities concerning the degradation of recalcitrant organic compounds into readily biodegradable compounds or their complete mineralization into harmless products such as carbon dioxide and water employing AOPs have been promoted.

Among various AOPs, heterogeneous photocatalysis -which employs different semiconductors as photocatalysts- is believed to be most promising due to its low cost and negligible production of by-products. The successful application of photocatalysis in different areas such as environmental purification, renewable energy production, and the design of “self cleaning” surfaces coated with metal oxide materials, increased the interest in research concerning this topic during the last few decades. Until today titanium dioxide ( $\text{TiO}_2$ ) is considered to be the most reliable photocatalyst considering its high activity under irradiation with UV (A) photons with wavelengths  $\lambda < 390$  nm and its stability during repeated catalytic cycles. Moreover, the multi-faceted functional properties of  $\text{TiO}_2$ , such as its chemical, thermal, and mechanical stability have further promoted its application for photocatalytic water treatment.

During the last few decades a broad fundamental understanding of the mechanisms involved in the photocatalytic process has been obtained. However, there are still several fundamental issues, and even mechanistic details in the field of photocatalysis that remain unclear. Additionally, several reaction mechanisms and kinetic models have been proposed for the interpretation of a large number of experimental data concerning  $\text{TiO}_2$ -assisted photooxidation reactions. Despite the huge progress reached in the fundamental knowledge of these topics, several assumptions taken as “truths” by the scientific community have been challenged by the findings of surface science studies on  $\text{TiO}_2$  reported during the first decade of this century. Specifically, the new insights into the surface chemistry of  $\text{TiO}_2$  highlighted

the utmost role of the adsorption of molecules onto the TiO<sub>2</sub> surface for the photocatalytic process. Furthermore, it has been demonstrated that the kinetics and mechanisms of photocatalytic reactions are affected by several intrinsic and extrinsic parameters of the photocatalytic material.

This PhD thesis aims to elucidate the kinetics and mechanisms of photocatalytic oxidation reactions taking into account the aforementioned new insights.

This task has been approached by, first of all, carrying out an experimental study comprising TiO<sub>2</sub>-surface/substrate interactions. Secondly, by establishing the relationship of these surface/substrate interactions with the kinetics of the photocatalytic oxidation reactions of selected model compound. Furthermore, the design and synthesis of new photocatalysts as well as the interpretation of their photocatalytic activity are presented.

The topics of this doctoral dissertation are discussed in detail in the following six chapters comprising three peer-reviewed published articles.

### **Chapter 1: Introduction**

Because each article has its own particular introduction and reference sections, the objective of this chapter is not to present an exhaustive review of all topics covered in this thesis. Rather, this section presents a general overview on TiO<sub>2</sub> photocatalysis. Additionally, a book chapter is presented aiming to show the importance of TiO<sub>2</sub> surface science for photocatalysis with a particular focus on the relevance of the ATR-FTIR spectroscopy for the comprehension of the TiO<sub>2</sub>-surface/substrate interactions during the photocatalytic process.

**Scope of the thesis.** The aims and objectives of this investigation are also presented in this section.

**Chapter 2: *TiO<sub>2</sub>-surface/substrate interaction*.** This section includes the following article:

- M. Faycal Atitar, Ralf Dillert, and Detlef W. Bahnemann. Surface Interactions between Imazapyr and the TiO<sub>2</sub> Surface: An *in Situ* ATR-FTIR Study. *J Phys Chem C* 121(2017): 4293–4303.

**Chapter 3: *Kinetics, adsorption and photocatalytic reactions.*** This section includes the following article:

- M. Faycal Atitar, Asmae Bouziani, Ralf Dillert, Mohamed El Azzouzi, Detlef W. Bahnemann. Photocatalytic Degradation of the Herbicide Imazapyr: Do the Initial Degradation Rates Correlate with the Adsorption Kinetics and Isotherms? *Catal. Sci. Technol.* 8 (2018): 985-995.

**Chapter 4: *Mesoporous TiO<sub>2</sub> nanocrystals as efficient photocatalysts.*** This section includes the following article:

- M. Faycal Atitar, Adel A. Ismail, S.A. Al-Sayari, Detlef Bahnemann, D. Afanasev, A.V. Emeline. Mesoporous TiO<sub>2</sub> Nanocrystals as Efficient Photocatalysts: Impact of Calcination Temperature and Phase Transformation on Photocatalytic Performance. *Chem Eng J* 264 (2015): 417–424.

**Chapter 5: *Summarizing discussion.*** Discussion of the results presented in the previous chapters.

**Chapter 6: *Conclusions and outlook.*** General conclusions and perspectives of the work are reviewed in this section.



# Table of Contents

<b>Chapter 1: Introduction</b> .....	<b>1</b>
<b>1.1. Titanium dioxide (TiO<sub>2</sub>)</b> .....	<b>2</b>
<b>1.2. TiO<sub>2</sub> Photocatalysis</b> .....	<b>4</b>
<b>1.3. The relevance of ATR-FTIR spectroscopy in semiconductor photocatalysis</b> .....	<b>14</b>
<b>1.4. Scope of the Thesis</b> .....	<b>46</b>
<b>Chapter 2: Surface Interactions between Imazapyr and the TiO<sub>2</sub> Surface: An <i>in Situ</i> ATR-FTIR Study</b> .....	<b>49</b>
<b>2.1. Abstract</b> .....	<b>50</b>
<b>2.2. Introduction</b> .....	<b>50</b>
<b>2.3. Materials and Methods</b> .....	<b>52</b>
<b>2.4. Results and Discussion</b> .....	<b>55</b>
<b>2.5. Conclusions</b> .....	<b>70</b>
<b>2.6. Acknowledgments</b> .....	<b>70</b>
<b>2.7. References</b> .....	<b>71</b>
<b>2.9. Supporting Information</b> .....	<b>76</b>
<b>Chapter 3: Do The Initial Degradation Rates Correlate with The Adsorption Kinetics and Isotherms?</b> .....	<b>79</b>
<b>3.1. Abstract</b> .....	<b>80</b>
<b>3.2. Introduction</b> .....	<b>80</b>
<b>3.3. Experimental section</b> .....	<b>84</b>
<b>3.4. Results</b> .....	<b>85</b>
<b>3.5. Discussion</b> .....	<b>94</b>
<b>3.6. Conclusion</b> .....	<b>100</b>

<b>3.7. Acknowledgments</b> .....	<b>101</b>
<b>3.8. References</b> .....	<b>102</b>
<b>3.9. Supporting Information</b> .....	<b>105</b>
<b>Chapter 4: Mesoporous TiO<sub>2</sub> Nanocrystals as Efficient Photocatalysts: Impact of Calcination Temperature and Phase Transformation on Photocatalytic Performance</b> .....	<b>115</b>
<b>4.1. Abstract</b> .....	<b>116</b>
<b>4.2. Introduction</b> .....	<b>116</b>
<b>4.3. Experimental section</b> .....	<b>117</b>
<b>4.4. Results and Discussion</b> .....	<b>121</b>
<b>4.5. Conclusions</b> .....	<b>130</b>
<b>4.6. Acknowledgments</b> .....	<b>131</b>
<b>4.7. References</b> .....	<b>132</b>
<b>Chapter 5: Summarizing Discussion</b> .....	<b>135</b>
<b>Chapter 6 : Conclusion and Outlook</b> .....	<b>149</b>
<b>List of Publications</b> .....	
<b>Curriculum vitae</b> .....	



# Chapter 1

## Introduction

The demand for the earth's limited supply of freshwater has increased over the past decade, due to the exponential growth of the human population and the economic development. Thus, clean and sustainable energy production along with environmental concerns have emerged as top issues and challenges for the humanity. In this context, protection of natural water resources and development of new technologies for water purification and wastewater treatment became a key environmental concern of the 21st century.

Two major types of pollutants derived from technological and agricultural sources could be identified to encompass all others sources of pollutants. Technological pollutants are produced from human made sources, i.e., industrial, chemical, etc.

The compounds derived from these sources usually exhibit low solubility in water. Therefore, a separate layer of these compounds is formed on the surface that negatively affects the physical properties of the water (oxygen uptake, surface tension), which in turn also hampers living organism, which are in contact with the surface. The second major type of pollutants is produced by the high concentrations of nutrients that leach into the soil and drain into water sources mainly from agriculture.

Both organic and inorganic chemicals come into contact with ground and surface water sources. These inorganic chemicals include heavy metals, nitrates, and organometallics (especially tin compounds) [1]. General classes of organic compounds of environmental concern include: solvents, volatile organics, chlorinated volatile organics, dioxins, pesticides, chlorophenols, asbestos, and a plethora of aromatics from sewage [1]. Although this is not an exhaustive list, nevertheless it highlights the fact that many of these compounds are mildly soluble in water and are toxic to all forms of life.

In order to overcome this problem, the research and industrial community is challenged to develop advanced analytical, biochemical, and physicochemical methods for water purification. This challenge called for new technologies and made the use of sunlight a very attractive route that considers semiconductor photocatalysis

as one of the most promising advanced oxidation processes, as well as an alternative to the conventional processes.

Semiconductor photocatalysis has proved in the last decade to be a powerful tool for the destruction and remediation of highly toxic pollutants, for the purification of polluted water and air, for self-cleaning surfaces coated with metal oxide materials, and for the production of energy by splitting water into molecular hydrogen and molecular oxygen [1–3]. This technology relies on the use of metal chalcogenides or oxides to generate oxidizing holes, which directly react with the molecules adsorbed on the surface of the photocatalyst.

Many semiconductor materials have been used as photocatalysts for the photocatalytic degradation of organic molecules. The most commonly studied semiconductors include titanium dioxide ( $\text{TiO}_2$ ), zinc oxide ( $\text{ZnO}$ ), tungsten trioxide ( $\text{WO}_3$ ), hematite ( $\text{Fe}_2\text{O}_3$ ), and zinc sulphide ( $\text{ZnS}$ ) [4]. Nevertheless,  $\text{TiO}_2$  due to its low cost, abundance, high activity, and stability under a variety of conditions is the most reliable and widely used material today [5,6].

### 1.1. Titanium dioxide ( $\text{TiO}_2$ )

Titanium dioxide exists as three different polymorphs: anatase, rutile, and brookite as shown in Figure 1.1. Rutile is thermodynamically the most stable form of  $\text{TiO}_2$ . The metastable anatase and brookite phases convert irreversibly to the rutile phase upon calcination at temperatures exceeding  $600\text{ }^\circ\text{C}$  [7]. Anatase and rutile exhibit a tetragonal unit-cell structure, while brookite crystalizes in a more complex orthorhombic cell as shown in Figure 1.1. In all three forms, titanium ( $\text{Ti}^{4+}$ ) atoms are coordinated to six oxygen ( $\text{O}^{2-}$ ) atoms, forming  $\text{TiO}_6$  octahedra [7,8].

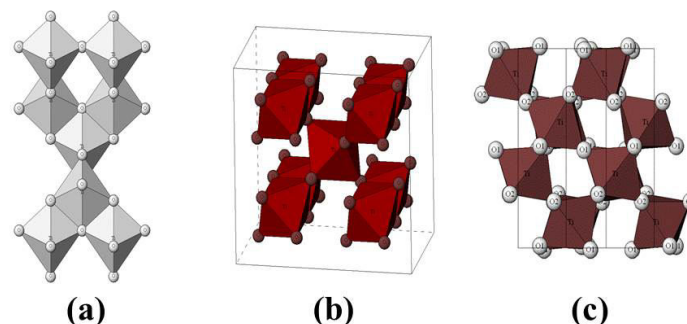


**Figure 1.1.** Crystallographic structure of  $\text{TiO}_2$  (a) anatase (tetragonal), (b) rutile (tetragonal), and (c) brookite (orthorhombic). (Reprinted with permission from Katsuhiro Nomura ([nomura-k@aist.go.jp](mailto:nomura-k@aist.go.jp); <http://staff.aist.go.jp/nomura-k/english/itsc/gallery-e.htm>) Copyright (2002)).

The rutile form of TiO<sub>2</sub> is widely used as pigment in paints, plastics, cosmetics, and other products [7]. In 1972, Honda and Fujishima discovered the photosensitization effect of a TiO<sub>2</sub> electrode for the water splitting [9]. Since then, enormous efforts have been devoted to the use of TiO<sub>2</sub> for many promising applications in areas ranging from photovoltaics and photocatalysis to photo-electrochromics and sensors [1,5,10]. The wide applications of TiO<sub>2</sub> can be practically divided into two categories such as “energy” and “environmental”. These applications depend not only on the properties of the employed TiO<sub>2</sub>, but also on the type and modifications of TiO<sub>2</sub>, as well as on the interactions of TiO<sub>2</sub> with the surrounding environment [7,8].

Similar to several semiconductors, TiO<sub>2</sub> is considered to be a wide band gap semiconductor comprising a conduction band (CB) and a valence band (VB) with a rather broad band gap energy ( $E_g \geq 3.0$  eV). Furthermore, it is also known that the CB and VB of TiO<sub>2</sub> are respectively made up of Ti 3d and O 2p orbitals [11,12]. The electronic structures of the three TiO<sub>2</sub> polymorphs are different due to the different local crystal environments of the Ti and O atoms in the unit cells of each crystalline phase. The band gap energy is reported to be 3.0 eV for rutile [8], 3.2 eV for anatase [8], and 3.31 eV for brookite [13].

In the present work, the commercial photocatalyst powder Evonik Degussa Aeroxide TiO<sub>2</sub> P25 was used. The material contains a unique combination of anatase 80% and rutile 20% crystal structure (the band gap energy of Aeroxide TiO<sub>2</sub> P25 is reported as 3.2 eV) [14]. This material is frequently used as a standard material for many applications. The present work also deals with the preparation of photocatalytically active TiO<sub>2</sub> nanomaterials with different porosity and mixed crystal phases. The activity of the newly synthesized material is compared with that of Aeroxide TiO<sub>2</sub> P25.

TiO<sub>2</sub> can be prepared both in the form of powder or as thin films. There are various synthetic routes reported in the literature that provide particles with the desired characteristics (i.e., crystallite phase & size, morphology, and uniformity), and also with a concern to their cost and yield. The most important ones used for the large scale production of commercial products are flame pyrolysis, and processes such as sol-gel, hydrothermal, or solvothermal [7]. A prominent example of a commercial product synthesized using flame pyrolysis is Evonik Degussa Aeroxide TiO<sub>2</sub> P25 where highly crystalline TiO<sub>2</sub> nanoparticles are obtained through the reaction of

vaporized titanium tetrachloride ( $\text{TiCl}_4$ ) with oxygen and hydrogen in the gas phase at high temperatures exceeding  $1000\text{ }^\circ\text{C}$  [15].

Wet-chemical approaches are popular and convenient to obtain homogeneous  $\text{TiO}_2$  materials with controlled stoichiometry and/or complex morphology. They are based on the combination of hydrolysis and condensation reactions of metal halide or alkoxide precursors in water or oxygen-containing organic solvents. Depending on the degree of condensation, these reactions can lead to molecular nanoclusters, nanoparticles, or polymer-like metal oxides. This sequence of reactions is known as the sol-gel method [16]. In a typical sol-gel synthesis, an inorganic precursor  $\text{TiR}_4$  is dissolved in water or a mixture of solvents. This precursor is rapidly hydrolyzed to yield  $\text{Ti}(\text{OH})_x\text{R}_{4-x}$ , which then undergoes condensation through either substitution or addition reactions to give titanium dioxide [16].

The preparation of mesoporous materials is mainly concerned with the building of monodispersed and mesosized pore spaces (2–50 nm) [17]. Such materials are characterized by their huge surface area and good accessibility of the pores. The synthesis of mesoporous  $\text{TiO}_2$  materials has been extensively studied with or without the use of organic surfactant templates such as amphiphilic poly(alkyleneoxide) block copolymers [7,17,18], which act as the structure directing agents.

## 1.2. $\text{TiO}_2$ Photocatalysis

The photocatalytic process involves several oxidation and reduction reactions in which light is used to activate a substance (the photocatalyst) thus accelerating the rate of the chemical reactions without being involved in the reactions.

$\text{TiO}_2$  is a photocatalyst with a band gap of  $\approx 3.2\text{ eV}$  that absorbs light in the UV range ( $\lambda < 390\text{ nm}$ ). This light energy is used to excite electrons from the filled valence band to the conduction band. The charge carriers thus generated, i.e., the electron ( $e^-$ ) in the conduction band (a reducing agent) and the hole ( $h^+$ ) in the valence band (an oxidizing agent), migrate to the surface. If an organic molecule is adsorbed on the surface of the photocatalyst, it may undergo an oxidation reaction either directly by the photogenerated conduction band holes or indirectly via hydroxyl radicals,  $\cdot\text{OH}$ , produced from the oxidation of water or via a reductive pathway, or through the reaction of superoxide radicals generated by trapping of the photo-generated electrons by molecular oxygen. Additionally, the generated hydroxyl radical may

also diffuse into the bulk solution resulting in the oxidation of organic molecules even if they are not adsorbed. The whole process can be represented by the following Figure 1.2. and the chemical equations (1.1) to (1.7) [1,19].

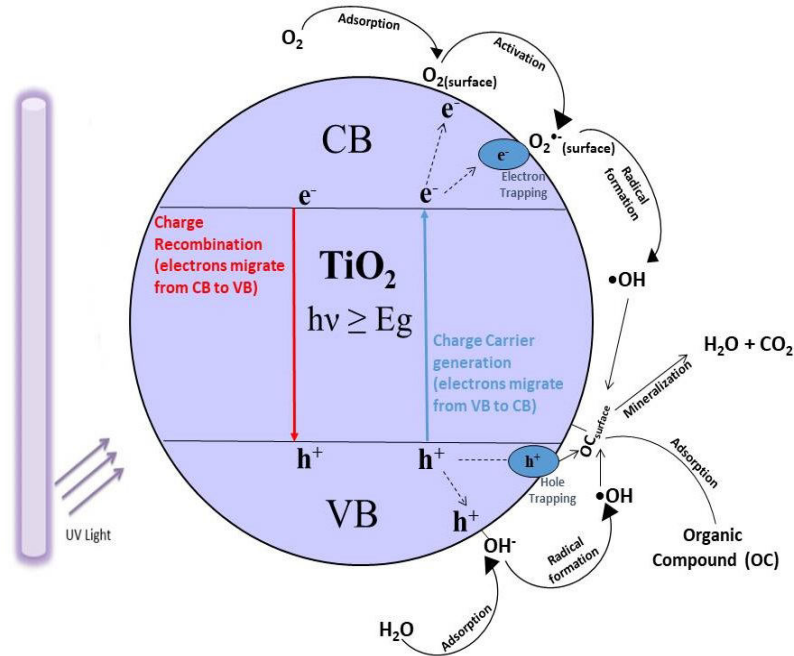
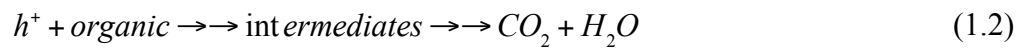


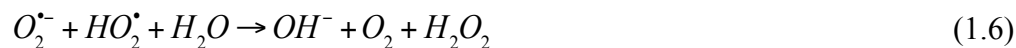
**Figure 1.2.** Mechanism of the heterogeneous photocatalytic process



Oxidative reaction:



Reductive reaction:



The role and the importance of each of these steps for the photocatalytic degradation of organic pollutants is still not completely clear. The hydroxyl radical ( $\cdot OH$ ) generated in (1.3) and (1.7) is considered to be the primary oxidant, while the presence of molecular oxygen ( $O_2$ ) can prevent the recombination of the electron-hole pair. The  $\cdot OH$  radical may react with organic compounds resulting in the

formation of various reaction intermediates depending on the nature of the compound [1,20]. These intermediates may further react with  $\cdot\text{OH}$  radicals to produce the final degradation products such as  $\text{CO}_2$  and  $\text{H}_2\text{O}$ . However, several publications have shown that the direct oxidation of organic molecules with trapped holes is also possible and sometimes the dominant process [21,22].

In spite of several contributions by different research groups concerning the understanding of the mechanisms involved in the photocatalytic process [2,21–25], there are still several fundamental issues, approaches, and mechanisms that remain unclear in this field.

The photocatalytic process for the degradation of organic pollutants on irradiated  $\text{TiO}_2$  is highly complex. The complexity of the process derives from the different reaction steps, intermediate by-products, and the diversity of reaction pathways involved in the process. For various specific cases, the relative role of holes, radicals, and surface charge are still under debate. On the other hand, like most heterogeneous reactions, it is assumed that the reaction occurs in the adsorbed phase. The task of developing a reliable rate law, which could be generally applicable to different pollutants and conditions, is therefore very difficult.

A complete kinetic analysis involves the study of reaction rates which requires the understanding of the mechanisms by which the reactants are converted to the products. Kinetic experiments are usually performed to study the photo-degradation of the target compounds. The results of such measurements show that reaction rates depend on the concentration of the reactants (and products) in a way that can be expressed in terms of differential equations known as rate laws. A common way to express the reaction rate is to use the power law as shown in equation (1.8) [26].

$$r = \frac{dC}{dt} = -kC^n \quad (1.8)$$

where  $k$  is the rate constant and  $n$  is the order of the reaction.

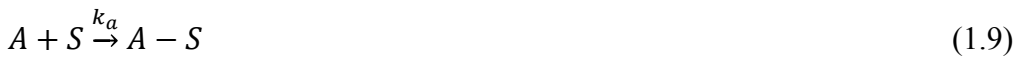
Some photocatalytic reactions obey a zero-order rate law and therefore exhibit a rate that is independent of the concentration of the reactant. However, first and second order reactions are more common in photocatalysis [26].

Heterogeneous catalysis is an important research area for the chemical industry due to its wide application. Photocatalytic reactions depend on the fact that at least one reactant is adsorbed (usually chemisorbed) on the surface of the catalyst [26]. For this reason, adsorption-desorption phenomena and interfacial reactions are usually of

major importance for the understanding of the mechanisms involved in photocatalysis [27]. Since the rate of a photocatalytic reaction depends on the adsorbed amount of the reactant, the adsorption equilibrium is usually described by a simple but plausible Langmuir isotherm, based on the following assumptions [26]:

1. The surface is uniform and all sites are equivalent.
2. There is no interaction between adsorbed molecules.
3. The ability to adsorb at a given site is independent of the occupation of the neighbouring sites.
4. The extent of adsorption is not beyond one complete monolayer coverage.

The dynamic equilibrium of the adsorption of a molecule A is:



The rate of adsorption ( $r_a$ ) is given by:

$$r_a = k_a(n_{ts} - n_{os})C \quad (1.10)$$

For the desorption:



and the rate of desorption is:

$$r_d = k_d n_{os} \quad (1.12)$$

Where  $S$  is the sorption site,  $n_{ts}$  is the total amount of surface sorption sites,  $C$  is the concentration of molecule A,  $n_{os}$  is the fraction of occupied sorption sites and  $k_a$  and  $k_d$  are the kinetic constants.

The Langmuir isotherm can be derived by looking on the amount of occupied sites at the photocatalyst surface under equilibrium conditions where the rates of adsorption and desorption are equal:

$$\frac{dn_{os}}{dt} = +k_a(n_{ts} - n_{os})C - k_d n_{os} = 0 \quad (1.13)$$

$$+k_a n_{ts} C - k_a n_{os} C - k_d n_{os} = 0 \quad (1.14)$$

$$n_{os}(k_a C + k_d) = k_a n_{ts} C \quad (1.15)$$

$$n_{os} = \frac{k_a n_{ts} C}{k_a C + k_d} = n_{ts} \frac{\frac{k_a}{k_d} C}{1 + \frac{k_a}{k_d} C} \quad (1.16)$$

This can be written as:

$$n_{os} = n_{ts} \frac{K_L C}{1 + K_L C} \quad (1.17)$$

or as the fractional coverage:

$$\theta = \frac{n_{os}}{n_{ts}} = \frac{K_L C}{1 + K_L C} \quad (1.18)$$

with  $K_L = \frac{k_a}{k_d}$

#### Nomenclature

$C$	$\text{mol L}^{-1}$	amount concentration of the dissolved (non-adsorbed) probe molecule in the suspension
$k_a$	$\text{L mol}^{-1} \text{s}^{-1}$	rate constant of adsorption
$k_d$	$\text{s}^{-1}$	rate constant of desorption
$k'_r$	$\text{mol}^{-1} \text{s}^{-1}$	rate constant of the photocatalytic reaction
$k_r$	$\text{mol L}^{-1} \text{s}^{-1}$	maximum rate of the photocatalytic reaction
$K_L$	$\text{mol}^{-1}$	Langmuir adsorption constant
$K_{LH}$	$\text{mol}^{-1}$	constant in Langmuir-Hinshelwood rate law
$n_{os}$	$\text{mol}$	amount of occupied sites
$n_{ox}$	$\text{mol}$	amount of oxidizing species at the photocatalyst surface
$n_{ts}$	$\text{mol}$	total amount of surface sites
$t$	$\text{min}$	time
$V$	$\text{L}$	total volume of suspension

The Langmuir-Hinshelwood model was developed using the Langmuir isotherm, assuming that a slow step reaction takes place after the adsorption equilibrium. This model was applied to interpret the kinetic data of heterogeneous photoreactions [1,24,28]. The rate of a unimolecular surface reaction is proportional to the surface coverage [29], and can be expressed as follows:

$$\frac{dC}{dt} = \frac{k'_r n_{ox} n_{os}}{V} \quad (1.19)$$

The Langmuir-Hinshelwood rate law is derived employing the amount balance of sites at the photocatalyst surface occupied by the probe molecule during the photocatalytic reaction:



$$\frac{dn_{os}}{dt} = +k_a(n_{ts} - n_{os})C - k_d n_{os} - k'_r n_{ox} n_{os} \quad (1.20)$$

Under steady state conditions, i.e.,  $\frac{dn_{os}}{dt} = 0$ , it can be written

$$+k_a n_{ts} C - k_a n_{os} C - k_d n_{os} - k'_r n_{ox} n_{os} = k_a (n_{ts} C - n_{os} k_a C + k_d + k'_r n_{ox}) = 0 \quad (1.21)$$

and after rearrangement

$$n_{os} = \frac{k_a n_{ts} C}{k_a C + k_d + k'_r n_{ox}} \quad (1.22)$$

Inserting Equation (1.22) into the Equation (1.19) yields

$$\frac{dC}{dt} = \frac{k'_r n_{ox} n_{ts}}{V} \times \frac{k_a C}{k_a C + k_d + k'_r n_{ox}} = \frac{k'_r n_{ox} n_{ts}}{V} \times \frac{\frac{k_a}{k_d + k'_r n_{ox}} C}{1 + \frac{k_a}{k_d + k'_r n_{ox}} C} \quad (1.23)$$

With the abbreviations  $k_r = \frac{k'_r n_{ox} n_{ts}}{V}$  and  $K_{LH} = \frac{k_a}{k_d + k'_r n_{ox}}$  Equation (1.24) yields Equation (1.25).

$$\frac{dC}{dt} = k_r \frac{K_{LH} C}{1 + K_{LH} C} \quad (1.25)$$

As mentioned before, the interpretation of the results of kinetic studies concerning TiO<sub>2</sub> photocatalytic reactions for water treatment, as well as the elucidation of the underlying mechanisms today rely largely on the kinetic adsorption model of Langmuir–Hinshelwood (LH) including classical or modified rate forms [1,24,28,30–32]. However, the values of  $K_L$  (obtained from the Langmuir adsorption isotherm) and those of  $K_{LH}$  (obtained from the photocatalytic reaction) may differ from each other. This is usually explained by the fact that the photocatalytic reaction is influenced by several parameters such as the absence or presence of chemisorption, the reaction mechanisms (through direct hole transfer or via the intermediate formation of OH radicals), the formation of intermediates, the presence and/or absence of molecular oxygen in the system, the photon flux, the total number of adsorption sites, and the overall properties of the photocatalyst [28,30–37].

It is important to point out that the photocatalytic process proceeds efficiently only under aerated conditions, and molecular oxygen (O<sub>2</sub>) may therefore enhance the photocatalytic reaction induced by photoexcited e<sup>-</sup> and positive hole h<sup>+</sup>. A plausible mechanism by which O<sub>2</sub> participates is the capture of e<sup>-</sup> to produce the relatively stable superoxide anion radical O<sub>2</sub><sup>•-</sup>, and retards the charge carrier recombination

[38,39]. The dependence of the photocatalytic reaction rate from the concentration of molecular oxygen present in the suspension has been explained by O<sub>2</sub> adsorption and depletion, both in the dark and during illumination, at the photocatalyst surface [4]. The Langmuir-Hinshelwood model assumes that the adsorption of the reactant has to occur before oxidation takes place. Furthermore, it is considered that only one substrate molecule may bind at each surface site without competition with other organic and/or inorganic compounds present in the suspension. On the other hand, the classical Langmuir-Hinshelwood model of catalysis specifies a bimolecular reaction between reactants both being in an adsorption equilibrium. The Eley-Rideal model has been used as an alternative mechanism to interpret the kinetics of photocatalytic reactions in gaseous or liquid phase. This model assumes a reaction between one non-adsorbed reactant and one adsorbed reactant [40].

## References

- [1] M.R. Hoffmann, S.T. Martin, W. Choi, D.W. Bahnemann, Environmental Applications of Semiconductor Photocatalysis, *Chem. Rev.* 95 (1995) 69–96. doi:10.1021/cr00033a004.
- [2] J. Schneider, M. Matsuoka, M. Takeuchi, J. Zhang, Y. Horiuchi, M. Anpo, D.W. Bahnemann, Understanding TiO<sub>2</sub> Photocatalysis: Mechanisms and Materials, *Chem. Rev.* 114 (2014) 9919–9986. doi:10.1021/cr5001892.
- [3] F. De Angelis, C. Di Valentin, S. Fantacci, A. Vittadini, A. Selloni, Theoretical Studies on Anatase and Less Common TiO<sub>2</sub> Phases: Bulk, Surfaces, and Nanomaterials, *Chem. Rev.* 114 (2014) 9708–53. doi:10.1021/cr500055q.
- [4] M.A. Fox, M.T. Dulay, Heterogeneous photocatalysis, *Chem. Rev.* 93 (1993) 341–357. doi:10.1021/cr00017a016.
- [5] A.L. Linsebigler, G. Lu, J.T. Yates, Photocatalysis on TiO<sub>2</sub> Surfaces: Principles, Mechanisms, and Selected Results, *Chem. Rev.* 95 (1995) 735–758. doi:10.1021/cr00035a013.
- [6] K. Hashimoto, H. Irie, A. Fujishima, TiO<sub>2</sub> Photocatalysis: A Historical Overview and Future Prospects, *Jpn. J. Appl. Phys.* 44 (2006) 8269–8285.
- [7] X. Chen, S.S. Mao, Titanium dioxide nanomaterials: Synthesis, properties, modifications and applications, *Chem. Rev.* 107 (2007) 2891–2959. doi:10.1021/cr0500535.
- [8] M. Pelaez, N.T. Nolan, S.C. Pillai, M.K. Seery, P. Falaras, A.G. Kontos, P.S.M. Dunlop, J.W.J. Hamilton, J.A. Byrne, K. O’Shea, M.H. Entezari, D.D. Dionysiou, A review on the visible light active titanium dioxide photocatalysts for environmental applications, *Appl. Catal. B Environ.* 125 (2012) 331–349. doi:10.1016/j.apcatb.2012.05.036.
- [9] A. Fujishima, K. Honda, Electrochemical Photolysis of Water at a Semiconductor Electrode, *Nature.* 238 (1972) 37–38. doi:10.1038/238037a0.
- [10] M. Grätzel, Photoelectrochemical Cells, *Nature.* 414 (2001) 338–344. doi:10.1038/35104607.
- [11] H. Yan, X. Wang, M. Yao, X. Yao, Band structure design of semiconductors for enhanced photocatalytic activity: The case of TiO<sub>2</sub>, *Prog. Nat. Sci. Mater. Int.* 23 (2013) 402–407. doi:10.1016/j.pnsc.2013.06.002.
- [12] S. Di Mo, W.Y. Ching, Electronic and optical properties of three phases of titanium dioxide: Rutile, anatase, and brookite, *Phys. Rev. B.* 51 (1995) 13023–13032. doi:10.1103/PhysRevB.51.13023.
- [13] T.A. Kandiel, A. Feldhoff, L. Robben, R. Dillert, D.W. Bahnemann, Tailored titanium dioxide nanomaterials: anatase nanoparticles and brookite nanorods as highly active photocatalysts, *Chem. Mater.* 22 (2010) 2050–2060. doi:10.1021/cm903472p.
- [14] D.C. Hurum, A.G. Agrios, K.A. Gray, T. Rajh, M.C. Thurnauer, Explaining the enhanced photocatalytic activity of Degussa P25 mixed-phase TiO<sub>2</sub> using EPR, *J. Phys. Chem. B.* 107 (2003) 4545–4549. doi:10.1021/Jp0273934.
- [15] Degussa, Verfahren zum Reinigen von hochdispersen Oxyden von Metallen bzw. Metalloiden, DE762723, 1942.
- [16] D.P. MacWan, P.N. Dave, S. Chaturvedi, A review on nano-TiO<sub>2</sub> sol-gel type

- syntheses and its applications, *J. Mater. Sci.* 46 (2011) 3669–3686. doi:10.1007/s10853-011-5378-y.
- [17] W. Li, Z. Wu, J. Wang, A.A. Elzatahry, D. Zhao, A perspective on mesoporous TiO<sub>2</sub> materials, *Chem. Mater.* 26 (2014) 287–298. doi:10.1021/cm4014859.
- [18] L. Robben, A.A. Ismail, S.J. Lohmeier, A. Feldhoff, D.W. Bahnemann, J.-C. Buhl, Facile Synthesis of Highly Ordered Mesoporous and Well Crystalline TiO<sub>2</sub>: Impact of Different Gas Atmosphere and Calcination Temperatures on Structural Properties, *Chem. Mater.* 24 (2012) 1268–1275. doi:10.1021/cm203203b.
- [19] W. Bahnemann, M. Muneer, M.M. Haque, Titanium dioxide-mediated photocatalysed degradation of few selected organic pollutants in aqueous suspensions, *Catal. Today.* 124 (2007) 133–148. doi:10.1016/j.cattod.2007.03.031.
- [20] J.-M. Herrmann, Heterogeneous photocatalysis: fundamentals and applications to the removal of various types of aqueous pollutants, *Catal. Today.* 53 (1999) 115–129. doi:10.1016/S0920-5861(99)00107-8.
- [21] D.W. Bahnemann, M. Hilgendorff, R. Memming, Charge carrier dynamics at TiO<sub>2</sub> particles: reactivity of free and trapped holes, *J. Phys. Chem. B.* 101 (1997) 4265–4275. doi:10.1021/jp9639915.
- [22] J. Montoya, M. Atitar, F., D.W. Bahnemann, J. and Peral, P. Salvador, Comprehensive Kinetic and Mechanistic Analysis of TiO<sub>2</sub> Photocatalytic Reactions According to the Direct-Indirect (DI) Model: II) Experimental Validation, *J. Phys. Chem. C.* 28 (2014) 14276–14290. doi:10.1021/jp4121657.
- [23] D. Bahnemann, D. Bockelmann, R. Goslich, Mechanistic studies of water detoxification in illuminated TiO<sub>2</sub> suspensions, *Sol. Energy Mater.* 24 (1991) 564–583. doi:10.1016/0165-1633(91)90091-X.
- [24] C.S. Turchi, D.F. Ollis, Photocatalytic degradation of organic water contaminants: Mechanisms involving hydroxyl radical attack, *J. Catal.* 122 (1990) 178–192. doi:10.1016/0021-9517(90)90269-P.
- [25] J.F. Montoya, J. Peral, P. Salvador, Comprehensive Kinetic and Mechanistic Analysis of TiO<sub>2</sub> Photocatalytic Reactions According to the Direct-Indirect Model: (I) Theoretical Approach, *J. Phys. Chem. C.* 118 (2014) 14266–14275. doi:10.1021/jp4121645.
- [26] P. Atkins, J. de Paula, *Physical Chemistry*, 7th ed, Oxford University Press, 2002.
- [27] U. Diebold, The surface science of titanium dioxide, *Surf. Sci. Rep.* 48 (2003) 53–229. doi:10.1016/S0167-5729(02)00100-0.
- [28] A. V Emeline, V.K. Ryabchuk, N. Serpone, Dogmas and misconceptions in heterogeneous photocatalysis. Some enlightened reflections, *J. Phys. Chem. B.* 109 (2005) 18515–18521. doi:10.1021/jp0523367.
- [29] D. Friedmann, C. Mendive, D. Bahnemann, TiO<sub>2</sub> for water treatment: Parameters affecting the kinetics and mechanisms of photocatalysis, *Appl. Catal. B Environ.* 99 (2010) 398–406. doi:10.1016/j.apcatb.2010.05.014.
- [30] D.F. Ollis, Kinetics of liquid phase photocatalyzed reactions: An illuminating approach, *J. Phys. Chem. B.* 109 (2005) 2439–2444. doi:10.1021/jp040236f.

- [31] B. Ohtani, Preparing Articles on Photocatalysis—Beyond the Illusions, Misconceptions, and Speculation, *Chem. Lett.* 37 (2008) 216–229. doi:10.1246/cl.2008.216.
- [32] D. Monllor-Satoca, R. Gómez, M. González-Hidalgo, P. Salvador, The ‘Direct-Indirect’ model: An alternative kinetic approach in heterogeneous photocatalysis based on the degree of interaction of dissolved pollutant species with the semiconductor surface, *Catal. Today.* 129 (2007) 247–255. doi:10.1016/j.cattod.2007.08.002.
- [33] F. Zhang, J. Zhao, T. Shen, H. Hidaka, E. Pelizzetti, N. Serpone, TiO<sub>2</sub>-assisted photodegradation of dye pollutants II. Adsorption and degradation kinetics of eosin in TiO<sub>2</sub> dispersions under visible light irradiation, *Appl. Catal. B Environ.* 15 (1998) 147–156.
- [34] J. Zhao, H. Oota, H. Hidaka, E. Pelizzetti, N. Serpone, Photodegradation of surfactants X. Comparison of the photo-oxidation of the aromatic moieties in sodium dodecylbenzene sulphonate and in sodium phenyldodecyl sulphonate at TiO<sub>2</sub>-H<sub>2</sub>O interfaces, *J. Photochem. Photobiol. A Chem.* 69 (1992) 251–256. doi:10.1016/1010-6030(92)85285-3.
- [35] A. Mills, S. Morris, Photomineralization of 4-chlorophenol sensitized by titanium dioxide: a study of the initial kinetics of carbon dioxide photogeneration, *J. Photochem. Photobiol. A Chem.* 71 (1993) 75–83. doi:10.1016/1010-6030(93)87012-C.
- [36] E.P. Melián, O.G. Díaz, J. Araña, J.M.D. Rodríguez, E.T. Rendón, J.A.H. Melián, Kinetics and adsorption comparative study on the photocatalytic degradation of o-, m- and p-cresol, *Catal. Today.* 129 (2007) 256–262. doi:10.1016/j.cattod.2007.08.003.
- [37] T. Sauer, G. Cesconeto Neto, H.J. José, R.F.P.M. Moreira, Kinetics of photocatalytic degradation of reactive dyes in a TiO<sub>2</sub> slurry reactor, *J. Photochem. Photobiol. A Chem.* 149 (2002) 147–154. doi:10.1016/S1010-6030(02)00015-1.
- [38] B. Ohtani, Y. Nohara, R. Abe, Role of molecular oxygen in photocatalytic oxidative decomposition of acetic acid by metal oxide particulate suspensions and thin film electrodes, *Electrochemistry.* 76 (2008) 147–149. doi:10.5796/electrochemistry.76.147.
- [39] A. Fujishima, X. Zhang, D. Tryk, TiO<sub>2</sub> photocatalysis and related surface phenomena, *Surf. Sci. Rep.* 63 (2008) 515–582. doi:10.1016/j.surfrep.2008.10.001.
- [40] P. Pichat, Photocatalytic degradation of pollutants in water and air: Basic concepts and applications, in: M. Tarr (Ed.), *Chem. Degrad. Methods Wastes Pollut. Environ. Ind. Appl.*, 1st ed., CRC Press, 2003: pp. 77–120.

**1.3. The relevance of ATR-FTIR spectroscopy in semiconductor photocatalysis**

*Mohamed Faycal Atitar, Hamza Belhadj, Ralf Dillert and Detlef W. Bahnemann*

Published in “Emerging Pollutants in the Environment – Current and Further Implications”.

Edited by Marcelo L. Larramendy and Sonia Soloneski, InTech 2015, pp 203-229.

### 1.3.1. Abstract

Attenuated total reflection Fourier-transform infrared (ATR-FTIR) spectroscopy has a high potential for investigating a wide range of samples and systems. In photocatalysis, various interfacial phenomena can be studied using this technique, including pH-dependent adsorption and photodegradation of probe molecules. The analysis of the processes occurring at the interface of thin particle films deposited on the surface of an ATR crystal, either in the liquid or the gas phase, is perhaps the best way to elucidate the mechanism of adsorption and heterogeneous photocatalytic reactions. This chapter summarizes the recent advances and applications of ATR-FTIR techniques in semiconductor photocatalysis. A brief outlook at some of the possible investigations in this area is provided and the different proposed adsorption and photocatalytic degradation mechanisms are discussed.

**Keywords:** Adsorption, attenuated total reflection Fourier-transform infrared (ATR-FTIR), photocatalysis, semiconductor, spectroscopy, thin films, TiO<sub>2</sub>

### 1.3.2 Introduction

The expanding interest in environmental and energy issues led to the consideration of heterogeneous photocatalysis as one of the most promising advanced oxidation processes. The interest in this scientific field has increased in the last decade since photocatalysis is assumed to be a powerful tool for the destruction and remediation of highly toxic pollutants, the purification of polluted water and air, the development of self-cleaning surfaces coated with semiconducting metal oxide materials, and the conversion of solar energy into chemical energy [1–3]. Many semiconductor materials have been tested as photocatalysts, nevertheless, due to its low cost, abundance, high activity, and stability under a variety of conditions. Titanium dioxide (TiO<sub>2</sub>) is the most reliable and widely used material [4, 5]. Accordingly, there has been a tremendous amount of research on diverse aspects of TiO<sub>2</sub> (nano)materials, ranging from their synthesis, characterization, and applications to atomic scale, to experimental and theoretical investigations of their fundamental physical and chemical properties [1, 5–7]. Despite these investigations, there remains a need to better understand the reaction mechanisms of the transformation of organic molecules occurring during TiO<sub>2</sub> photocatalysis.

Surface science plays a prominent role in mechanistic investigations concerning the photocatalytic process, providing a unique approach to understand bulk, surface, and interfacial phenomena occurring at the TiO<sub>2</sub> surface [6, 8, 9]. According to several proposed photocatalytic mechanisms [10, 11], an important point for the conversion of the molecules on TiO<sub>2</sub> is the physical and electronic structure of the adsorbed state of the molecules. How a molecule binds onto the TiO<sub>2</sub> surface influences its electronic structure, as well as its redox properties. *Inter alia*, coverage, thermal stability, and reactivity, adsorption structure and site, are all important factors [8]. The interest in surface techniques to investigate liquid-solid and gas-solid interfacial chemistry has grown due to the importance of the information they provide. Few surface spectroscopic techniques are adequate to perform *in situ* analyses of interfacial interactions. For example, sum-frequency vibrational spectroscopy is restricted to planar solid-solution interfaces [12], infrared ellipsometry is considered mainly as a technique for the analysis of thin solid films rather than of interfacial species [13], and surface enhanced Raman spectroscopy (SERS) requires the presence of metals on the surface. Thus, this complicates the more widespread applicability of SERS [14, 15].

IR spectroscopy is the oldest and most commonly used method for identifying both organic and inorganic chemicals, as well as for providing specific information on molecular structure, chemical bonding, and molecular environment. Being a powerful tool for qualitative and quantitative studies, it can be applied to study solids, liquids, or gaseous samples [16]. Recently, IR spectroscopy has been applied *in situ* to study surface reactions on immersed solids such as oxides. This has been achieved with particle films via internal reflection or attenuated total reflection (ATR-FTIR) methods. Investigating several metal oxide solid particles in suspensions or deposited as thin films on ATR crystals, these developments have led to *in situ* ATR-FTIR studies of adsorption and chemical reactions on a variety of solid-liquid and/or solid-gas interfaces in the photocatalysis context [17–24]. The ATR-FTIR technique has proved to be a powerful tool for probing binding mechanisms and for characterizing the adsorption of organic molecules onto metal oxide surfaces in liquid media.

This book chapter focuses on the application of this technique in the above-mentioned context. An overview of the investigations that have been performed to date will be given, analyzing the different experimental procedures, and summarizing



the performed investigation of surface interactions. An in-depth analysis of the different proposed adsorption and photocatalytic reaction mechanisms on TiO<sub>2</sub>, as well as on other metal oxides also employed in photocatalysis will be given. To complement this overview, results and interpretations of quantum chemical calculations will also be presented.

### 1.3.2.1. History and brief overview of ATR-FTIR spectroscopy

Infrared absorption spectroscopy (IR) has contributed for more than fifty years to the molecular view on a wide variety of systems. The selection rule for a vibrational mode of a molecule to be IR active is that there is a change of the electric dipole moment of the molecule upon absorption of light. The absorption of infrared light due to the excitation from the ground vibrational energy level to a higher energy level provides information concerning molecular structure and molecular interactions [15, 25, 26]. Due to the existence of the wide absorption spectra database in the mid-infrared region (4000–400 cm<sup>-1</sup>), infrared spectroscopy is considered as a universal technique since many molecules have strong absorbances in this region [27].

Fourier-transform infrared (FTIR) spectroscopy is a well-established technique based on the idea of the interference of radiation between two beams to yield an interferogram. The latter is a signal produced as a function of the change of path length between the two beams. The two domains of distance and frequency are interconvertible by the mathematical Fourier transformation method.

ATR spectroscopy was introduced simultaneously by Harrik [28] and Fahrenfort [29] based upon the total internal reflection phenomena. In this approach, IR spectra are recorded for a sample material that is in contact with an internal reflection element (IRE). The IR beam is focused onto the edge of the IRE, reflected through the IRE, and then directed to the detector (cf. Figure 1.3.) [26, 27]. In this case, all the light reflects off the internal surface of the IRE, hence explaining the term total internal reflection [27]. The internal reflection element (IRE) or ATR crystal has, in most cases, a higher refractive index ( $n_1$ ) as compared to the sample ( $n_2$ ). Another important parameter is the incidence angle  $\theta$  that can be determined from the refractive indexes of the sample ( $n_2$ ) and the IRE ( $n_1$ ):

$$\theta = \sin^{-1}\left(\frac{n_2}{n_1}\right) \quad (1.26)$$

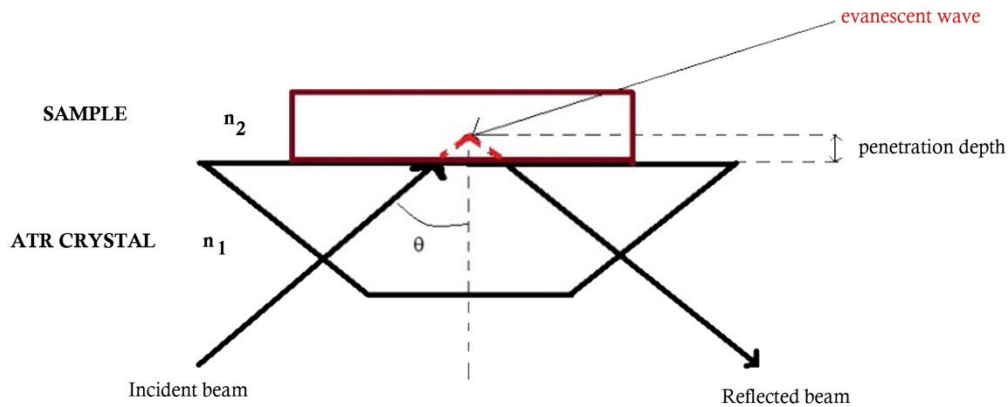


**Figure 1.3.** Schematic diagram of a horizontal ATR sampling accessory illustrating the important parameters [16].

The major applications of the ATR method are in the mid-IR region. However, the range has been extended to the near-IR, the far-IR, as well as to the UV and visible spectral regions. Therefore, it is of great importance to choose a suitable ATR crystal for a given application. The most common ATR crystals with their respective refractive indexes and some other relevant properties are summarized in Table 1.1.

Since the IR beam should penetrate the sample, the penetration depth ( $d_p$ ) is one of the important parameters in ATR-FTIR spectroscopy. The measure of the depth that the infrared beam enters into the sample is defined by equation (1.27):

$$d_p = \frac{1}{[2\pi W n_1 (\sin^2 \theta - n_{21}^2)^{\frac{1}{2}}]} \quad (1.27)$$

where  $d_p$  is the depth of penetration,  $W$  the wavenumber,  $n_1$  the refractive index of the ATR crystal,  $\theta$  the angle of incidence, and  $n_{21}$  the fraction  $\frac{n_2}{n_1}$ .

Each of the parameters mentioned above has important messages to teach us about the ATR technique and its application. Readers interested in details of the theory of ATR should consult the respective literature [16, 25, 27].

Material	Refractive index	Wavenumber range (cm <sup>-1</sup> )	d <sub>p</sub> (μm)	References
Diamond	2.4	45000–2500	1.35–1.66	[30][31][32]
Germanium (Ge)	4	5500–870	0.65–0.73	[30][31][32]
Zinc Selenide (ZnSe)	2.41	20000–650	1.22–1.66	[30][31][32]
AMTIR (As/Ge/Se glass)	2.5	11000–750	1.46	[30]
Silicon (Si)	3.4	-	0.84–1.17	[30][32]
Thallium bromoiodide (KRS-5)	2.37	20000–250	1.22–1.73	[30][32]
Cd telluride (CdTe)	2.67	10000–450	-	[31]
Sapphire (Al <sub>2</sub> O <sub>3</sub> )	1.74	25000–1800	-	[31]
Zinc Sulfide (ZnS)	2.2	17000–950	2.34	[31][32]
Cubic Zirconia (ZrO <sub>2</sub> )	2.15	25000–1800	-	[31]

**Table 1.1.** Relevant properties of some common ATR crystals.

### 1.3.2.2. Experimental processing

One of the advantages of the ATR-FTIR technique is that an experiment can be easily conducted to study the interactions between a chosen probe molecule and the surface of different metal oxides. The whole procedure consists in the preparation of a thin film of nanoparticles of the chosen metal oxide on the ATR crystal. This thin film should be stable, at least during the experiment, and its thickness should allow the penetration of the IR beam to reach the interface, e.g., the sample solution above the oxide layer. A thin homogeneous layer of the nanoparticles on the ATR crystal is generally produced from their suspension in an adequate solvent. This suspension is carefully drop-casted on the IRE material. Examples of the preparation of these thin layers, especially those made of TiO<sub>2</sub>, can be found elsewhere [18, 19, 23, 33].

It is worth noting that the contact between the probe molecule and the layer can lead to a change in some operational parameters such as pH, temperature, and ionic

strength of the supernatant solution. Therefore, studies on adsorption phenomena are better carried out employing flow cell reactors either in the liquid or the gas phase (see Figure 1.4a) where the solution or the dispersant circulate continuously over the layer. This allows the control of the above-mentioned parameters and the monitoring of the evolution in time of the system under different conditions. As an alternative, a sample batch system can also be employed where the inlet and outlet are closed (Figure 1.4b) [23].

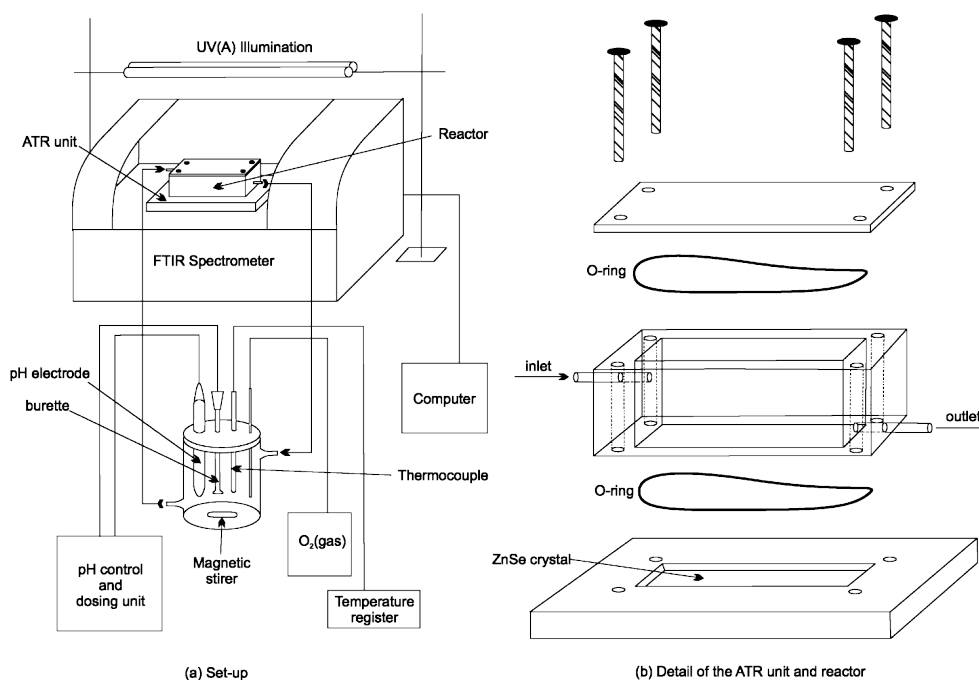


**Figure 1.4.** Flow cell reactor for ATR-FTIR spectroscopic studies (Reproduced from [23] with permission of the PCCP Owner Societies).

Prior to coating the ATR crystal, a spectrum of the blank ATR crystal is collected for spectral processing. Mainly, two different approaches can be used for the spectral processing. The first one is the normalization of the spectra of the ligand to that of the matrix (solvent at the pH of interest in the liquid phase or dispersant in the gas phase) from which a spectrum is collected. The probe molecule is then introduced and the corresponding spectrum is collected. The spectrum of the probe molecule is then referenced to the background spectrum (solvent/dispersant). The second approach is as follows: after preparing the thin film, a spectrum of the solvent at the pH of interest (or of the dispersant in the gas phase) is collected; the probe molecule is introduced and a spectrum is collected; the single beam spectrum of both solvent/dispersant and of the probe molecule in the solvent/dispersant is referenced

to the blank ATR crystal to obtain the absorbance spectra of each. Subsequently, the absorbance spectrum of the solvent/dispersant is subtracted from the spectrum of the probe molecule. To collect spectra for the probe molecule alone the same experimental process is used but without the nanoparticle thin layer [30].

### **1.3.3. Probing interfacial reactions by ATR-FTIR investigations**

#### **1.3.3.1. Metal oxide-water interface**

Considering its relevance to semiconductor photocatalysis, water splitting, and other important applications, the interaction of water with metal oxide surfaces, especially TiO<sub>2</sub>, has been the focus of several experimental and theoretical investigations over the last decades [3, 4, 6, 8, 34–36]. Molecular, dissociated, and undissociated states of water adsorbed at a solid surface have been suggested. In addition to that, a mixture of these adsorption states is possible.

ATR-FTIR spectroscopy is one of the suitable techniques to investigate the adsorption of water molecules on a metal oxide surface under a wide range of conditions [37–39]. From many perspectives, numerous experimental and theoretical water adsorption studies have been conducted by means of ATR-FTIR spectroscopy [17, 37, 40, 41].

Figure 1.5. depicts the typical spectra of water adsorbed on TiO<sub>2</sub> (anatase/rutile Evonik-Degussa Aeroxide TiO<sub>2</sub> P25) [38]. The broad absorption band at around 3600–2800 cm<sup>-1</sup> and the small peak at 3696 cm<sup>-1</sup> are well-known to be the stretching vibration modes of the H<sub>2</sub>O molecules, which have complex interactions through hydrogen bonds, and the end part of polymerically chained H<sub>2</sub>O molecules without hydrogen bonds, respectively. The broad band contains not only the components of the H<sub>2</sub>O molecules with different numbers of hydrogen bonds but also the Fermi resonance attributed to the overtone absorption of the bending mode  $\delta$  (H<sub>2</sub>O) at 1637 cm<sup>-1</sup>. Therefore, it is difficult to analyze the detailed adsorption state of the polymerically chained H<sub>2</sub>O molecules on metal oxide surfaces only from FTIR (mid-infrared) measurements [38]. However, based on the information obtained from such IR spectra, ATR-FTIR spectroscopy has been used for the characterization and identification of intermediate mechanisms involved in environmental interfaces [42], mainly during photocatalytic oxidation processes induced at the TiO<sub>2</sub>-water interface [37,40].

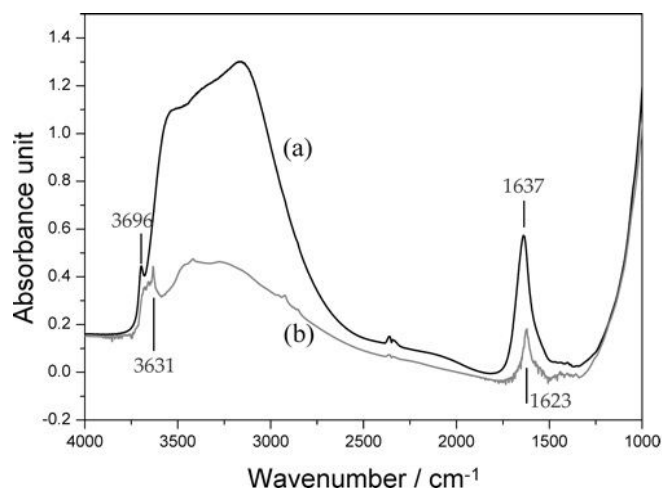


**Figure 1.5.** FT-IR (MIR) absorption spectra of TiO<sub>2</sub> (Evonik-Degussa Aeroxide TiO<sub>2</sub> P25) in air (a) and after evacuation at room temperature for 1 h (b) (Reprinted with permission from Takeuchi M, Martra G, Coluccia S, Anpo M. Investigations of the Structure of H<sub>2</sub>O Clusters Adsorbed on TiO<sub>2</sub> Surfaces by Near-Infrared Absorption Spectroscopy. *Journal of Physical Chemistry B*; 109(15):7387–91. Copyright (2005) American Chemical Society).

Starting from the hypothesis that adsorbed H<sub>2</sub>O changes its conformation due to the co-adsorption of cyclohexane on TiO<sub>2</sub> (anatase, Sachtleben Hombikat UV100), Almeida et al. [40] have shown with the help of additional DFT (Density Functional Theory) calculations, yielding the adsorption energy and the structure of the water molecule at different hydration levels (Figure 1.6.), that at least three layers of water are formed during the adsorption process. The first layer includes only chemisorbed H<sub>2</sub>O molecules. The second hydration level includes physisorbed (H-bonded) H<sub>2</sub>O molecules on surface OH sites, and the highest hydration level contains an additional adsorbed water layer. The dissociative chemisorption of water is assumed to be energetically favored. In addition to that, dissociative chemisorption of water generates at least two different Ti-OH groups. At least one of these two new OH sites contains an oxygen atom originally originating from the TiO<sub>2</sub> lattice structure [40]. This finding allowed the authors to provide a spectral and structural interpretation of the mode of adsorption of cyclohexanone on the hydrated TiO<sub>2</sub> surface [40].

	(100)	(101)	(001)
Structures			
Hydration ( $\text{H}_2\text{O}/\text{nm}^2$ )	6.2	4.8	2.3
Energy (kJ/mol)	-68.5	-65.7	-184.7
Structures			
Hydration ( $\text{H}_2\text{O}/\text{nm}^2$ )	9.3	9.6	7.0
Energy (kJ/mol)	-61.7	-67.1	-97.4
Structures			
Hydration ( $\text{H}_2\text{O}/\text{nm}^2$ )	18.5	16.8	16.4
Energy (kJ/mol)	-61.0	-57.1	-72.6

**Figure 1.6.** Adsorption energies and structures of  $\text{H}_2\text{O}$  on  $\text{TiO}_2$  (100), (101), and (001) facets, at different hydration levels (Reprinted with permission from Almeida A, Calatayud M. Combined ATR-FTIR and DFT Study of Cyclohexanone Adsorption on Hydrated  $\text{TiO}_2$  Anatase Surfaces. *Journal of Physical Chemistry C*; 115(29):14164–14172. Copyright (2011) American Chemical Society).

Besides of that, several research reports have identified and specified the different bending modes and structures of water on the  $\text{TiO}_2$  surface during, before, and after UV light irradiation. It has been reported that UV irradiation induces a structural ordering of the adsorbed water layer [43], or results in an increase in the amount of surface OH groups, thus increasing the hydrophilicity of the  $\text{TiO}_2$  surface [44]. Mendive et al. [37] have revealed by ATR-FTIR studies that the disaggregation of particle agglomerates plays an important role in UV illuminated aqueous  $\text{TiO}_2$  nanoparticulate systems.

However, it should be noted here that the exact nature of the adsorption of water is still a matter of discussion in the field of metal oxide (especially of  $\text{TiO}_2$ ) photocatalysis. This is a consequence of the diverse possibilities of interpretation arising from the combination of experimental results obtained by ATR-FTIR spectroscopy and by other techniques. Obviously, there is not yet a general consensus on the mechanism of adsorption of water on  $\text{TiO}_2$ .

### 1.3.3.2. Interactions of probe molecules with the metal oxide surface

ATR-FTIR spectroscopy yields important insight into the surface speciation of probe molecules adsorbed on nanomaterials [30]. Chemical or inner sphere adsorption is generally studied when it is expected that the probe molecule is able to coordinate with the metal ions of the substrate covering the ATR crystal [15].

Investigations of the interaction of a large number of ligands on metal oxide, metal hydroxide, and metal oxyhydroxide systems have been performed employing ATR-FTIR spectroscopy [26]. The objective of these investigations is to obtain an insight into the chemical nature of these interactions, being either qualitative such as the mode of adsorption and the surface speciation, or quantitative such as the kinetics and the surface coverage.

It is worth to note that TiO<sub>2</sub> nanoparticles are much more extensively used as substrates as compared with other metal oxides. The adsorption of organic compounds bearing common functional groups such as acids [23, 45, 46], amino acids [47], phenolic compounds [11, 48], and a few complex heteroaromatic compounds [49–52] has been studied in detail (cf. Table 1.3.).

As an example, a typical ATR-FTIR spectrum of an aqueous solution of the herbicide imazapyr in the absence and presence of a TiO<sub>2</sub> layer is presented in Figure 1.7. The reliability of information obtained from the IR spectra is dependent mainly upon the correct assignment of the vibrational modes by comparison with published spectroscopic data [15, 30]. Mudunkotuwa et al. have presented a summary of several common IR absorption band frequencies (Table 1.2.) [30]. Furthermore, the infrared spectral data collected for coordination compounds [53] are very useful when interpreting the spectra of adsorbates, which mostly resemble those of ligands of coordination compounds [15]. In addition to that, the interpretation of the increase in the intensities of the bands of functional groups, as well as the shifting of these bands either to the blue or to the red spectral regions also provide important information concerning the type of interaction between adsorbate and surface. The interpretation of IR bands is very helpful for a qualitative analysis, e.g., concerning the points of interactions, the modes of adsorption, and the molecular speciation, respectively.



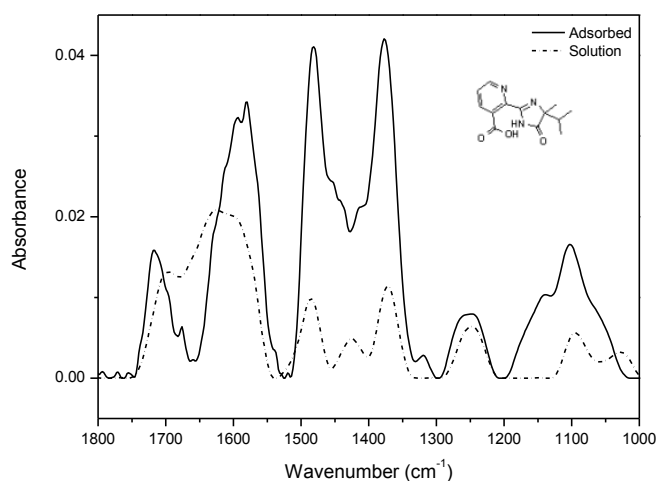


**Figure 1.7.** ATR-FTIR spectra of  $8 \times 10^{-3} \text{ mol L}^{-1}$  imazapyr aqueous solution at pH 3 (dashed lines); and  $2 \times 10^{-3} \text{ mol L}^{-1}$  imazapyr aqueous solution in contact with a  $\text{TiO}_2$  film (solid lines). Reference spectra were of water in contact with the bare ZnSe prism and of the bare  $\text{TiO}_2$  film respectively [54].

Vibrational Mode	Wavenumber ( $\text{cm}^{-1}$ )
$\nu(\text{C}=\text{O})$	1730–1720
$\nu_{\text{asym}}(\text{COO}^-)$	1620–1590
$\nu_{\text{sym}}(\text{COO}^-)$	1410–1390
$\delta_{\text{asym}}(\text{NH}_3^+)$	1630
$\delta_{\text{sym}}(\text{NH}_3^+)$	1571
$\nu_{\text{asym}}(\text{CH}_2)$	2920
$\nu_{\text{sc}}(\text{CH}_2)$	1442–1438
$\nu_{\text{w}}(\text{CH}_2)$	1400–1200
$\nu_{\text{r}}(\text{CH}_2)$	730–720
$\nu_{\text{sym}}(\text{NH})$	3300–3100
$\nu_{\text{sym}}(\text{C}=\text{O})^{\text{major}} + \nu_{\text{sym}}(\text{C}-\text{N})^{\text{minor}}$	1700–1600 (Amide I)
$\nu_{\text{sym}}(\text{C}-\text{N}) + \delta(\text{N}-\text{H})_{\text{out of phase}}$	1580–1510 (Amide II)
$\nu_{\text{sym}}(\text{C}-\text{N}) + \delta(\text{N}-\text{H})_{\text{in phase}}$	1400–1200 (Amide III)

**Table 1.2.** IR absorption frequencies of common organic functional groups (Adapted from [30] with permission of The Royal Society of Chemistry).

As mentioned above, the complexity of the obtained IR spectra usually requires the combination of different techniques to enable their interpretation. Generally, the deductions resulting from the analysis of the IR spectra have to be supported by the results of other experimental techniques and/or by theoretical calculations. Several experimental and theoretical studies on the adsorption of aliphatic mono- and dicarboxylic acids on metal oxide surfaces have been performed [46]. It is assumed that the binding of carboxylates at the solid metal oxide surface occurs in several ways such as physisorption through electrostatic attraction and hydrogen bonding, and chemisorption in different modes including monodentate, bridged bidentate, and chelating bidentate adsorbed structures [55–57]. These different binding modes can be distinguished in an infrared spectrum by the difference  $\Delta\nu_{a-s}$  of the frequencies of the asymmetric and the symmetric mode of the carboxylate stretching vibration. By comparing the  $\Delta\nu_{a-s}$  of free aqueous carboxylate,  $\Delta\nu_{a-s}$  (free), to the  $\Delta\nu_{a-s}$  (adsorbed) values measured in transition metal complexes, the following correlations were found [46, 56, 58]:

$\Delta\nu_{a-s}$  (adsorbed) >  $\Delta\nu_{a-s}$  (free): monodentate coordination

$\Delta\nu_{a-s}$  (adsorbed) <  $\Delta\nu_{a-s}$  (free): bidentate chelating or bridging

$\Delta\nu_{a-s}$  (adsorbed)  $\ll$   $\Delta\nu_{a-s}$  (free): bidentate chelating, unless short metal-metal bonds are present

DFT calculations have been performed by Vittadini et al. for several possible adsorption conformations of formic acid and sodium formate on the anatase surface to support the interpretation of ATR-FTIR spectra measured of formic acid adsorbed on the  $\text{TiO}_2$  surface [59]. The comparison of the calculated results with this experimental information enabled the identification of seven different surface species (see Figure 1.8.). On the hydrated surface, both  $\text{HCOOH}$  and  $\text{HCOONa}$  preferentially form inner-sphere adsorption complexes.  $\text{HCOOH}$  as monodentate adsorbate dissociates due to the interaction with a nearby water molecule, while  $\text{HCOONa}$  prefers a bridging bidentate structure [59].

Mono-carboxylic acids, i.e., formic and acetic acid, were found to bind on  $\text{ZrO}_2$  and  $\text{Ta}_2\text{O}_5$  surfaces in both protonated and deprotonated carboxylic acid forms indicating a bridging bidentate adsorption. Under the experimental conditions of this work no adsorption of formic acid onto  $\text{TiO}_2$  and  $\text{Al}_2\text{O}_3$  was observed [46].

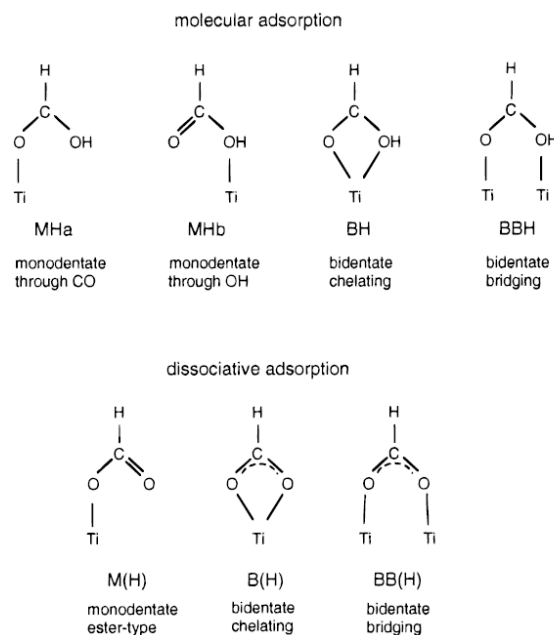


**Figure 1.8.** Possible configurations for HCOOH and HCOO<sup>-</sup> species bound to metal cations (Reprinted with permission from Vittadini A, Selloni A, Rotzinger FP, Grätzel M. Formic Acid Adsorption on Dry and Hydrated TiO<sub>2</sub> Anatase (101) Surfaces by DFT Calculations. *Journal of Physical Chemistry B*; 104(101):1300–1306. Copyright (2000) American Chemical Society).

Dicarboxylic acids adsorb much more strongly to oxide surfaces than monocarboxylic acids due to both electrostatic and chemical interactions.

Oxalic acid is one of the most investigated molecules in this regard [18, 45, 58, 60, 61]. Based on a series of spectra recorded at varying different experimental parameters (concentration, pH, and ionic strength), and supported by the comparison of these spectra with those of the aqueous [Fe(Ox)<sub>y</sub>]<sub>z</sub> complex, Hug et al. [18] described several surface complexes formed during the adsorption of oxalic acid at the TiO<sub>2</sub> P25 surface. The obtained data strongly support the assumption that oxalate forms specific inner-sphere coordination complexes with surface Ti<sup>4+</sup> sites. These complexes are formed through bidentate bridging or monodentate binding modes.

Mendive et al. have published several papers presenting experimental results of their investigation of the TiO<sub>2</sub>-oxalic acid system using both pure anatase and rutile phases. In addition to that, data of quantum chemical calculations using Modified Symmetrically Orthogonalized Intermediate Neglect of Differential Overlap (MSINDO) have been presented to yield a complete insight into the TiO<sub>2</sub>-oxalate system [23, 24, 62, 63]. A detailed analysis of the experimental ATR-FTIR data and the data obtained from theoretical calculations (IR spectra (Figure 1.9.) and

calculated bending energies) has led to the suggestion of different adsorbate structures of oxalic acid either on anatase or on rutile nanoparticles (Figure 1.10.). By comparison between both TiO<sub>2</sub> phases (anatase and rutile), the difference as well as the similarity in the adsorption of oxalate can be explained either by the mode of adsorption, the structure of the surface complexes, the surface speciation of either TiO<sub>2</sub> phases, or the adsorption energies.

Young et al. [45] have published the results of an ATR-FTIR study focused on the adsorption-desorption kinetics of oxalic acid on the anatase TiO<sub>2</sub> surface. The measured spectra were not found to be well resolved. However, based on the absorbance versus time behavior, the authors were able to extract the pseudo-first-order rate constants corresponding to the three expected adsorbed species of oxalic acid at the TiO<sub>2</sub> surface.

Furthermore, Mendive et al. [61] have proposed the mechanism of the photocatalytic degradation of oxalic acid with the help of the above mentioned experimental and theoretical investigations [24, 63]. The possible pathways for the formation of oxalic acid photoproducts, as well as the role of the TiO<sub>2</sub> surface as active surface have been discussed in detail [61]. An example of the proposed degradation pathways of the oxalic acid surface complexes is depicted in Figure 1.11.

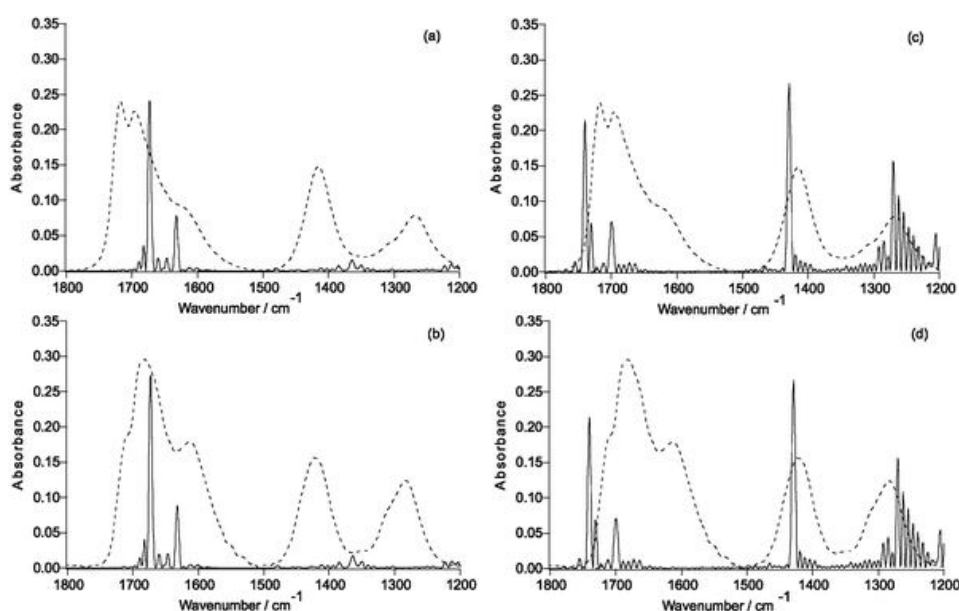


**Figure 1.9.** Experimental and calculated FTIR spectra of oxalic acid on anatase (Reproduced from [23] with permission of the PCCP Owner Societies).

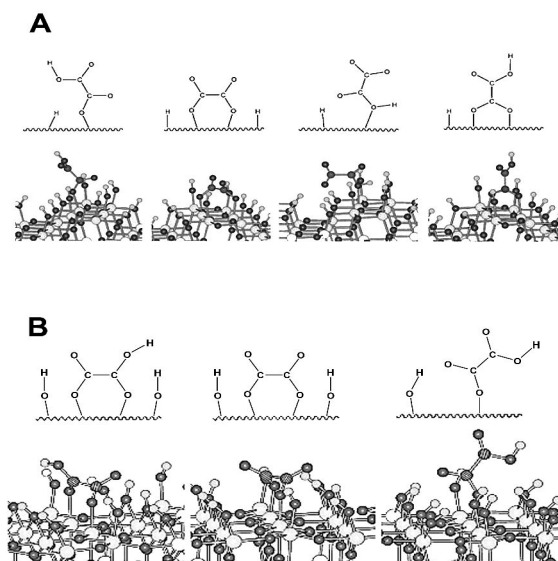


**Figure 1.10.** Adsorbed structures of oxalic acid on anatase (A) (Reproduced from [24] with permission of the PCCP Owner Societies) and Rutile (B) (Reproduced from [63] with permission of the PCCP owner Societies) in equilibrium in the dark. A scheme of every structure is provided. Ti, O, H and C atoms are represented by large light, dark, small light and dark-dashed spheres respectively.

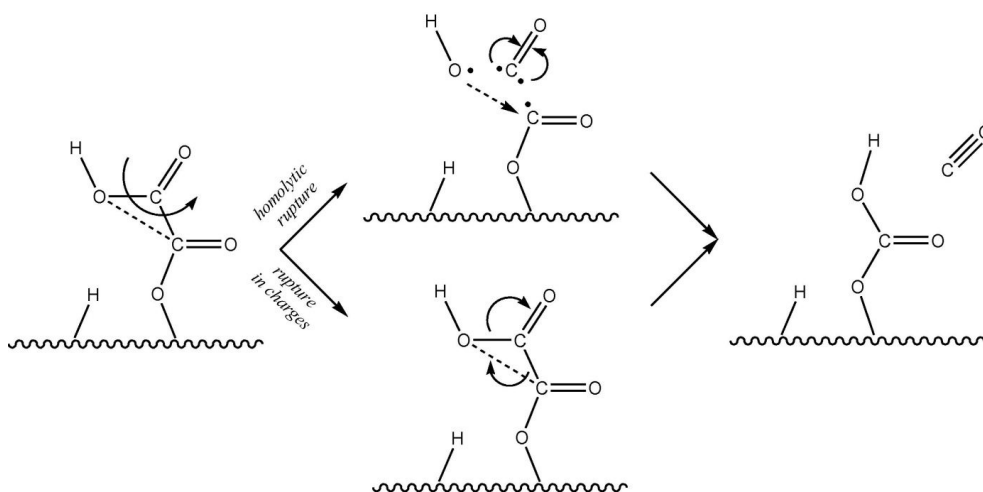


**Figure 1.11.** Possible photocatalytic degradation pathways of species adsorbed on anatase (Reprinted from Oxalic Acid at the  $\text{TiO}_2$ /Water Interface under UV(A) Illumination: Surface Reaction Mechanisms, Cecilia B. Mendive, Thomas Bredow, Jenny Schneider, Miguel Blesa, Detlef Bahnemann. *Journal of Catalysis* 2015, 322:60-72, Copyright (2015), with permission from Elsevier).

As mentioned in the introduction of this chapter, the direct evidence for the formation of structurally different surface complexes is an important step in the

understanding of metal oxide photocatalysis, especially of TiO<sub>2</sub> photocatalysis. This is due to the fact that the reactivity and the pathways for product formation are determined by the structures of the formed surface species during the dark adsorption. Recently, Montoya et al. [11] have investigated the interaction of the TiO<sub>2</sub> surface with three probe molecules, *e.g.*, formic acid, benzene, and phenol employing ATR-FTIR spectroscopy. Based upon the analysis of the IR spectra (Figure 1.12.), assumptions have been made concerning the physisorption of benzene (no changes have been observed in the spectra with and without the TiO<sub>2</sub> layer), the strong chemisorption of formic acid, and also the role of the solvent (water or acetonitrile) for the adsorption mode of phenol. Based on these results, the authors provided an insight into the mode of interaction of the probe molecules with the TiO<sub>2</sub> surface (chemisorption or physisorption) (Figure 1.13.). In addition to that, they discussed the photocatalytic oxidation mechanism induced either by the reaction of surface trapped holes with the adsorbate (direct pathway) or the reaction of photocatalytically generated  $\cdot\text{OH}$  radicals with the physisorbed molecules (indirect pathway). The authors concluded that formic acid is directly oxidized due to its strong chemisorption onto the TiO<sub>2</sub> surface, while physisorbed benzene is indirectly oxidized. For phenol the authors suggested a combination of both pathways [10, 11].

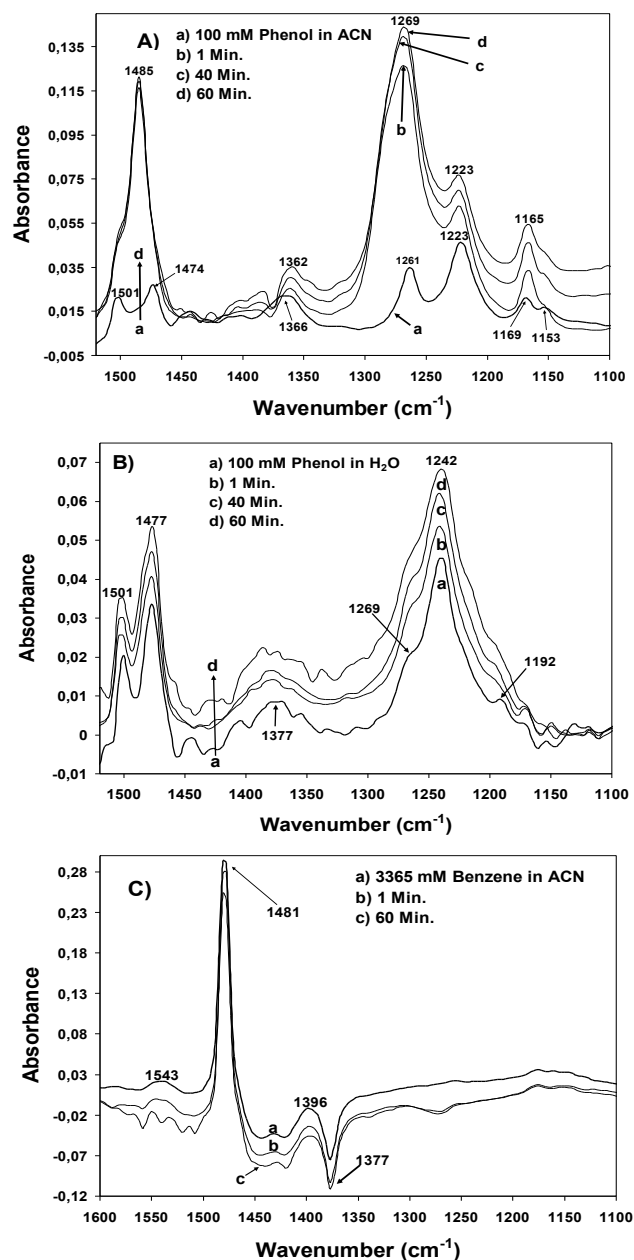


**Figure 1.12.** ATR-FTIR spectra of: A) a 100 mM solution of acetonitrile dissolved phenol, in the absence (a) and in the presence of an anatase film under different TiO<sub>2</sub>-Phenol contact times (b-d); B) a 100 mM solution of water dissolved phenol (pH 3) in the absence (a) and in the presence of a TiO<sub>2</sub> anatase film, under different TiO<sub>2</sub>-Phenol contact times (b-d); C) a 3365 mM solution of acetonitrile dissolved benzene in absence (a) and presence of a TiO<sub>2</sub> anatase film under different TiO<sub>2</sub>-Benzene contact times (b-c) (Reprinted with permission from Montoya JF, Atitar FM, Bahnemann DW, Peral J, Salvador P. Comprehensive Kinetic and Mechanistic Analysis of TiO<sub>2</sub> Photocatalytic Reactions According to the Direct-Indirect (DI) Model: II) Experimental Validation. Journal of Physical Chemistry C; 28(118):14276–14290. Copyright (2014) American Chemical Society).

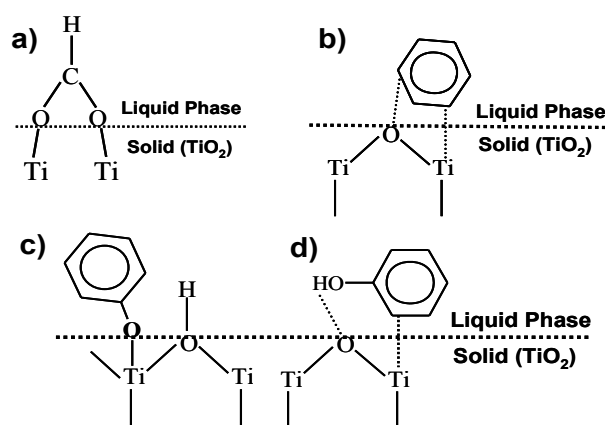


**Figure 1.13.** Interaction modes of benzene, formic acid and phenol, model organic compounds with the  $\text{TiO}_2$  surface (Reprinted with permission from Montoya JF, Atitar FM, Bahnemann DW, Peral J, Salvador P. Comprehensive Kinetic and Mechanistic Analysis of  $\text{TiO}_2$  Photocatalytic Reactions According to the Direct-Indirect (DI) Model: II) Experimental Validation. *Journal of Physical Chemistry C*; 28(118):14276–90. Copyright (2014) American Chemical Society).

In addition to the presented examples, several experimental and theoretical studies have been performed concerning the adsorption and various photocatalytic reactions by means of the ATR-FTIR technique. Table 1.3. presents a survey of published data on the adsorption as well as the photooxidation of aqueous organic compounds on metal oxide surfaces studied by means of ATR-FTIR spectroscopy.

Adsorbate or reactant	Material	Study	Ref
Acetic acid	Rutile	Adsorption	[64]
Acetate	Rutile	Adsorption	[65]
Acrylic acid	P25	Adsorption	[66]
Poly(Acrylic acid)	Hematite	Adsorption	[67]
L- $\alpha$ -alanine	P25	Adsorption	[68]
Amino acid	P25	Photo- Oxidation	[69]
	Au/ $\text{TiO}_2$		
p-Arsanilic acid	Iron-(Oxyhydr)Oxides	Adsorption	[70],[71]
Aspartic acid	$\text{TiO}_2$ ( <i>synthesis</i> )	Adsorption	[72]
Benzoic acid / benzoate	Aluminum Hydroxide	Adsorption	[73]
Boric acid	Hydrous Ferric Oxide	Adsorption	[74]



Adsorbate or reactant	Material	Study	Ref
		Photo- Oxidation	[75]
	P25	Adsorption	[76]
Catechol	TiO <sub>2</sub> ( <i>synthesis</i> )	Adsorption	
	Cr <sub>2</sub> O <sub>3</sub>	Adsorption	[48]
	MnO <sub>2</sub>	Adsorption	
	Fe <sub>2</sub> O <sub>3</sub>	Adsorption	
4-Chlorocatechol	P25	Adsorption	[77]
Citric acid	Rutile	Adsorption	[64]
	Anatase	Adsorption	[78]
<i>m</i> -Cresol			
<i>o</i> -Cresol	P25	Adsorption	[76]
		Adsorption	
Cyclohexane	UV100	Photo- Oxidation	[33],[79]
Cyclohexanone	TiO <sub>2</sub> ( <i>synthesis</i> )	Adsorption	[80]
Cysteine	P25	Adsorption	[47]
Dextrin	Anatase	Adsorption	[22]
Dicarboxylates		Photo- Oxidation	
$\alpha$ -hydroxydicarboxylates	Fe(III)(hydr)oxides	Oxidation	[81]
Dihydroxyphenylalanine	Rutile	Adsorption	[82]
Dimethylarsinic acid	Iron-(Oxyhydr)Oxides	Adsorption	[70]
E. Coli	P25	Photo- Oxidation	[83]
Ethanol	TiO <sub>2</sub> ( <i>synthesis</i> )	Photo- Oxidation	[84]
	Rutile	Adsorption	[64]
Formic acid	TiO <sub>2</sub> ( <i>synthesis</i> )	Adsorption	[55]

<b>Adsorbate or reactant</b>	<b>Material</b>	<b>Study</b>	<b>Ref</b>
Formate	Rutile	Adsorption	[65]
Fumaric acid	Hematite	Adsorption	[85]
Gallic acid	P25	Photo- Oxidation	[86]
Glutamic acid	TiO <sub>2</sub> ( <i>synthesis</i> )	Adsorption	[72]
Glyoxylic acid	P25	Adsorption	[87]
Isopropyl		Adsorption	
Methylphosphonofluoridate	P25	Photo- Oxidation	[88]
Lactic acid	P25	Adsorption	[66]
Maleic acid	Hematite	Adsorption	[85]
Malonate	Rutile Anatase	Adsorption	[58]
Malonic acid	Au/TiO <sub>2</sub> ( <i>synthesis</i> )	Photo- Oxidation	[89]
	P25		[90]
Nicotinic acid	TiO <sub>2</sub> ( <i>synthesis</i> )	Adsorption	[51]
Nitrate	Al <sub>2</sub> O <sub>3</sub>	Adsorption	[91]
<i>o</i> -Phthalic acid	Hematite	Adsorption	[92]
Oxalate	Anatase Rutile	Adsorption	[58]
	Anatase	Photo- Oxidation	[61]
Oxalic acid	Rutile Anatase	Adsorption	[45]
	Anatase	Adsorption	[11]
Phenol	P25	Photo- Oxidation	[93]
4,4'-Bis(2-	Rutile	Photo-	[94]

Adsorbate or reactant	Material	Study	Ref
sulfostyryl)biphenyl	Anatase	Oxidation	
	Hematite		
	$\delta$ -Alumina		
	Lepidocrocite		
$\beta$ -Picoline	TiO <sub>2</sub> ( <i>synthesis</i> )	Adsorption	[51]
Polyacrylates	Hematite	Adsorption	[95]
1,2-propylene glycol	P25	Photo- Oxidation	[93]
Pyridine	P25	Adsorption	[96]
Pyruvic Acid	P25	Adsorption	[66]
Pyridine-3-carbaldehyde	TiO <sub>2</sub> ( <i>synthesis</i> )		[97]
		adsorption	[51]
Ru-bpy	TiO <sub>2</sub> ( <i>synthesis</i> )	Adsorption	[98]
	Rutile		
Succinate	Anatase	Adsorption	[58]
	Lepidocrocite		
Succinic acid	Hematite	Adsorption	[85]
	P25	Photo- Oxidation	[90]
	TiO <sub>2</sub> ( <i>synthesis</i> )	Photo- Oxidation	[99]
Toluene	P25-TiO <sub>2</sub>	Oxidation	[100]

**Table 1.3.** Selection of previously published ATR-FTIR studies concerning the adsorption and photooxidation of common ligands on metal oxides surfaces.

#### 1.3.4. Concluding remarks

The ATR-FTIR technique offers the chance to obtain novel information concerning interfacial processes *in situ*. This information can be used to explain surface reaction mechanisms. Hence, ATR-FTIR studies are becoming increasingly popular as an

investigative technique and may now be considered as one tool of choice in the field of interfacial chemistry when compared to other techniques, particularly in obtaining data under ambient conditions. This is due to the major advantages of ATR-FTIR spectroscopy such as the *in situ* data collection, as well as the high sensitivity, simplicity, and rapidity of the measurements.

The use of ATR-FTIR in the area of photocatalysis is of great importance since it provides both qualitative and quantitative molecular insight into interfacial processes occurring in the dark (adsorption) and under UV illumination (adsorption/desorption and chemical reactions). The information obtained will often be the key for a deeper understanding of the mechanisms occurring in metal oxide photocatalysis.

### **Acknowledgments**

The present study was performed within the project “Establishment of the Laboratory of Photoactive Nanocomposite Materials” (No. 14.750.31.0016) supported by a Grant from the Government of the Russian Federation. M. Faycal Atitar gratefully acknowledges a scholarship from the DAAD in the Frame of a Sandwich-Program.

## References

1. Hoffmann MR, Martin ST, Choi W, Bahnemann DW. Environmental Applications of Semiconductor Photocatalysis. *Chemical Reviews* 1995;95(1):69–96.
2. Schneider J, Matsuoka M, Takeuchi M, Zhang J, Horiuchi Y, Anpo M, Bahnemann DW. Understanding TiO<sub>2</sub> Photocatalysis: Mechanisms and Materials. *Chemical Reviews* 2014;114: 9919-9986.
3. De Angelis F, Di Valentin C, Fantacci S, Vittadini A, Selloni A. Theoretical Studies on Anatase and Less Common TiO<sub>2</sub> Phases: Bulk, Surfaces, and Nanomaterials. *Chemical Reviews* 2014;114(19):9708–9753.
4. Linsebigler A, Lu G, Jr JY. Photocatalysis on TiO<sub>2</sub> Surfaces: Principles, Mechanisms, and Selected Results. *Chemical Reviews* 1995;95:735–758.
5. Hashimoto K, Irie H, Fujishima A. TiO<sub>2</sub> Photocatalysis: A Historical Overview and Future Prospects. *Japanese Journal of Applied Physics* 2006;44(12):8269–8285.
6. Diebold U. The Surface Science of Titanium Dioxide. *Surface Science Reports* 2003;48(5-8):53–229.
7. Ismail AA, Bahnemann DW. Photochemical Splitting of Water for Hydrogen Production by Photocatalysis: A Review. *Solar Energy Materials and Solar Cells* 2014;128:85–101.
8. Henderson MA. A Surface Science Perspective on TiO<sub>2</sub> Photocatalysis. *Surface Science Reports* 2011;66(6-7):185–297.
9. Fujishima A, Zhang X, Tryk D. TiO<sub>2</sub> Photocatalysis and Related Surface Phenomena. *Surface Science Reports* 2008;63(12):515–582.
10. Montoya JF, Peral J, Salvador P. Comprehensive Kinetic and Mechanistic Analysis of TiO<sub>2</sub> Photocatalytic Reactions According to the Direct–Indirect Model: (I) Theoretical Approach. *Journal of Physical Chemistry C* 2014;118(26):14266–14275.
11. Montoya J, Atitar, FM, Bahnemann DW, Peral J and, Salvador P. Comprehensive Kinetic and Mechanistic Analysis of TiO<sub>2</sub> Photocatalytic Reactions According to the Direct-Indirect (DI) Model: II) Experimental Validation. *Journal of Physical Chemistry C* 2014;28(118):14276–14290.
12. Miranda PB, Shen YR. Liquid Interfaces: A Study by Sum-Frequency Vibrational Spectroscopy. *Journal of Physical Chemistry B* 1999;103(17):3292–307.
13. Drevillon B. Spectroscopic Ellipsometry in the Infrared Range. *Thin Solid Films* 1998;313-314:625–630.

14. Michael JW, Shouzhong Z, Ho YHC. The New Interfacial Ubiquity of Surface-Enhanced Raman Spectroscopy Analytical Chemistry 2000; 72: 38–47.
15. McQuillan AJ. Probing Solid–Solution Interfacial Chemistry with ATR-IR Spectroscopy of Particle Films. Advanced Materials 2001;13(12-13):1034–1038.
16. Simonescu C. Advanced Aspects of Spectroscopy. Akhyar Farrukh M (ed.). InTech 2012. ISBN: 978-953-51-0715-6. Available from : <http://www.intechopen.com/books/advanced-aspects-of-spectroscopy>.
17. Tejedor MI, Anderson MA. In Situ Attenuated Total Reflection Fourier Transform Infrared Studies of the Goethite (α-FeOOH)-Aqueous Solution Interface. Langmuir 1986;2(2):203–210.
18. Hug S, Sulzberger B. In situ Fourier Transform Infrared Spectroscopic Evidence for the Formation of Several Different Surface Complexes of Oxalate on TiO<sub>2</sub> in the Aqueous Phase. Langmuir 1994;18(12):3587–3597.
19. Connor P, Dobson K, McQuillan AJ. New Sol-gel Attenuated Total Reflection Infrared Spectroscopic Method for Analysis of Adsorption at Metal Oxide Surfaces in Aqueous Solutions. Chelation of TiO<sub>2</sub>, ZrO<sub>2</sub>, and Al<sub>2</sub>O<sub>3</sub> Surfaces by Catechol, 8-Quinololinol, and Acetylacetone. Langmuir 1995;(6):4193–4195.
20. Roddick-Lanzilotta A, Connor P, McQuillan AJ. An In Situ Infrared Spectroscopic Study of the Adsorption of Lysine to TiO<sub>2</sub> from an Aqueous Solution. Langmuir 1998;(17):6479–6484.
21. Roddick-Lanzilotta A, McQuillan AJ. An In Situ Infrared Spectroscopic Investigation of Lysine Peptide and Polylysine Adsorption to TiO<sub>2</sub> from Aqueous Solutions. Journal of Colloid and Interface Science 1999;217(1):194–202.
22. Beaussart A, Petrone L, Mierczynska-Vasilev A, McQuillan AJ, Beattie DA. In Situ ATR FTIR Study of Dextrin Adsorption on Anatase TiO<sub>2</sub>. Langmuir 2012;28(9):4233–4240.
23. Mendive CB, Bredow T, Blesa MA, Bahnemann DW. ATR-FTIR Measurements and Quantum Chemical Calculations Concerning the Adsorption and Photoreaction of Oxalic Acid on TiO<sub>2</sub>. Physical Chemistry Chemical Physics PCCP 2006;8(27):3232–3247.
24. Mendive CB, Bredow T, Feldhoff A, Blesa MA, Bahnemann DW. Adsorption of Oxalate on Anatase (100) and Rutile (110) Surfaces in Aqueous Systems: Experimental Results vs. Theoretical Predictions. Physical Chemistry Chemical Physics 2009;11(11):1794–1808.
25. Stuart B. Infrared Spectroscopy : Fundamentals and Applications. Wiley 2004.

26. Hind AR, Bhargava SK, McKinnon A. At the Solid/Liquid Interface: FTIR/ATR — The Tool of Choice. *Advances in Colloid and Interface Science* 2001;93(1-3):91–114.
27. Smith BC. *Fundamentals of Fourier Transform Infrared Spectroscopy (Second Edition)*. CRC Press Taylor & Francis Group 2011.
28. Harrick NJ. Surface Chemistry from Spectral Analysis of Totally Internally Reflected Radiation. *Journal of Physical Chemistry* 1960;64(9):1110–1114.
29. Fahrenfort J. Attenuated Total Reflection : A New Principle for the Production of Useful Infrared Reflection Spectra of Organic Compounds. *Spectrochimica Acta* 1961;17(7):698–709.
30. Mudunkotuwa IA, Al Minshid A, Grassian VH. ATR-FTIR Spectroscopy as a Tool to Probe Surface Adsorption on Nanoparticles at the Liquid-Solid Interface in Environmentally and Biologically Relevant Media. *Analyst* 2014;139(5):870–881.
31. Khoshhesab ZM. *Infrared Spectroscopy - Materials Science, Engineering and Technology*. Theophile T (ed). InTech 2012. ISBN:978-953-51-0537-4. Available from: <http://www.intechopen.com/books/infrared-spectroscopy-materials-science-engineering-and-technology/fundamental-of-reflectance-ir-spectroscopy>
32. Vigano C, Ruyschaert JM, Goormaghtigh E. Sensor Applications of Attenuated Total Reflection Infrared Spectroscopy. *Talanta* 2005;65(5):1132–1142.
33. Almeida AR, Moulijn JA, Mul G. In Situ ATR-FTIR Study on the Selective Photo-oxidation of Cyclohexane over Anatase TiO<sub>2</sub>. *Journal of Physical Chemistry C* 2008;112(5):1552–1561.
34. Bourikas K, Kordulis C, Lycourghiotis A. Titanium Dioxide (Anatase and Rutile): Surface Chemistry, Liquid-Solid Interface Chemistry, and Scientific Synthesis of Supported Catalysts. *Chemical Reviews* 2014;114:9754–9823.
35. Hodgson A, Haq S. Water Adsorption and the Wetting of Metal Surfaces. *Surface Science Reports* 2009;64(9):381–451.
36. Henderson M. The Interaction of Water with Solid Surfaces: Fundamental Aspects Revisited. *Surface Science Reports* 2002;46(1-8):1–308.
37. Mendive CB, Hansmann D, Bredow T, Bahnemann D. New Insights into the Mechanism of TiO<sub>2</sub> Photocatalysis: Thermal Processes beyond the Electron–Hole Creation. *Journal of Physical Chemistry C* 2011;115(40):19676–85.
38. Takeuchi M, Martra G, Coluccia S, Anpo M. Investigations of the Structure of H<sub>2</sub>O Clusters Adsorbed on TiO<sub>2</sub> Surfaces by Near-Infrared Absorption Spectroscopy. *Journal of Physical Chemistry B* 2005;109(15):7387–7391.

39. Warren D, McQuillan AJ. Influence of Adsorbed Water on Phonon and UV-Induced IR Absorptions of TiO<sub>2</sub> Photocatalytic Particle Films. *Journal of Physical Chemistry B* 2004;19373–19379.
40. Almeida AR, Calatayud M, Tielens F, Moulijn JA, Mul G. Combined ATR-FTIR and DFT Study of Cyclohexanone Adsorption on Hydrated TiO<sub>2</sub> Anatase Surfaces. *Journal of Physical Chemistry C* 2011;115(29):14164–14172.
41. Li G, Li L, Boerio-Goates J, Woodfield BF. High Purity Anatase TiO<sub>2</sub> Nanocrystals: Near Room-Temperature Synthesis, Grain Growth Kinetics, and Surface Hydration Chemistry. *Journal of American Chemical Society* 2005;127(24):8659–8666.
42. Rubasinghege G, Grassian VH. Role(s) of Adsorbed Water in the Surface Chemistry of Environmental Interfaces. *Chemical Communications (Cambridge)* 2013;49(30):3071–3094.
43. Uosaki K, Yano T, Nihonyanagi S. Interfacial Water Structure at As-prepared and UV-induced Hydrophilic TiO<sub>2</sub> Surfaces Studied by Sum Frequency Generation Spectroscopy and Quartz Crystal Microbalance. *Journal of Physical Chemistry B* 2004;108(50):19086–19088.
44. Sakai N, Fujishima A, Watanabe T, Hashimoto K. Quantitative Evaluation of the Photoinduced Hydrophilic Conversion Properties of TiO<sub>2</sub> Thin Film Surfaces by the Reciprocal of Contact Angle. *Journal of Physical Chemistry B* 2003;107(4):1028–1035.
45. Young AG, McQuillan AJ. Adsorption/Desorption Kinetics from ATR-IR Spectroscopy. Aqueous Oxalic Acid on Anatase TiO<sub>2</sub>. *Langmuir* 2009;25(6):3538–3548.
46. Dobson KD, McQuillan AJ. In Situ Infrared Spectroscopic Analysis of the Adsorption of Aliphatic Carboxylic Acids to TiO<sub>2</sub>, ZrO<sub>2</sub>, Al<sub>2</sub>O<sub>3</sub>, and Ta<sub>2</sub>O<sub>5</sub> from Aqueous Solutions. *Spectrochimica Acta Part A Molecular and Biomolecular Spectroscopy* 1999;55(7-8):1395–1405.
47. Begonja S, Rodenas L, Borghi EB, Morando PJ. Adsorption of Cysteine on TiO<sub>2</sub> at Different pH Values: Surface Complexes Characterization by FTIR-ATR and Langmuir Isotherms Analysis. *Colloids and Surfaces A: Physicochemical and Engineering Aspects* 2012;403:114–120.
48. Gulley-Stahl H, Hogan PA, Schmidt WL, Wall SJ, Buhrlage A, Bullen HA. Surface Complexation of Catechol to Metal Oxides: An ATR-FTIR, Adsorption, and Dissolution Study. *Environmental Science and Technology* 2010;44(11):4116–4121.
49. Popova G. In Situ FTIR Study of Pyridine-3-carbaldehyde Adsorption on TiO<sub>2</sub> (Anatase) and V-Ti-O Catalyst. *Reaction Kinetics and Catalysis Letters* 2004;83(2):353–360.



50. Chernobay GB, Chesalov YA, Baltakhinov VP, Popova GY, Andrushkevich TV. In Situ FTIR Study of  $\beta$ -picoline Transformations on V–Ti–O Catalysts. *Catalysis Today* 2011;164(1):58–61.
51. Chesalov YA, Chernobay GB, Andrushkevich TV. FTIR Study of the Surface Complexes of  $\beta$ -picoline, 3-pyridine-carbaldehyde and Nicotinic acid on Sulfated TiO<sub>2</sub> (Anatase). *Journal of Molecular Catalysis A: Chemical* 2013;373:96–107.
52. Koczoń P, Dobrowolski JC, Lewandowski W, Mazurek AP. Experimental and Theoretical IR and Raman Spectra of Picolinic, Nicotinic and Isonicotinic Acids. *Journal of Molecular Structure* 2003;655(1):89–95.
53. Nakamoto K. *Infrared and Raman Spectra of Inorganic and Coordination Compounds: Part B: Applications in Coordination, Organometallic, and Bioinorganic Chemistry*. 6th edition. Wiley 2008.
54. Atitar MF, Dillert R, Bahnemann DW. An In Situ ATR-FTIR Study of the Adsorption of Imazapyr Herbicide onto TiO<sub>2</sub> Surface. Unpublished Results.
55. Nanayakkara CE, Dillon JK, Grassian VH. Surface Adsorption and Photochemistry of Gas-Phase Formic Acid on TiO<sub>2</sub> Nanoparticles: The Role of Adsorbed Water in Surface Coordination, Adsorption Kinetics, and Rate of Photoproduct Formation. *Journal of Physical Chemistry C* 2014;118(44):25487–25495.
56. Petrone L, McQuillan AJ. Alginate Ion Adsorption on a TiO<sub>2</sub> Particle Film and Interactions of Adsorbed Alginate with Calcium Ions Investigated by Attenuated Total Reflection Infrared (ATR-IR) Spectroscopy. *Applied Spectroscopy* 2011;65(10):1162–1169.
57. Qu Q, Geng H, Peng R, Cui Q, Gu X, Li F, Wang M. Chemically Binding Carboxylic Acids onto TiO<sub>2</sub> Nanoparticles with Adjustable Coverage by Solvothermal Strategy. *Langmuir* 2010;26(12):9539–46.
58. Hug SJ, Bahnemann DW. Infrared Spectra of Oxalate, Malonate and Succinate Adsorbed on the Aqueous Surface of Rutile, Anatase and Lepidocrocite Measured with In Situ ATR-FTIR. *Journal of Electron Spectroscopy and Related Phenomena* 2006;150(2-3):208–219.
59. Vittadini A, Selloni A, Rotzinger FP, Grätzel M. Formic Acid Adsorption on Dry and Hydrated TiO<sub>2</sub> Anatase (101) Surfaces by DFT Calculations. *Journal of Physical Chemistry B* 2000;104(101):1300–1306.
60. Mendive CB, Blesa MA, Bahnemann DW. The Adsorption and Photodegradation of Oxalic Acid at the TiO<sub>2</sub> Surface. *Water Science and Technology* 2005;55(12):139–145.
61. Mendive CB, Bredow T, Schneider J, Blesa M, Bahnemann DW. Oxalic Acid at the TiO<sub>2</sub>/Water Interface under UV(A) Illumination: Surface Reaction Mechanisms. *Journal of Catalysis* 2015;322:60–72.

62. Mendive CB, Bahnemann DW, Blesa MA. Microscopic Characterization of the Photocatalytic Oxidation of Oxalic Acid Adsorbed onto TiO<sub>2</sub> by FTIR-ATR. *Catalysis Today* 2005;101(3-4):237–244.
63. Mendive CB, Bredow T, Feldhoff A, Blesa MA, Bahnemann DW. Adsorption of Oxalate on Rutile Particles in Aqueous Solutions: A Spectroscopic, Electron-Microscopic and Theoretical Study. *Physical Chemistry Chemical Physics PCCP* 2008;10:1960–1974.
64. Ojamäe L, Aulin C, Pedersen H, Käll P-O. IR and Quantum-Chemical Studies of Carboxylic Acid and Glycine Adsorption on Rutile TiO<sub>2</sub> Nanoparticles. *Journal of Colloid and Interface Science* 2006;296(1):71–78.
65. Rotzinger FP, Kesselman-Truttmann JM, Hug SJ, Shklover V, Grätzel M. Structure and Vibrational Spectrum of Formate and Acetate Adsorbed from Aqueous Solution onto the TiO<sub>2</sub> Rutile (110) Surface. *Journal of Physical Chemistry B* 2004;108(16):5004–5017.
66. Chen Y, Lin Y-F, Peng Z, Lin J. Transmission FT-IR Study on the Adsorption and Reactions of Lactic Acid and Poly(lactic Acid) on TiO<sub>2</sub>. *Journal of Physical Chemistry C* 2010;114(41):17720–17727.
67. Kirwan LJ, Fawell PD, Van Bronswijk W. In Situ FTIR-ATR Examination of Poly(acrylic Acid) Adsorbed onto Hematite at Low pH. *Langmuir* 2003;19(14):5802–5807.
68. Martra G, Horikoshi S, Anpo M, Coluccia S, Hidaka H. FTIR Study of Adsorption and Photodegradation of L- $\alpha$ -alanine on TiO<sub>2</sub> Powder. *Research on Chemical Intermediates* 2002;28(4):359–371.
69. Dolamic I, Bürgi T. In Situ ATR-IR Study on the Photocatalytic Decomposition of Amino Acids over Au/TiO<sub>2</sub> and TiO<sub>2</sub>. *Journal of Physical Chemistry C* 2011;115(5):2228–2234.
70. Mitchell W, Goldberg S, Al-Abadleh HA. In Situ ATR-FTIR and Surface Complexation Modeling Studies on the Adsorption of Dimethylarsinic Acid and p-Arsanilic Acid on Iron-(oxyhydr)Oxides. *Journal of Colloid and Interface Science* 2011;358(2):534–540.
71. Depalma S, Cowen S, Hoang T, Al-Abadleh HA. Adsorption Thermodynamics of p-Arsanilic Acid on Iron (Oxyhydr)Oxides: In-Situ ATR-FTIR Studies. *Environmental Science and Technology* 2008;42(6):1922–1927.
72. Roddick-Lanzilotta A, McQuillan AJ. An In Situ Infrared Spectroscopic Study of Glutamic Acid and of Aspartic Acid Adsorbed on TiO<sub>2</sub>: Implications for the Biocompatibility of Titanium. *Journal of Colloid and Interface Science* 2000;227(1):48–54.
73. Guan X, Chen G, Shang C. ATR-FTIR and XPS Study on the Structure of Complexes Formed upon the Adsorption of Simple Organic Acids on

- Aluminum Hydroxide. *Journal of Environmental Science* 2007;19(4):438–443.
74. Peak D, Luther GW, Sparks DL. ATR-FTIR Spectroscopic Studies of Boric Acid Adsorption on Hydrous Ferric Oxide. *Geochimica et Cosmochimica Acta* 2003;67(14):2551–2560.
75. Araujo PZ, Mendive CB, Rodenas LA. G, Morando PJ, Regazzoni AE, Blesa MA, Bahnemann DW. FT-IR-ATR as a Tool to Probe Photocatalytic Interfaces. *Colloids and Surfaces A: Physicochemical and Engineering Aspects* 2005;265(1-3):73–80.
76. Araña J, Pulido Melián E, Rodríguez López VM, Peña Alonso A, Doña Rodríguez JM, González Díaz O, Perez Pena J. Photocatalytic Degradation of Phenol and Phenolic Compounds Part I. Adsorption and FTIR Study. *Journal of Hazardous Materials* 2007;146(3):520–528.
77. Martin ST, Kesselman JM, Park DS, Lewis NS, Hoffmann MR. Surface Structures of 4-Chlorocatechol Adsorbed on Titanium Dioxide. *Environmental Science and Technology* 1996;30(8):2535–2542.
78. Mudunkotuwa IA, Grassian VH. Citric Acid Adsorption on TiO<sub>2</sub> Nanoparticles in Aqueous Suspensions at Acidic and Circumneutral pH: Surface Coverage, Surface Speciation, and Its Impact on Nanoparticle-Nanoparticle Interactions. *Journal of American Chemical Society*. 2010;132(42):14986–14994.
79. Hernández-Alonso MD, Almeida AR, Moulijn JA, Mul G. Identification of the Role of Surface Acidity in the Deactivation of TiO<sub>2</sub> in the Selective Photo-Oxidation of Cyclohexane. *Catalysis Today* 2009;143(3-4):326–333.
80. Almeida A, Moulijn J, Mul G. Photocatalytic Oxidation of Cyclohexane over TiO<sub>2</sub>: Evidence for a Mars–Van Krevelen Mechanism. *Journal of Physical Chemistry C* 2011;1330–1338.
81. Borer P, Hug SJ. Photo-Redox Reactions of Dicarboxylates and  $\alpha$ -Hydroxydicarboxylates at the Surface of Fe(III)(hydr)Oxides Followed with in Situ ATR-FTIR Spectroscopy. *Journal of Colloid and Interface Science* 2014;416:44–53.
82. Bahri S, Jonsson CM, Jonsson CL, Azzolini D, Sverjensky DA, Hazen RM. Adsorption and Surface Complexation Study of L-DOPA on Rutile ( $\alpha$ -TiO<sub>2</sub>) in NaCl Solutions. *Environmental Science and Technology* 2011;45(9):3959–3966.
83. Nadtochenko VA, Rincon AG, Stanca SE, Kiwi J. Dynamics of E.coli Membrane Cell Peroxidation During TiO<sub>2</sub> Photocatalysis Studied by ATR-FTIR Spectroscopy and AFM Microscopy. *Journal of Photochemical and Photobiological Science A Chemistry* 2005;169(2):131–137.

84. Tan J, Yang L, Kang Q, Cai Q. In Situ ATR-FTIR and UV-Visible Spectroscopy Study of Photocatalytic Oxidation of Ethanol over TiO<sub>2</sub> Nanotubes. *Analytical Letters* 2011;44(6):1114–1125.
85. Hwang YS, Lenhart JJ. Adsorption of C<sub>4</sub>-dicarboxylic Acids at the Hematite/Water Interface. *Langmuir* 2008;24(24):13934–13943.
86. Araujo PZ, Morando PJ, Martínez E, Blesa MA. Time Evolution of Surface Speciation During Heterogeneous Photocatalysis: Gallic Acid on Titanium Dioxide. *Applied Catalysis B Environmental* 2012;125:215–221.
87. Ekström GN, McQuillan AJ. In Situ Infrared Spectroscopy of Glyoxylic Acid Adsorption and Photocatalysis on TiO<sub>2</sub> in Aqueous Solution. *Journal of Physical Chemistry B* 1999;103(48):10562–10565.
88. Hirakawa T, Sato K, Komano A, Kishi S, Nishimoto CK, Mera N, Kugishima M, Sano T, Ichinose H, Negishi N, Seto Y, Takeuchi K. Experimental Study on Adsorption and Photocatalytic Decomposition of Isopropyl Methylphosphonofluoridate at Surface of TiO<sub>2</sub> Photocatalyst. *Journal of Physical Chemistry C* 2010;114(5):2305–2314.
89. Hu X, Burgi T. Photoinduced Electron Transfer and Photodegradation of Malonic Acid at Au/TiO<sub>2</sub> Investigated by In Situ ATR-IR Spectroscopy. *Applied Catalysis A General* 2012;449:139–144.
90. Dolamic I, Burgi T. Photocatalysis of Dicarboxylic Acids over TiO<sub>2</sub>: An In Situ ATR-IR Study. *Journal of Catalysis* 2007;248(2):268–276.
91. Baltrusaitis J, Schuttlefield J, Jensen JH, Grassian VH. FTIR Spectroscopy Combined with Quantum Chemical Calculations to Investigate Adsorbed Nitrate on Aluminium Oxide Surfaces in the Presence and Absence of Co-adsorbed Water. *Physical Chemistry Chemical Physics PCCP* 2007;9(36):4970–4980.
92. Hwang YS, Liu J, Lenhart JJ, Hadad CM. Surface Complexes of Phthalic Acid at the Hematite/Water Interface. *Journal of Colloid and Interface Science* 2007;307(1):124–134.
93. Araña J, Tello Rendón E, Doña Rodríguez JM, Herrera Melián JA, González Díaz O, Pérez Peña J. High Concentrated Phenol and 1,2-propylene Glycol Water Solutions Treatment by Photocatalysis. *Applied Catalysis B Environmental* 2001;30(1-2):1–10.
94. Kesselman-Truttman JM, Hug SJ. Photodegradation of 4,4'-Bis(2-sulfostyryl)biphenyl (DSBP) on Metal Oxides Followed by In Situ ATR-FTIR Spectroscopy. *Environmental Science and Technology* 1999;33(18):3171–3176.
95. Bronswijk W Van, Kirwan LJ, Fawell PD. In Situ Adsorption Densities of Polyacrylates on Hematite Nano-particle Films as Determined by ATR-FTIR Spectroscopy. *Vibrational Spectroscopy* 2006;41(2):176–181.

96. Green IX, Buda C, Zhang Z, Neurock M, Yates JT. IR Spectroscopic Measurement of Diffusion Kinetics of Chemisorbed Pyridine through TiO<sub>2</sub> Particles. *Journal of Physical Chemistry C* 2010;114(39):16649–16659.
97. Popova GY, Chesalov YA, Andrushkevich TV. In situ FTIR Study of Pyridine-3-carbaldehyde Adsorption on TiO<sub>2</sub> (Anatase) and V-Ti-O Catalyst. *Reaction Kinetics and Catalysis Letters*. 2004;83(2):353–360.
98. Pe C, Kador L, Peng B, Thelakkat M. Characterization of the Adsorption of Ru-bpy Dyes on Mesoporous TiO<sub>2</sub> Films with UV - Vis , Raman , and FTIR Spectroscopies. *Journal of Physical Chemistry B* 2006;110(17):8723–8730.
99. Maira A, Coronado J, Augugliaro V, Yeung K, Conesa J, Soria J. Fourier Transform Infrared Study of the Performance of Nanostructured TiO<sub>2</sub> Particles for the Photocatalytic Oxidation of Gaseous Toluene. *Journal of Catalysis* 2001;202(2):413–420.
100. Lin H, Long J, Gu Q, Zhang W, Ruan R, Li Z, Wang X. In Situ IR Study of Surface Hydroxyl Species of Dehydrated TiO<sub>2</sub>: Towards Understanding Pivotal Surface Processes of TiO<sub>2</sub> Photocatalytic Oxidation of Toluene. *Physical Chemistry Chemical Physics* 2012;14(26):9468–9474.

#### **1.4. Scope of the Thesis**

The introduction section contains only few examples of the topics under debate in the field of photocatalysis. However, many additional issues related to these topics still remain unclear or are matter of discussion.

The aim of this PhD thesis is to elucidate some relevant features of the photocatalytic degradation mechanism of organic pollutants in water. Although this topic has been widely studied, there is still space for new fundamental interpretations.

The main objective is to shed some light on the important process occurring at solid-liquid interfaces because interactions at these interfaces are considered to be the main key for the photocatalytic process. These interactions are influenced by several parameters. From the mechanistic point of view, the type and mode of the adsorption, the semiconductor surface charges, as well as the intermediate species (i.e., surface complexes) play a major role in the adsorption and the photocatalytic degradation. Here, the goal is to draw attention to the fact that understanding the surface interactions between the photocatalyst surface and the model organic compound is a primary step for the understanding of the overall process either in the dark or under illumination.

On the other hand, and from the kinetic point of view, the role of the adsorption in the kinetics of the photocatalytic degradation is also still a matter of discussion. The Langmuir-Hinshelwood model, when it applies, gives insight into the mechanism of the photocatalytic process. However, to the best of our knowledge, this model takes only the adsorption isotherms of the two adsorbates involved into account. The kinetics of the adsorption and their correlation with the kinetics of the photocatalytic reaction occurring either at/or near the surface of the semiconductor are still unclear. Hence, the objective of this work is to study the kinetics of the adsorption as well as the photocatalytic reaction to figure out whether they correlate. Furthermore, this knowledge should provide an insight on the role of the adsorption process on the photocatalytic degradation mechanism of the organic pollutants.

The photocatalytic performance is also influenced by the photocatalyst. Besides the understanding of the mechanism, one of the aims of this thesis is to synthesize mesoporous TiO<sub>2</sub> materials as well as to focus on the relationship between the effect of the calcination temperature, the phase transformation, and the surface area of the synthesized mesoporous photocatalyst.

The above-mentioned issues will contribute to a new understanding of photocatalytic reactions using alternative approaches and interpretations as compared with the conventional kinetic models. All these issues have been studied at the TiO<sub>2</sub>/Water interfaces. The model organic pollutant chosen for these issues is a herbicide from the imidazolinone family (i.e., Imazapyr). Furthermore the commercial type Evonik Degussa Aeroxide TiO<sub>2</sub> P25 was used as the photocatalyst.



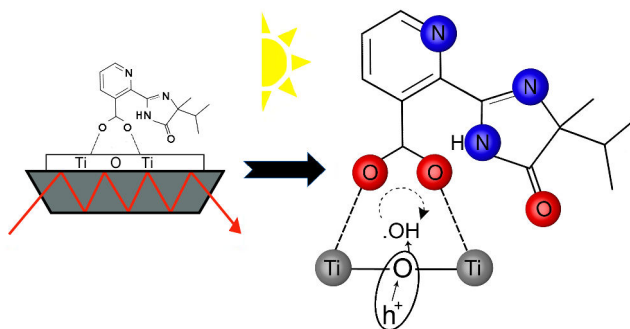


## Chapter 2

### Surface Interactions between Imazapyr and the TiO<sub>2</sub> Surface: An *in Situ* ATR-FTIR Study

M. Faycal Atitar, Ralf Dillert, and Detlef W. Bahnemann

Published in Journal of Physical Chemistry C, 2017, 121(8), pp 4293-4303



## 2.1. Abstract

Herein we present a detailed report concerning the mode of surface interactions between imazapyr, 2-(4-methyl-5-oxo-4-propan-2-yl-1*H*-imidazol-2-yl)pyridine-3-carboxylic acid, and the TiO<sub>2</sub> surface. Adsorption of imazapyr onto a TiO<sub>2</sub> film has been investigated *in situ* using attenuated total reflection Fourier transform infrared (ATR-FTIR) spectroscopy. The adsorption of imazapyr is pH dependent and occurs through electrostatic interactions and chemical bonding between the probe molecule and the charged TiO<sub>2</sub> surface involving different functional groups of imazapyr species present in solution. Based upon the ATR-FTIR spectra of imazapyr recorded at different pH values, it is concluded that the adsorption of imazapyr onto the TiO<sub>2</sub> surface is favored at pH values below the TiO<sub>2</sub>'s point of zero charge. Upon adsorption, the carboxylic acid group of imazapyr binds at surface Ti(IV) centers mainly as a bridging ligand at pH < p*H*<sub>zpc</sub>. With increasing pH values, the binding of imazapyr to the surface becomes less favorable. Furthermore, evidence is presented for additional contributions of other binding modes. Attempting to understand the influence of these interactions on the initial photocatalytic degradation rate of imazapyr, the results of this study confirm experimentally the aspects of the photocatalytic oxidation mechanism of imazapyr discussed previously on the basis of semiempirical calculations [Osajima *et al.* Monatshefte für Chemie - Chem. Mon. **2007**, 139, 7–11, and Carrier *et al.* Appl. Catal. B Environ. **2006**, 65, 11–20].

## 2.2. Introduction

According to several proposed photocatalytic mechanisms, the binding mode of specific molecules to the photocatalyst surface is affecting their light-induced transformation.<sup>1–4</sup> The interaction of the target molecule, acting as either electron donor or acceptor, with the surface of a semiconducting nanomaterial is determined by the surface chemistry intrinsic to the respective class of compounds.<sup>5</sup> The effect of the adsorption of organic substrate molecules onto the photocatalyst surface on the former's photocatalytic degradation rate was the topic of several publications.<sup>6–8</sup> Kormann *et al.* determined the photocatalytic degradation rates of trichloroacetic acid and chloroethylammonium in the presence of anatase TiO<sub>2</sub>, being the photocatalyst, and varied the pH of the aqueous suspensions. Supported by the results of theoretical calculations these authors discussed the influence of the binding

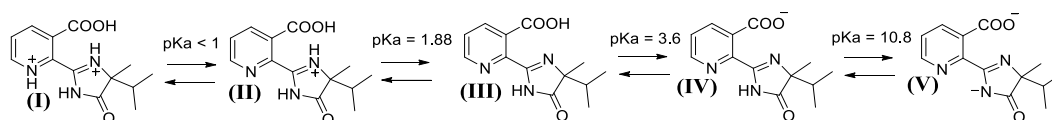
mode as well as of the concentration of the surface complexes on the photocatalytic degradation rates as a function of the pH. They concluded that the pH-dependent adsorption of the probe molecules onto the TiO<sub>2</sub> particles determines their photoreactivity.<sup>9</sup>

It is well-known that the surface of TiO<sub>2</sub> is positively charged at pH values below the point of zero charge (pH<sub>pzc</sub>) of the TiO<sub>2</sub> sample, neutral at the pH<sub>pzc</sub>, and negatively charged at pH values above the pH<sub>pzc</sub>. The pH<sub>pzc</sub> of the widely used photocatalyst Evonik Aeroxide TiO<sub>2</sub> P25 is reported to be in the range of 6.25 to 6.9.<sup>5,10</sup> Furthermore, in both the anatase and the rutile structure, the Ti<sup>4+</sup> cation is surrounded by four O<sup>2-</sup> anions at the surface.

Imazapyr, 2-(4-methyl-5-oxo-4-propan-2-yl-1*H*-imidazol-2-yl)pyridine-3-carboxylic acid, being a heteroaromatic molecule, is a nonselective herbicide which belongs to the imidazolinone family.<sup>11</sup> The photocatalytic oxidation of imazapyr has been studied previously using commercial TiO<sub>2</sub><sup>12-15</sup> as well as newly synthesized mesoporous TiO<sub>2</sub> materials.<sup>16,17</sup>

Imazapyr dissolved in water presents five distinct species depending on the pH of the solution (Scheme 2.1).<sup>15</sup> According to this scheme depending on the pH of the suspension, different types of interactions between the probe molecule and the charged TiO<sub>2</sub> surface are expected.

**Scheme 2.1.** Different Forms of Imazapyr As a Function of the pH.



At  $1.9 < \text{pH} < 3.6$  the neutral form of imazapyr (III in Scheme 2.1.) will be the main species interacting with the positively charged TiO<sub>2</sub> surface. At  $3.6 < \text{pH} < \text{pH}_{\text{pzc}}$  (TiO<sub>2</sub>) the deprotonated and thus negatively charged imazapyr (IV) is interacting with the positive TiO<sub>2</sub> surface, while at  $\text{pH}_{\text{pzc}}$  (TiO<sub>2</sub>) <  $\text{pH} < 10.8$  the negatively charged imazapyr molecule (IV) is interacting with a TiO<sub>2</sub> surface which is also negatively charged. Therefore, strong electrostatic attraction or repulsion, respectively, is expected to affect the amount of imazapyr adsorbed onto the TiO<sub>2</sub> surface, as well as the binding mode between this organic probe molecule and the oxide surface, resulting in pH-dependent photocatalytic reaction rates during the UV(A) irradiation of the suspension.

The characterization of the adsorption mode of organic molecules onto metal oxide surfaces in liquid media is often performed *in situ* by means of attenuated total reflectance Fourier transform infrared (ATR-FTIR) spectroscopy.<sup>18,19</sup> This technique has been extensively used to investigate the adsorption of several probe molecules at the TiO<sub>2</sub> surface.<sup>2,20-26</sup> The molecular information acquired from this technique allows the determination of the adsorption mode, including conformational and structural changes of the coordinated adsorbate.<sup>18,27</sup>

The interactions of the different functional groups of imazapyr with the TiO<sub>2</sub> surface as well as varying amounts of adsorbed imazapyr species are expected to depend on the pH of the suspension being in contact with the TiO<sub>2</sub> layer. Furthermore, the occurrence of both chemical and electrostatic interactions between the TiO<sub>2</sub> surface and the probe molecule is possible. Hence, the aim of the current work is to elucidate the mode of interaction between imazapyr and the TiO<sub>2</sub> surface in the dark using ATR-FTIR spectroscopy. The information obtained from this technique will provide a deeper understanding of the mechanism of the photocatalytic oxidation of imazapyr. Hence, photocatalytic experiments and an *in situ* ATR-FTIR investigation of the imazapyr adsorption on Evonik Aeroxide TiO<sub>2</sub>-P25 have been performed varying the pH of the suspension.

### 2.3. Materials and Methods

**Materials.** The photocatalyst employed in this work was Evonik Aeroxide TiO<sub>2</sub> P25 (mainly anatase with a rutile content of ca. 20%, a primary particle size of around 21 nm, and a BET surface area of 50 m<sup>2</sup> g<sup>-1</sup>). It was used as received. All other reagents were of analytical grade and were used without any previous purification. The water used in all experiments was deionized water (resistivity = 18.2 MΩ cm) collected from a Sartorius Arium 611 deionizer.

**Photocatalytic Degradation Experiments.** An amount of 625 mg of the TiO<sub>2</sub> powder was dispersed in 250 mL of an aqueous KClO<sub>4</sub> solution (10 mmol L<sup>-1</sup>, KClO<sub>4</sub> was added to keep the ionic strength of the solution constant throughout the experimental run<sup>28</sup>) by sonication and shaking in an ultrasonic bath for 15 min resulting in a catalyst concentration  $C_{\text{cat}} = 2.5 \text{ g L}^{-1}$  which has been found to yield the highest photocatalytic degradation rates (details will be published elsewhere).

Subsequently, an aliquot from an aqueous stock solution of imazapyr (7.65 mmol L<sup>-1</sup>) was added to reach the desired initial imazapyr concentration of 0.08 mmol L<sup>-1</sup>. The pH value of the suspension was adjusted either using HNO<sub>3</sub> or KOH standard solutions. The suspensions were stirred overnight in a borosilicate glass beaker at 300 rpm to attain adsorption equilibrium. Photocatalytic degradation experiments were conducted in the “blackbody reactor” described by Emeline *et al.*<sup>29</sup> This reactor consists of a beaker containing the mechanically stirred TiO<sub>2</sub> suspension. The light beam is directed by an optical fiber from the light source (365 nm LED OEM module from OMICRON Lasertechnik) through a small area inlet into an inner quartz cavity located in the center of the beaker.

**HPLC Analysis.** Sample analysis from the study of the photocatalytic degradation of imazapyr was carried out employing a high performance liquid chromatography (HPLC) system composed of a LCP 4100 ECOM Tech Lab pump and a LCD 2084 ECOM Techlab UV Detector adjusted to 254 nm. A Kinetex 2.6 μm C18 100 Å column from Phenomenex (150 × 4.6 mm) working at room temperature was the stationary phase, and a mixture of acetonitrile and water (40:60 %v/v) adjusted to pH 3 by adding H<sub>3</sub>PO<sub>4</sub> was used as a mobile phase. With the flow rate kept constant at 0.8 mL min<sup>-1</sup> the peak of imazapyr was observed at a retention time of 4.60 min. A calibration curve (R<sup>2</sup>=0.999) was obtained by measuring 6 different imazapyr concentrations in the range between 0 and 0.08 mmol L<sup>-1</sup>. Before illumination, 1 mL of the previously equilibrated suspension was analyzed by HPLC to determine the initial equilibrium concentration of the probe molecule. During illumination samples were taken at regular time intervals and were analyzed after filtration through a Millipore syringe filter.

**ATR-FTIR Measurements.** The spectrometer used in this study was a Bruker IFS 66 infrared spectrometer equipped with a deuterated triglycine sulfate (DTGS) detector. The ATR accessory used was a Pike Technologies horizontal unit with demountable plate containing a removable ZnSe ATR crystal set at 45° angle of incidence, thus allowing nine upper face reflections. The dimensions of the ZnSe ATR element were 6.8 × 72 mm<sup>2</sup> on the horizontal probe face with a thickness of 4 mm. The wavenumber range was 4000–800 cm<sup>-1</sup> with a spectral resolution of 4 cm<sup>-1</sup>.

To avoid spectral interferences due to material degradation, polyoxymethylene (POM) and borosilicate glass, which both are chemically resistant to the employed solutions, were employed to construct the solution compartment and the reactor windows, respectively.

The closed solution compartment is attached to the upper part of the ZnSe ATR crystal to ensure continuous flow of the solution across the surface of the TiO<sub>2</sub>-coated crystal. This setup allows the control of experimental parameters such as pH and ionic strength of the bulk adsorbent during the experiment (Supporting Information Figure S2.1.). More details are given in ref<sup>25</sup>.

The TiO<sub>2</sub> layer on the ATR crystal was prepared according to a coating procedure previously published by Hug and Sulzberger.<sup>26</sup> Specifically, an aliquot of 400  $\mu\text{L}$  of an aqueous 5.75  $\text{g L}^{-1}$  TiO<sub>2</sub> suspension was placed on the surface of the ZnSe ATR crystal. This small volume was simply spread by manually balancing the unit. This thin suspension layer was dried at ambient temperature in a desiccator. The thus obtained coverage of the final dry particle layer was 2.3  $\text{g m}^{-2}$ , and the layer appeared homogeneous under visual inspection. In the original preparation by Hug and Sulzberger,<sup>26</sup> atomic force microscopy (AFM) measurements of the layers with a coverage of 2.3  $\text{g m}^{-2}$  were reported to exhibit a thickness of  $1.7 \pm 0.3 \mu\text{m}$ .

The interferometer and the infrared light path were constantly purged with argon and the sampling chamber with nitrogen. The final spectra represent the average of 325 scans. To minimize spectral interference resulting from the presence of a varying amount of water vapor and carbon dioxide present in the main body of the instrument “reference spectra” have been subtracted from the sample single-channel spectra (atmospheric compensation). After measuring the ATR-FTIR spectrum of the TiO<sub>2</sub>-coated ATR crystal (as background spectrum) the surface was equilibrated with an aqueous solution free of imazapyr (blank solution). The pH of the blank solution was fixed and carefully kept constant at the desired pH value with a programmed dosing unit. The ionic strength of the aqueous phase was adjusted by adding KClO<sub>4</sub> to obtain a concentration of 10  $\text{mmol L}^{-1}$ . The solution compartment was filled with 10 mL of the blank solution, and then a background spectrum was collected. Afterward the solvent was substituted by 10 mL of the solution containing the probe molecule imazapyr. Spectra were collected in 10–30 min intervals over a total period of 180 min. In preliminary studies, solution phase spectra were collected in the absence of TiO<sub>2</sub> film at different concentrations, with peaks only being observed at

imazapyr concentrations above 4 mmol L<sup>-1</sup>. To avoid any solution phase contribution toward the spectral intensity for the adsorbed species, the imazapyr concentration was chosen to be 2 mmol L<sup>-1</sup> for the adsorption study. Before data analysis the background spectra were subtracted from the spectrum obtained in the presence of imazapyr.

## 2.4. Results and Discussion

The influence of the pH on the photocatalytic degradation of imazapyr in aqueous TiO<sub>2</sub> suspensions was studied at the same pH values (pH 3, 5, 7, and 9) employed in the ATR-FTIR study. These pH values were chosen above (pH 3 and 5) and below (pH 7 and 9) the point of zero charge of the employed photocatalyst, i.e.,  $\sim\text{pH}_{\text{pzc}}=6.9$  for Evonik Aeroxide TiO<sub>2</sub> P25.<sup>10</sup> To gain an overview concerning the photocatalytic degradation of imazapyr molecules in the presence of TiO<sub>2</sub> the analysis of the results will focus mainly on the pH values 3 and 9. In the entire investigated pH range imazapyr is mainly present as neutral or deprotonated species, respectively (III and IV in Scheme 2.1.), according to the calculated distribution of the different imazapyr species using reported<sup>15</sup> acid–base dissociation constants.

**Photocatalytic Degradation Experiments.** The photocatalytic degradation experiments have been conducted following two different experimental protocols. In the first procedure the initial pH was adjusted to the desired pH value, with the concentration of imazapyr and the variation of the pH value being monitored during the subsequent UV (A) irradiation. A second set of experiments has been performed under the same experimental conditions (initial imazapyr concentration, optimal catalyst concentration, and pH) but keeping the pH constant employing the so-called pH stat method<sup>30</sup> during the UV (A) irradiation.

In all experimental runs the imazapyr concentration was found to decrease with irradiation time. A first-order kinetics fitting ( $R^2 \geq 0.994$ ) of the thus obtained concentration vs time plots (Supporting Information Figure S2.2) enables the calculation of the respective first-order rate constants; the resulting initial degradation rates were calculated by multiplying these rate constants with the corresponding initial imazapyr concentration and allow the comparison of the imazapyr degradation under different pH conditions.

Figure 2.1a shows the dependence of the initial degradation rate of imazapyr on the initial pH of the suspension; the inset shows the variation of pH during the experimental runs. Only a small change of approximately 0.1 pH units is observed during UV(A) irradiation at pH 3. However, a significant variation of the pH is observed at the initial pH values 5, 7, and 9.

Figure 2.1b shows the pH-dependence of the initial degradation rate in experimental runs performed at constant pH using the pH stat method. As can be seen from these figures the initial photocatalytic degradation rate of imazapyr decreases with increasing pH value.

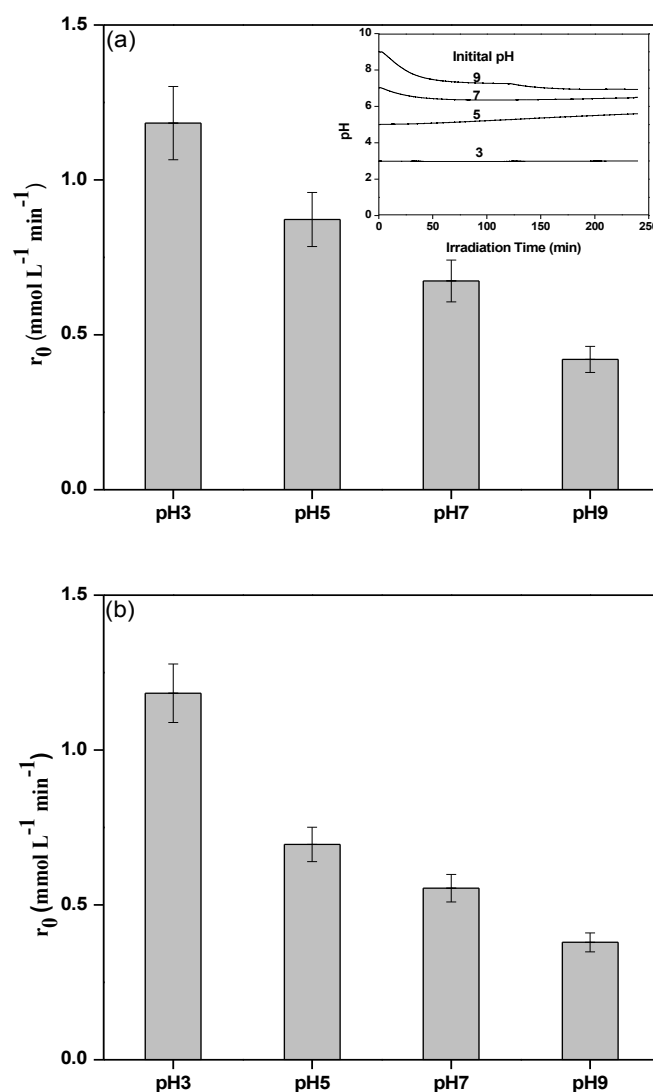


**Figure 2.1.** (a) Initial imazapyr degradation rate as a function of the pH of the suspension and the variation of the pH value during the UV illumination (inset). (b) Initial imazapyr degradation rate as a function of the pH of the suspension at constant pH (pH stat method).



Similar results have been reported by Carrier *et al.*<sup>15</sup> and by Osajima *et al.*<sup>14</sup> These authors have concluded that the observed dependence of the degradation rate on the pH of the suspension is due to the interactions between the ionizable functional groups of imazapyr and the titania surface.

The imazapyr adsorption isotherms obtained between pH 3 and pH 9 revealed decreasing amounts of imazapyr adsorbed onto the TiO<sub>2</sub> surface with increasing pH (data not shown). Note that imazapyr is an ionic species with three p*K*<sub>a</sub> values (1.88, 3.60, and 10.80) and that the TiO<sub>2</sub> surface is positively charged in acidic media and negatively charged in alkaline media. Since adsorption of the probe molecule at the TiO<sub>2</sub> surface is considered to be a prerequisite for a photocatalytic reaction, the experimental results presented in Figure 2.1. consequently indicate that at pH 9 a fraction of the negatively charged imazapyr ions present in the suspension is adsorbed at the negatively charged TiO<sub>2</sub> surface.

**ATR-FTIR Investigations.** IR spectra of imazapyr in solution as well as adsorbed onto the Aeroxide TiO<sub>2</sub> P25 surface have been collected at the before mentioned pH values (Figures 2.2–2.5). Meaningful IR bands were observed in the wavenumber range from 1800 to 950 cm<sup>-1</sup>. In this range strong overlapping peaks associated with CO, COO, CC, and CN vibrations as well as CH, NH, and OH vibrations can be expected to occur. Due to the superposition of these peaks a tentative assignment of the observed bands was made consulting several published references<sup>2,18,31–35</sup> as well as papers discussing the IR spectra of adsorbed molecules having similar functional groups as imazapyr (i.e., a pyridine ring with a carboxylic acid, an imidazole ring, and an oxo group) such as nicotinic acid,<sup>36–40</sup> pyridine,<sup>41–45</sup> carboxylate and carboxylic acids,<sup>20,21,26,46,47</sup> as well as several amino acids.<sup>48–51</sup>

**Spectra of Homogeneous Imazapyr Solutions.** Figure 2.2. shows the IR spectra of homogeneous aqueous solutions of imazapyr at pH 3 and pH 9 in the wavenumber range from 1800 to 950 cm<sup>-1</sup>. The results shown in this figure demonstrate that the positions as well as the intensity of some peaks are strongly affected by the pH of the solution as expected considering the pH-dependent protonation and deprotonation of the probe molecule. It can be readily calculated from the respective p*K*<sub>a</sub> values (vide supra) that approximately 75% of the imazapyr is present in its neutral form (species III in Scheme 2.1.) at pH 3. On the other hand, at pH 9 almost 100% of the imazapyr is deprotonated resulting in the negatively charged molecule ion (species IV in

Scheme 2.1.) (calculated distribution of imazapyr species as a function of the pH value is shown in Supporting Information Table S2.1).

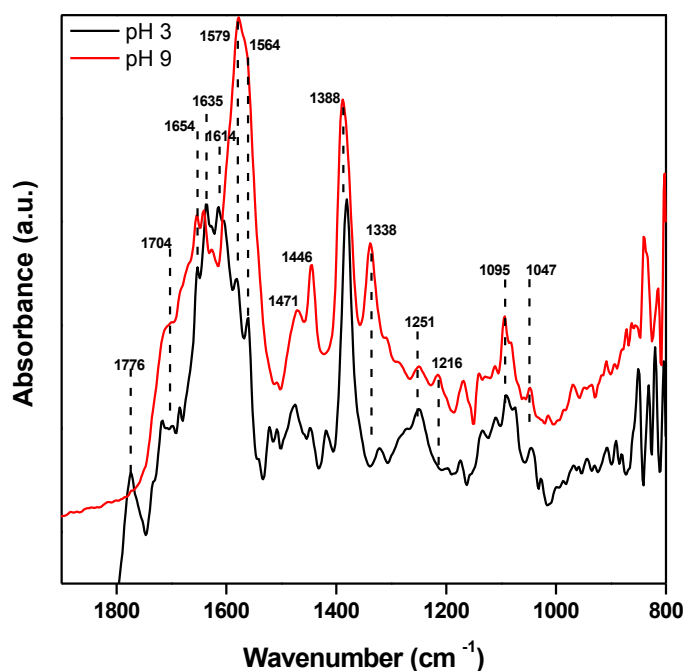


**Figure 2.2.** ATR-FTIR spectra of 12 mmol L<sup>-1</sup> solution of imazapyr in the absence of TiO<sub>2</sub> film at pH 3 (black line) and pH 9 (red line).

The presence of imazapyr in its protonated form in the solution at pH 3 is characterized by two main absorption features corresponding to the protonated carboxylic group of the probe molecule: the absorption band corresponding to a carbonyl stretch  $\nu(\text{C}=\text{O})$  at 1776 cm<sup>-1</sup> and  $\nu(\text{C}-\text{O}-\text{H})$  at 1251 cm<sup>-1</sup> (comprised of a mixture of C–O stretch and C–O–H bend that often yields a single, broad absorption band).<sup>52,53</sup> Imazapyr consists of a pyridine ring with a carboxylic group and an imidazole ring. This increases the structural complexity of imazapyr when compared to other amino acids. Mudunkotuwa *et al.*<sup>48</sup> have analyzed the solution phase spectra of histidine (imidazol ring, amine, and carboxylic group) and have assigned the broad band in the region 1627-1590 cm<sup>-1</sup> to the ring breathing  $\nu(\text{CC}) + \nu(\text{CN})$  and to the bending mode of the amine group. Furthermore, the contribution of the asymmetric carboxylate stretch has been observed as a shoulder at 1600 cm<sup>-1</sup>. Additionally, Wang *et al.*<sup>39</sup> have performed an ATR-FTIR study concerning the crystallization of nicotinic acid (that is a pyridine ring with a carboxylic group). The latter was present in both protonated and deprotonated form. The authors have observed a broad band in the region 1650-1550 cm<sup>-1</sup> and have assigned the peaks at

1640, 1605, and 1556 cm<sup>-1</sup> to ring deformation, NH bending mode, and asymmetric stretching of the COO group, respectively. Kokaislova *et al.*<sup>40</sup> have presented surface-enhanced infrared absorption spectra (SEIRA), as well as theoretically calculated spectra of nicotinic acid. The authors have assigned the bands at 1595 and 1583 cm<sup>-1</sup> to the ring breathing  $\nu(\text{CC})$  and to the  $\nu_a(\text{COO})$  coupled to the in-plane CH deformation, respectively. From the theoretical results, two additional bands at 1662 and 1635 cm<sup>-1</sup> have been assigned to the  $\nu(\text{CC}) + \nu(\text{CN})$  vibration modes.<sup>40</sup> This comparison allows the assignment of the broad band in the imazapyr spectrum at 1579–1564 cm<sup>-1</sup> to the ring breathing  $\nu(\text{CC})$  and the antisymmetrical stretching mode of the carboxylate ion ( $\nu_a(\text{COO})$ ) coupled to the in-plane CH deformation. The bands at 1654, 1635 and 1614 cm<sup>-1</sup> to the overlapping stretching modes  $\nu(\text{CC})$  and  $\nu(\text{CN})$  are coupled with the bending vibration of the NH group, respectively. Similar assignments have been reported elsewhere for dextrin, nicotinic acid, histidine, and lysine.<sup>35,37,38,40,48,50</sup> The symmetric stretching of the COO group ( $\nu_s(\text{COO})$ ) is observed at 1380 cm<sup>-1</sup>.<sup>38-40</sup>

As can be seen in Figure 2.2. the band centered at 1776 cm<sup>-1</sup> assigned to the carbonyl stretch of the carboxylic acid disappears as the pH is raised to pH 9. The peak at 1704 cm<sup>-1</sup> present at pH 9 is assigned to the carbonyl stretch of the imidazole ring. The intensity of the peak at 1251 cm<sup>-1</sup>, which has been assigned to vibrations of the protonated carboxyl group at pH 3, is decreased, as the pH is increased to pH 9. Hay *et al.*<sup>52</sup> have argued that the identification of the peak of  $\nu(\text{C-O-H})$  is difficult due to the overlap of bending and stretching modes, the strong H-bonding with solvent molecules, and the vibrational coupling with the C–C stretching mode. The weak bands, at 1251, and 1216 cm<sup>-1</sup>, observed at pH 9 are therefore assigned to ring vibrations (i.e., C–H deformation in plane).<sup>40,48</sup>

The position of the peaks at 1564 and 1388 cm<sup>-1</sup>, assigned to be, respectively, the antisymmetrical and symmetrical stretching mode of the carboxylate ion, remains unaffected by the change of pH.

The positions of the peaks at 1654, 1635, and 1625 cm<sup>-1</sup> as well as those centered at 1471, 1446, 1095, and 1047 cm<sup>-1</sup> are also found to be unaffected by the increase of the pH from pH 3 to pH 9, while the intensities of some bands have increased (i.e., 1579, 1471, 1388, and 1095 cm<sup>-1</sup>). Such an increase is indicative for functional groups involved in the deprotonation of the carboxylic acid group and the probable presence of the imazapyr molecule with a deprotonated imidazole ring (species V in

Scheme 2.1.) at pH 9. Barth *et al.*<sup>54</sup> have reported that CC and CN vibrations (especially in the region 1094-1113 cm<sup>-1</sup>) are sensitive to the imidazole ring deprotonation and are marker bands for the histidine deprotonation.

The comparison of our data with these previously published data<sup>40,48,54</sup> allows the assignment of the bands at 1654, 1635 and 1625 cm<sup>-1</sup> to the overlapping stretching modes  $\nu(\text{CC})$  and  $\nu(\text{CN})$  coupled with the bending vibration of the NH group, while the band at 1471 cm<sup>-1</sup> is assigned to  $\nu(\text{CN})$  and/or  $\delta(\text{C-H})$  ring vibrations. However, the bands with maxima at 1095 and 1047 cm<sup>-1</sup> cannot be ambiguously assigned to any simple vibrational mode but they rather correspond to coupled vibrations, i.e.,  $\nu(\text{CC})$ ,  $\nu(\text{CN})$ ,  $\delta(\text{CO})$ , and  $\gamma(\text{CH})$ , and other ring vibrations.<sup>32,33,35,40,48,53,55-57</sup> All assignments of the bands in the range from 1800 to 950 cm<sup>-1</sup> related to imazapyr functional groups are summarized in Table 1.

**Spectra of Imazapyr Adsorbed at the TiO<sub>2</sub> Surface.** An ATR-FTIR TiO<sub>2</sub>-substrate interaction study was performed to reveal the nature of the binding mode of imazapyr at the TiO<sub>2</sub> surface. Independent from the pH of the aqueous solution, the adsorption equilibrium was reached within 180 min since no further spectral changes are noted after this contact time. This spectroscopic result is confirmed by the investigation of the imazapyr adsorption kinetics in TiO<sub>2</sub> containing suspensions showing a constant imazapyr concentration in the supernatant liquid after 180 min (data not shown).

Upon contact of the imazapyr solution with the surface of the TiO<sub>2</sub> film at pH 3, a continuous increase of the absorbance within a contact time of 180 min is observed (Figure 2.3.). When compared to the spectrum of the homogeneous solution, small shifts of the position of the absorption maxima as well as changes in the relative intensity are noted (Figures 2.2. and 2.3.). Both phenomena are obviously related to the interaction between the TiO<sub>2</sub> surface and specific functionalities in the probe molecule.

After a contact time of 180 min between the aqueous solution and the TiO<sub>2</sub>-coated ATR crystal, the adsorption equilibrium is established. The bands centered at 1706 cm<sup>-1</sup>, 1568 cm<sup>-1</sup>, and at 1376 cm<sup>-1</sup> (cf. Figure 2.3. and the data presented in Table 2.1.) are the bands assigned to the different vibration modes of the carbonyl and the carboxyl groups of the probe molecule in homogeneous solution at pH 3. The  $\nu(\text{C=O})$  broad band at 1706 cm<sup>-1</sup> indicates that even the carbonyl group of the imidazole ring contributes to the overall interaction of imazapyr molecules with the

TiO<sub>2</sub> surface. The band at 1776 cm<sup>-1</sup> which corresponds to the stretching vibrational mode of the C=O in COOH (in the spectrum of imazapyr solution at pH 3) disappears in the spectrum of adsorbed imazapyr at pH 3. This could be explained by the hypothesis that the carboxylic group of imazapyr adsorbs predominately in its deprotonated form, and the double character of the C=O bond is lost.<sup>40</sup> The presence of two forms of molecularly adsorbed imazapyr is not excluded. Chesalov *et al.*<sup>36</sup> have studied the adsorption of nicotinic acid at the TiO<sub>2</sub> surface. They have identified two  $\nu(\text{C}=\text{O})$  bands at 1740 and 1660 cm<sup>-1</sup> for adsorbed nicotinic acid and thus concluded the formation of two different surface species. Furthermore, Kokaislova *et al.*<sup>40</sup> have shown that the C=O in COOH of nicotinic acid maintains its double bond character, and the frequency of the corresponding band is downshifted in the spectrum of nicotinic acid. In the case of imazapyr, the band at 1706 cm<sup>-1</sup> characterizes an imazapyr complex that is bound to the TiO<sub>2</sub> surface mainly via the carboxyl group of the pyridine ring with the involvement of the carbonyl group of the imidazole ring in the interaction. The same band is indicative of the carboxyl group of the pyridine ring, forming a strong hydrogen bond with the TiO<sub>2</sub> surface.<sup>36</sup>

The peaks at 1568 and 1376 cm<sup>-1</sup> are assigned to the asymmetric and symmetric mode of the carboxylate stretching vibration,  $\nu_a(\text{COO})$  and  $\nu_s(\text{COO})$ , respectively.<sup>38,40,49</sup> The peak positions of the overlapping  $\nu(\text{CC})$ ,  $\nu(\text{CN})$ , and  $\delta(\text{NH})$  vibrations of the pyridine and imidazole rings<sup>36,40,41,43,48</sup> observed at 1654, 1635, and 1614 cm<sup>-1</sup> in homogeneous solution are located in the presence of TiO<sub>2</sub> at 1654 (very weak), 1627, 1612, and 1598 cm<sup>-1</sup>, respectively.

In the homogeneous solution, at pH 3, two broad overlapping peaks centered at 1095 and 1047 cm<sup>-1</sup> are observed between 1200 and 1000 cm<sup>-1</sup>. These bands assigned to coupled  $\nu(\text{CO})$ ,  $\delta(\text{CH})$ ,  $\nu(\text{CC})$ ,  $\nu(\text{CN})$ ,  $\gamma(\text{CH})$ ,  $\delta(\text{CO})$ , and ring vibrations<sup>32,33</sup> are slightly shifted in the presence of TiO<sub>2</sub> and appear now in the range of 1200–850 cm<sup>-1</sup> with maxima at 1143 and 1103 cm<sup>-1</sup>.

Analogously to the temporal change of the spectra recorded at pH 3, shifts of the peak positions as well as very weak absorption bands are observed at pH 9 until the adsorption equilibrium is established (Figure 2.4.). The spectrum shows strong absorption bands between 1100 and 850 cm<sup>-1</sup> which are assigned to  $\nu(\text{CC})$ ,  $\nu(\text{CN})$ ,  $\gamma(\text{CH})$ , and other ring vibrations as concluded from the spectra obtained in the homogeneous aqueous solution.

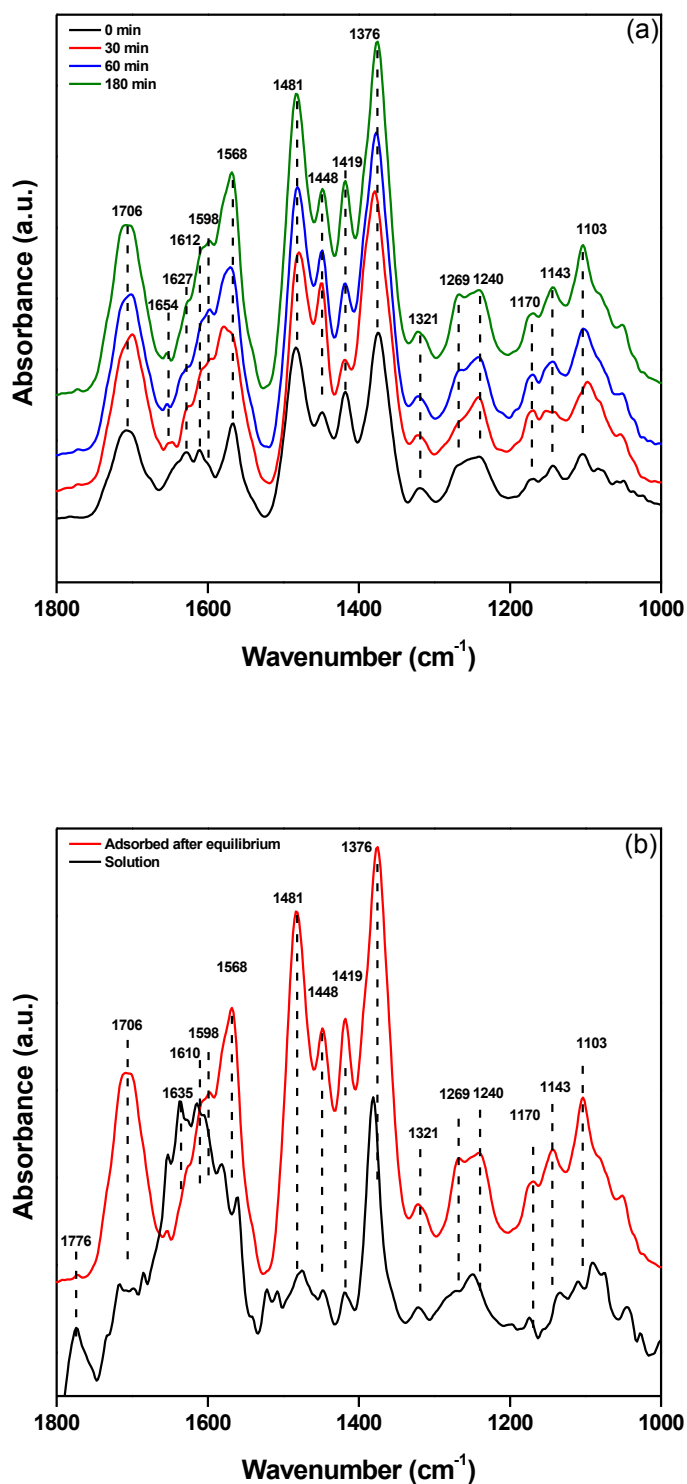


**Figure 2.3.** (a) ATR-FTIR spectra of an aqueous 2 mmol L<sup>-1</sup> solution of imazapyr in the presence of a TiO<sub>2</sub> film after different contact times at pH 3 and (b) spectra of imazapyr at pH 3 in the absence (black line) and in the presence of TiO<sub>2</sub> after equilibrium (red line).

A weak band at 1699 cm<sup>-1</sup> corresponds to the  $\nu(\text{C}=\text{O})$  vibrations. As mentioned during the discussion of the data observed at pH 3, the band is indicative for the

adsorption of imazapyr with the contribution of the carbonyl group of the imidazole ring. Furthermore, it is also assigned to the hydrogen bonding of the carboxyl group to the surface. The peaks at 1640, 1639, and 1488 cm<sup>-1</sup> are a superposition of  $\nu(\text{CN})$ ,  $\delta(\text{NH})$ , and  $\nu(\text{CC})$  ring vibrations, and the weak contributions of the asymmetric COO stretch is not excluded.<sup>48,58</sup> The symmetric COO stretch band is observed as a very weak absorption at 1368 cm<sup>-1</sup>. Furthermore, the peak with an absorbance maximum at 1238 cm<sup>-1</sup> results from a superposition of CC, CN, and CO vibrations.<sup>48,55,56</sup>

**Table 2.1.** Band Assignments for the Main IR Absorption Bands of an Aqueous Imazapyr Solution in the Absence and in the Presence of the TiO<sub>2</sub> Layer at pH 3 and 9.

Mode of Vibration*	Peak position / cm <sup>-1</sup>				Ref
	solution pH 3	solution pH 9	adsorbed pH 3	adsorbed pH 9	
$\nu(\text{C=O})$	1776	-	1706	1699	23,36,40,52
	1704	1704			
$\nu(\text{CN})+\nu(\text{CC})$	1654	1654	1654	1640	18,40,43
$\delta(\text{H}_2\text{O}),\nu(\text{CN},\text{CC})$	1635	1635	1635	1639	33,35,37,38,40,48,50,53
$\delta(\text{NH}),$	1614	1625	1610		
$\nu(\text{C=C})$	1579	1579	1598		
$\nu_a(\text{COO}), \delta(\text{CH})$	1564	1564	1568		35,38-40
$[\nu_s(\text{CN}), \delta(\text{CH})]_{\text{ring}}$	1471	1471	1481	1488	32,33,40,48
$\nu(\text{C=C})_N, \delta(\text{CH}_2)$	1446	1446	1448		35,37
$\nu_s(\text{C=N})+\nu_s(\text{CN})_{\text{ring}} +$ $\delta(\text{CH})$	1415		1419		37,48
$\nu_s(\text{COO})$	1380	1388	1376		38,39
$\nu(\text{CO}), \delta(\text{O-H}), \delta(\text{CH})$	1251	1251	1269		40,52,53
		1216	1240	1238	
$\nu(\text{CN}), \delta(\text{CH}), \nu(\text{CO}),$ $\delta(\text{CO}), \gamma(\text{CH}),$ ring vibrations	1095	1095	1143	1008	32,33,35,48,53,55-57
	1047	1047	1103	958	

\*  $\nu_{s/a}$  symmetric/asymmetric stretching vibration;  $\delta$  deformation/bending;  $\gamma$  twisting vibration. Note: The resolution is 4 cm<sup>-1</sup>.

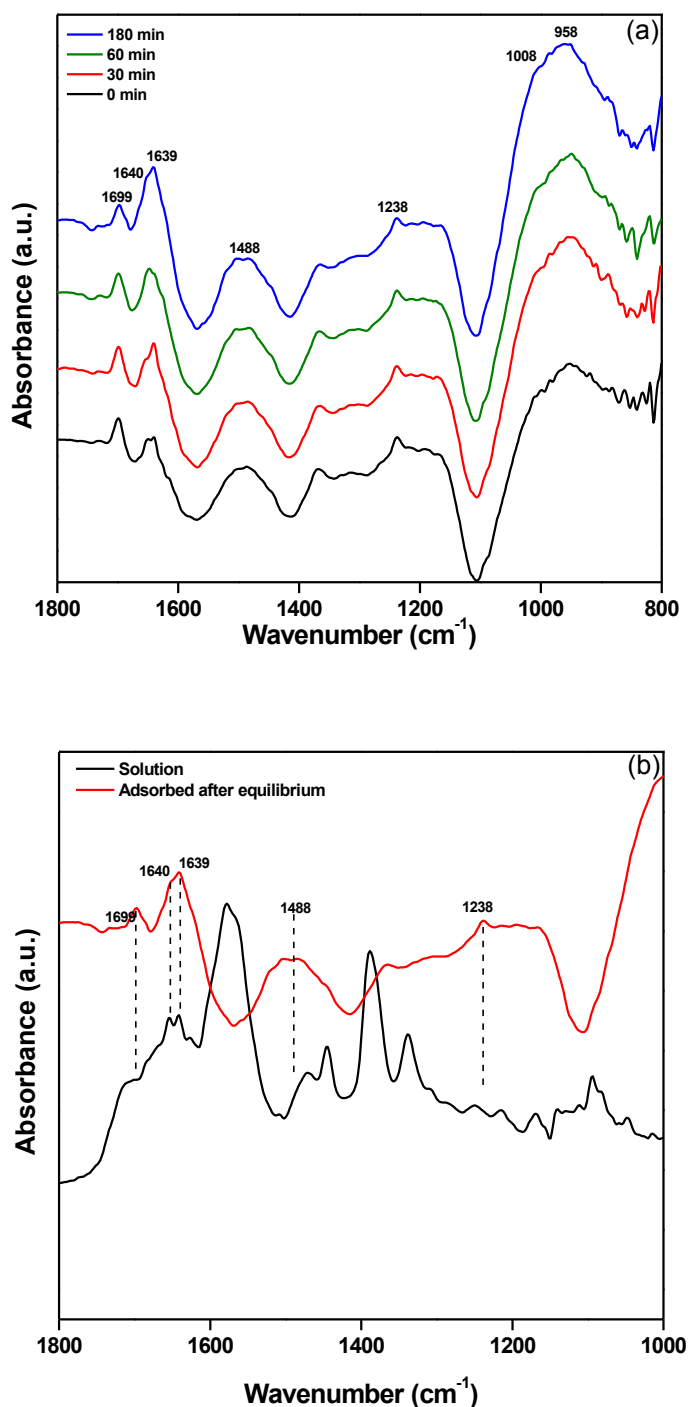


**Figure 2.4.** (a) ATR-FTIR Spectra of an aqueous 2 mmol L<sup>-1</sup> solution of imazapyr in the presence of the TiO<sub>2</sub> film after different contact times at pH 9 and (b) spectra of imazapyr at pH 9 in the absence (black line) and in the presence of TiO<sub>2</sub> after equilibrium (red line).

**Summarizing Discussion.** Figure 2.5. shows the spectra of imazapyr adsorbed on TiO<sub>2</sub> at all pH values investigated here (e.g., pH 3, 5, 7, and 9) after 180 min contact time, i.e., at equilibrium conditions. Upon increasing the pH from pH 3 to pH 9 (a) nearly all bands in the range between 1800 and 1500 cm<sup>-1</sup> are shifted to higher



wavenumbers; (b) the intensities of all peaks with wavenumbers  $>1100\text{ cm}^{-1}$  are decreased; and (c) the intensity of the broad band between  $1100$  and  $800\text{ cm}^{-1}$  is increased. The observed shifts in position and the changes in the peak intensities indicate the pH-dependent presence of different surface complexes formed during the contact between the aqueous imazapyr solution and the TiO<sub>2</sub> film. At pH 3 neutral as well as the negatively charged imazapyr molecules are present in the solution, and both are prone to interact with the positively charged TiO<sub>2</sub> surface *via* the carboxy group attached to the pyridine moiety of the molecule. The strong electrostatic attraction between the organic anion and the oxide surface results in the formation of carboxylate surface complexes with strong IR peaks centered at  $1568$  and  $1376\text{ cm}^{-1}$ .

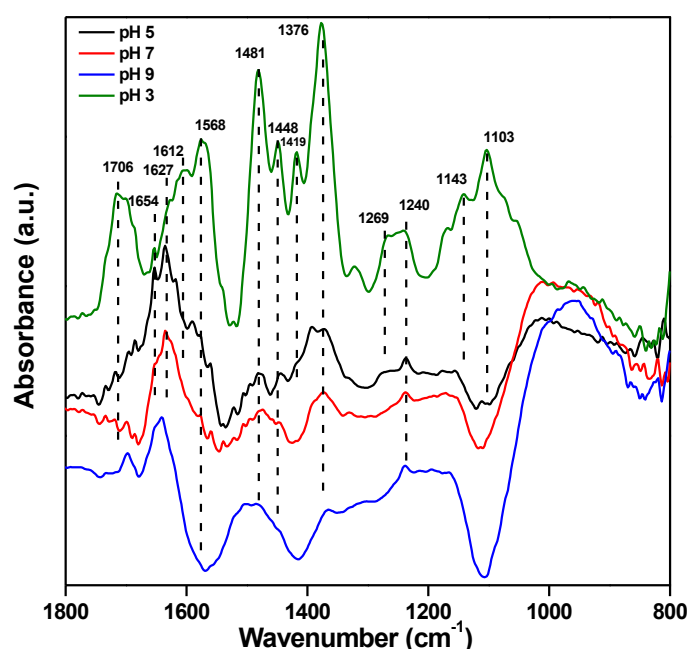


**Figure 2.5.** ATR-FTIR spectra of aqueous  $2\text{ mmol L}^{-1}$  imazapyr solutions measured at four different pH values in the presence of TiO<sub>2</sub> films after a contact time of 180 min.

At pH 9 the negatively charged imazapyr ion is the dominant organic species present in the solution. Since at this pH the TiO<sub>2</sub> surface is negatively charged as well, electrostatic repulsion prevents the formation of significant amounts of carboxylate surface complexes.<sup>15</sup>

The carboxylate group is separated from the TiO<sub>2</sub> surface by the pyridine ring; therefore, the IR peaks attributed to the COO group are weak at this pH. On the other

hand, the intensity of the broad bands between 1200 and 850 cm<sup>-1</sup> which have been assigned *inter alia* to superposed ring and CN vibrations is high, thus indicating an interaction between the TiO<sub>2</sub> surface and one of the heterocyclic rings present in the probe molecule. Since the N–C=O moiety of the imidazole ring facilitates the formation of a ring structure upon adsorption, the preferential formation of a surface complex having this structural element seems likely.<sup>59</sup>

The intensity of the broad band between 1200 and 850 cm<sup>-1</sup> is decreasing with decreasing pH, while the intensities of the peaks related to the COO group are increasing. The obvious explanation for this observation is a decreasing amount of the surface complex involving atoms present in the heterocyclic ring and an increasing amount of the carboxylate surface complex. These statements are not contradicting the results obtained by Osajima *et al.*,<sup>14</sup> who calculated the partial atomic charges (at the semiempirical AM1 level) of the imazapyr molecule and its ionized species.<sup>14</sup> Taking into account the charge of the TiO<sub>2</sub> surface, they have concluded that increasing the pH value of the suspension hinders the approach of the imazapyr molecules to the TiO<sub>2</sub> surface due to their electrostatic repulsion, thus inhibiting the intermit herbicide adsorption at the TiO<sub>2</sub> surface.

The interaction between the semiconductor surface and the imazapyr species is affected not only by the pH value but also by the ionic strength of the electrolyte. The Debye length determines length scale at which electrostatic interactions between charged particles are screened.<sup>60</sup> Furthermore, it has been suggested that the charging behavior of nanostructured surfaces may have important consequences for adsorption processes, as for the surface interactions. An incoming species, at a given distance from the surface of the order of one or two Debye lengths, will feel a reduced electric field compared to the case of interaction with a smooth surface. Iwafuji *et al.*<sup>61</sup> have studied the effect of adding different types of salts, in different concentrations, on the formation of the Langmuir monolayer of TiO<sub>2</sub>. The authors have concluded that increasing the concentration of ions causes the screening of a charged surface to increase, resulting in a decreased Debye length. Additionally the authors<sup>61</sup> have discussed two distinct effects of the salt, the structure making and structure breaking ions, which cause the interfacial water structure to increase or to be destroyed, respectively, by the promotion or destruction of hydrogen bonding. This result suggests that the formation of H-bonds in the subphase by the structure determining ions enhances the stability of the TiO<sub>2</sub>.<sup>61</sup>

Here the Debye lengths have been calculated to be 3.1 nm at pH 5 and 7 and 2.9 nm at pH 3 and 9. Since the present data have been obtained at nearly constant Debye lengths, the possible effect of the ionic strength cannot be considered in the context of the interpretation of the pH effect presented here. However, the probability of the screening of the before mentioned electrostatic repulsions between the negatively charged imazapyr and the negatively charged TiO<sub>2</sub> surface, or the formation of surface species due to the adsorption of the electrolyte, cannot be excluded. In view of the above, we consider that this critical issue should be further investigated.

Interactions between the COOH group of the probe molecule and the TiO<sub>2</sub> surface may occur in several ways such as physisorption through electrostatic attraction, hydrogen bonding, or chemisorption resulting in different types of surface complexes, e.g., monodentate, bidentate, and bridging type complexes.<sup>21,33,46,62</sup>

It has been shown that these different types of surface complexes can be distinguished by the comparison of the difference in wavenumber  $\Delta\nu_{a-s} = \nu_a - \nu_s$  between the asymmetric and the symmetric mode of the carboxylate stretching vibration in homogeneous solution ( $\Delta\nu_{a-s}(\text{free})$ ) and after adsorption at the oxide surface ( $\Delta\nu_{a-s}(\text{adsorbed})$ ).<sup>8</sup>

The respective analysis of the spectra (Figures 2.2–2.4) revealed that  $\Delta\nu_{a-s}(\text{adsorbed}) < \Delta\nu_{a-s}(\text{free})$ , indicating that imazapyr is covering the TiO<sub>2</sub> surface as a bidentate and/or bridging ligand over the pH range investigated here. Additional information concerning the structure of the adsorbates has been given by Osajima *et al.*<sup>14</sup> Based upon the calculated charge densities of the different imazapyr species in the aqueous phase, the dihedral angle equivalent to N3(imidazol)–C2(imidazol)–C2(pyridine)–N1(pyridine) is given as 212°. The authors have concluded that the adsorption occurs through the carboxylic oxygen. Furthermore, the interaction is more favorable between the deprotonated imazapyr molecule (species IV in scheme 2.1.) and the protonated TiO<sub>2</sub> surface as TiOH<sub>2</sub><sup>+</sup>. Kokaislova *et al.*<sup>40</sup> have reported that even in the preferred adsorption geometry of nicotinic acid, the  $\pi$ -electronic pyridine ring does not significantly contribute to the overall interaction of nicotinic acid (the  $\pi$ - $\pi$  intermolecular interactions are proposed to contribute to the arrangement of adsorbed molecular layer). It is worth to note that the preferred geometry of adsorbed nicotinic acid has been reported to be where the

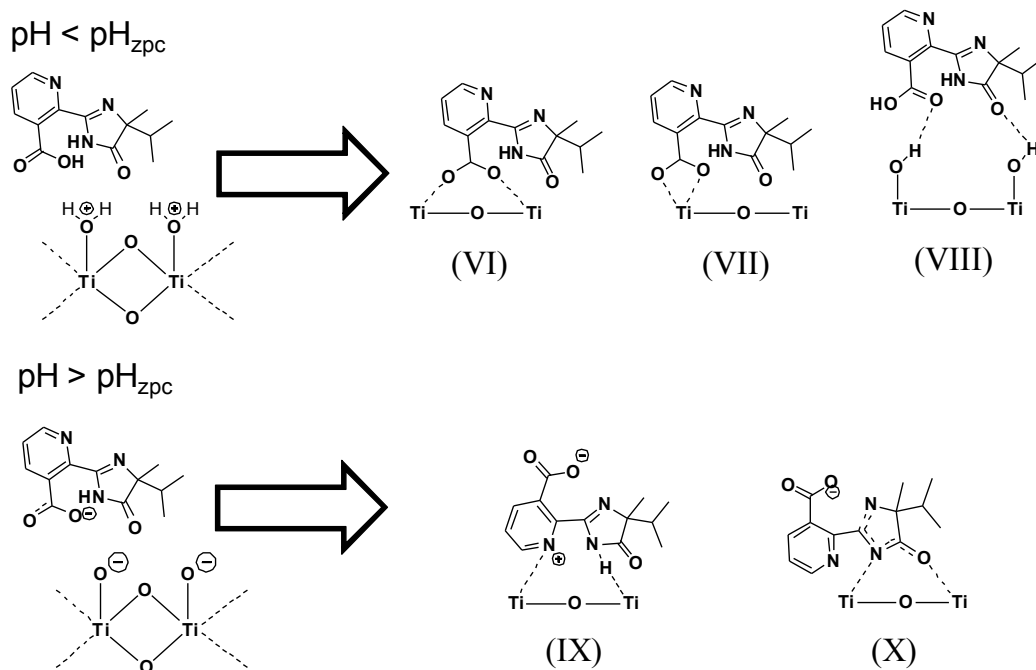
ring is almost perpendicularly oriented to the surface and the carboxylic acid to its proximity.<sup>40</sup>

Hence, the adsorption of imazapyr at the TiO<sub>2</sub> surface results in different surface-adsorbed species as depicted in Scheme 2.2. The predominant adsorbed structure at acidic pH is the one formed through the bridging mode (Species VI in Scheme 2.2.). However, it must be emphasized that the presence of the bidentate surface complex (species VII in Scheme 2.2.) as well as that of other surface complexes cannot be unequivocally excluded by this investigation.

As mentioned before, spectral evidence has been assigned to the contribution of the carboxyl group in the overall adsorption process. Species VI and VII (Scheme 2.2.) present possible structures where the adsorption of imazapyr takes place through the carboxylic group without any contribution of the carbonyl group of the imidazole ring. Furthermore, species VIII (Scheme 2.2.) represents the case where the carboxylic acid and/or the carbonyl group are linked to the TiO<sub>2</sub> surface via hydrogen bonds. The contribution of the carbonyl group of the imidazole ring in the overall interaction is not excluded.

It was mentioned before that the adsorption of imazapyr at the TiO<sub>2</sub> surface is hindered in alkaline media. Presumably, imazapyr adsorbs dissociatively through the contribution of the pyridine ring and the N–C=O moiety of the imidazole ring yielding species IX and X in Scheme 2.2. The presence of the adsorbates VI, VII, and VIII (Scheme 2.2.) proposed for acidic pH is not excluded in alkaline media. Furthermore, the presence of hydrogen-bonded and inner- or outer-sphere surface species (not proposed here) is not excluded in the overall interaction.

Usually, adsorption of the probe molecule is assumed to be a prerequisite for its photocatalytic conversion, and the photocatalytic reaction rate is assumed to be proportional to the coverage of the photocatalyst surface. With increasing pH the adsorption of imazapyr is inhibited; the surface coverage is decreased; and as expected the photocatalytic degradation rate of imazapyr is also found to decrease. Carrier *et al.*<sup>15</sup> who have studied the photocatalytic degradation of imazapyr, concluded from their experimental results in combination with electronic density calculations that the structure of the adsorbate affects the kinetics.

**Scheme 2.2.** Proposed Structures of Adsorbed Imazapyr Species on the TiO<sub>2</sub> Surface at Different pH Values.

Theoretical calculations performed by Osajima *et al.*<sup>14</sup> and by Carrier *et al.*<sup>15</sup> have shown that the preferential mode of adsorption of imazapyr is the bridging binding of the carboxylic group to the TiO<sub>2</sub> surface (VI scheme 2.2.). This has been confirmed experimentally in this work. Carrier *et al.*<sup>15</sup> have reported that the main product of the photocatalytic imazapyr degradation is formed by the direct hole oxidation of the carboxyl moiety attached to the pyridine ring followed by subsequent decarboxylation (Photo-Kolbe reaction).

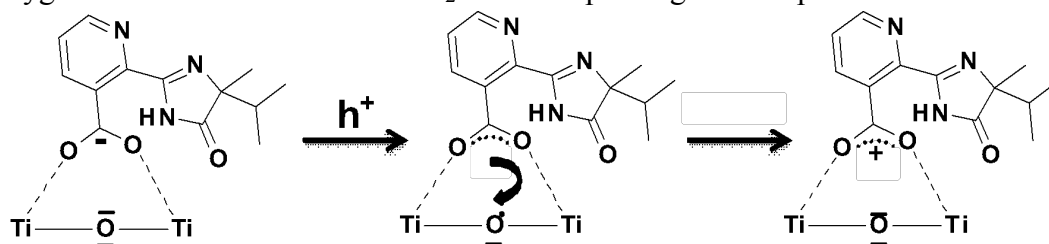
Carrier *et al.*<sup>15</sup> have reported that •OH radicals also play an important role in the photocatalytic degradation of imazapyr. The authors have determined the primary position for the •OH radical (an electrophilic species) attack (the atoms with the largest electron density) with the help of the calculation of electronic density of imazapyr. Furthermore, the authors have presented a detailed degradation pathway of imazapyr.

Recently, the role of bridging oxygen atoms as traps of photo-generated valence band holes leading to the photogeneration of terminal oxygen radicals able to react with the adsorbate species at the TiO<sub>2</sub> surface has been discussed.<sup>63,64</sup> The presence of terminal oxygen radicals at the TiO<sub>2</sub> surface offers an explanation for the mechanism of the photocatalytic degradation of imazapyr being adsorbed in a bridging form at pH 3: the TiO<sub>2</sub> surface oxygen atom located directly underneath the

adsorbed imazapyr species serves as a trap for a hole generated by the absorption of UV light. This leads to the generation of an oxygen-centered radical in the direct neighborhood to the target molecule enabling a facile interfacial electron transfer from the carboxylate group to this hole trap (Scheme 2.3.). Charge carrier diffusion from the interior of a particle to the surface can occur more rapidly with charges localized in the surface traps ( $e_{tr}^-$  and  $h_{tr}^+$ ) than the electron-hole recombination.

With increasing pH the amount of the adsorbed bridging imazapyr species decreases resulting in the observed decrease in the photocatalytic degradation rate, especially at pH 9 where the adsorption of imazapyr is very weak and the amount of the adsorbate (species VI in scheme 2) present at the surface is very low.

**Scheme 2.3.** Proposed Mechanism of the Interaction of Imazapyr with a Terminal Oxygen Radical Formed on the TiO<sub>2</sub> Surface upon Light Absorption.



## 2.5. Conclusions

Herein, the adsorption of imazapyr from aqueous solution onto a TiO<sub>2</sub> particle film was investigated by ATR-FTIR spectroscopy. The spectra revealed that imazapyr is strongly adsorbed at the TiO<sub>2</sub> surface forming bridging carboxylate complexes and other surface complexes involving the heterocyclic rings of this probe molecule. The relative amount of these species present at the TiO<sub>2</sub> surface is considerably affected by the pH. The high photocatalytic degradation rate of imazapyr observed at pH 3 in the presence of TiO<sub>2</sub> is thus attributed to the close proximity between suitable trap states for the photogenerated holes at the photocatalyst surface and the carboxylate group of the probe molecule.

## 2.6. Acknowledgments

M. Faycal Atitar gratefully acknowledges a scholarship from the DAAD in the frame of the Sandwich-Program. Financial support of the BMBF in the framework of an

international collaboration between Morocco and Germany is gratefully acknowledged (FKZ: 01DH12028). M.F.A thanks Pr. Alexey A. Tsyganenko from Department of Physics, St. Petersburg State University for fruitful discussions. The authors are thankful to the reviewers for the valuable suggestions and comments related to the spectral processing, as well as the effect of the ionic strength.

## 2.7. References

- (1) Montoya, J. F.; Peral, J.; Salvador, P. Comprehensive Kinetic and Mechanistic Analysis of TiO<sub>2</sub> Photocatalytic Reactions According to the Direct–Indirect Model: (I) Theoretical Approach. *J. Phys. Chem. C* **2014**, *118*, 14266–14275.
- (2) Montoya, J.; Atitar, F., M.; Bahnemann, D. W.; Peral, J. and; Salvador, P. Comprehensive Kinetic and Mechanistic Analysis of TiO<sub>2</sub> Photocatalytic Reactions According to the Direct-Indirect (DI) Model: II) Experimental Validation. *J. Phys. Chem. C* **2014**, *28*, 14276–14290.
- (3) Henderson, M. A. A Surface Science Perspective on TiO<sub>2</sub> Photocatalysis. *Surf. Sci. Rep.* **2011**, *66*, 185–297.
- (4) Friedmann, D.; Mendive, C.; Bahnemann, D. TiO<sub>2</sub> for Water Treatment: Parameters Affecting the Kinetics and Mechanisms of Photocatalysis. *Appl. Catal. B Environ.* **2010**, *99*, 398–406.
- (5) Hoffmann, M. R.; Martin, S. T.; Choi, W.; Bahnemann, D. W. Environmental Applications of Semiconductor Photocatalysis. *Chem. Rev.* **1995**, *95*, 69–96.
- (6) Canle L., M.; Santaballa, J. A.; Vulliet, E. On the Mechanism of TiO<sub>2</sub>-Photocatalyzed Degradation of Aniline Derivatives. *J. Photochem. Photobiol. A Chem.* **2005**, *175*, 192–200.
- (7) Lee, H.-S.; Hur, T.; Kim, S.; Kim, J.-H.; Lee, H.-I. Effects of pH and Surface Modification of TiO<sub>2</sub> with SiO<sub>x</sub> on the Photocatalytic Degradation of a Pyrimidine Derivative. *Catal. Today* **2003**, *84*, 173–180.
- (8) Choi, H.; Antoniou, M. G.; Pelaez, M.; De La Cruz, A. a.; Shoemaker, J. a.; Dionysiou, D. D. Mesoporous Nitrogen-Doped TiO<sub>2</sub> for the Photocatalytic Destruction of the Cyanobacterial Toxin Microcystin-LR under Visible Light Irradiation. *Environ. Sci. Technol.* **2007**, *41*, 7530–7535.
- (9) Kormann, C.; Bahnemann, D. W.; Hoffmann, M. R. Photolysis of Chloroform and Other Organic Molecules in Aqueous TiO<sub>2</sub> Suspensions. *Environ. Sci. Tech.* **1991**, *25*, 494–500.
- (10) Dutta, P. K.; Ray, A. K.; Sharma, V. K.; Millero, F. J. Adsorption of Arsenate and Arsenite on Titanium Dioxide Suspensions. *J. Colloid Interface Sci.* **2004**, *278*, 270–275.
- (11) Cox, C. Nonylphenol and Related Chemicals. *J. Pestic. reform* **1996**, *16*, 16–20.
- (12) Pizarro, P.; Guillard, C.; Perol, N.; Herrmann, J. M. Photocatalytic Degradation of Imazapyr in Water: Comparison of Activities of Different Supported and Unsupported TiO<sub>2</sub>-Based Catalysts. In *Catalysis Today*; 2005; Vol. 101, pp. 211–218.
- (13) Rumi Ishiki, R.; Mitsugu Ishiki, H.; Takashima, K. Photocatalytic Degradation

- of Imazethapyr Herbicide at TiO<sub>2</sub>/H<sub>2</sub>O Interface. *Chemosphere* **2005**, *58*, 1461–1469.
- (14) Osajima, J. A.; Ishiki, H. M.; Takashima, K. The Photocatalytic Degradation of Imazapyr. *Monatshefte für Chemie - Chem. Mon.* **2007**, *139*, 7–11.
- (15) Carrier, M.; Perol, N.; Herrmann, J.-M.; Bordes, C.; Horikoshi, S.; Paise, J. O.; Baudot, R.; Guillard, C. Kinetics and Reactional Pathway of Imazapyr Photocatalytic Degradation Influence of pH and Metallic Ions. *Appl. Catal. B Environ.* **2006**, *65*, 11–20.
- (16) Faycal Atitar, M.; Ismail, A. A.; Al-Sayari, S. A.; Bahnemann, D.; Afanasev, D.; Emeline, A. V. Mesoporous TiO<sub>2</sub> Nanocrystals as Efficient Photocatalysts: Impact of Calcination Temperature and Phase Transformation on Photocatalytic Performance. *Chem. Eng. J.* **2015**, *264*, 417–424.
- (17) Ismail, A. A.; Abdelfattah, I.; Atitar, M. F.; Robben, L.; Bouzid, H.; Al-Sayari, S. a.; Bahnemann, D. W. Photocatalytic Degradation of Imazapyr Using Mesoporous Al<sub>2</sub>O<sub>3</sub>-TiO<sub>2</sub> Nanocomposites. *Sep. Purif. Technol.* **2015**, *145*, 147–153.
- (18) Mudunkotuwa, I. A.; Minshid, A. Al; Grassian, V. H. ATR-FTIR Spectroscopy as a Tool to Probe Surface Adsorption on Nanoparticles at the Liquid-Solid Interface in Environmentally and Biologically Relevant Media. *Analyst* **2014**, *139*, 870–881.
- (19) McQuillan, A. J. Probing Solid–Solution Interfacial Chemistry with ATR-IR Spectroscopy of Particle Films. *Adv. Mater.* **2001**, *13*, 1034–1038.
- (20) Dobson, K. D.; McQuillan, A. J. In Situ Infrared Spectroscopic Analysis of the Adsorption of Aliphatic Carboxylic Acids to TiO<sub>2</sub>, ZrO<sub>2</sub>, Al<sub>2</sub>O<sub>3</sub>, and Ta<sub>2</sub>O<sub>5</sub> from Aqueous Solutions. *Spectrochim. Acta Part A Mol. Biomol. Spectrosc.* **1999**, *55*, 1395–1405.
- (21) Qu, Q.; Geng, H.; Peng, R.; Cui, Q.; Gu, X.; Li, F.; Wang, M. Chemically Binding Carboxylic Acids onto TiO<sub>2</sub> Nanoparticles with Adjustable Coverage by Solvothermal Strategy. *Langmuir* **2010**, *26*, 9539–9546.
- (22) Gulley-Stahl, H.; Hogan, P. A.; Schmidt, W. L.; Wall, S. J.; Buhrlage, A.; Bullen, H. A. Surface Complexation of Catechol to Metal Oxides: An ATR-FTIR, Adsorption, and Dissolution Study. *Environ. Sci. Technol.* **2010**, *44*, 4116–4121.
- (23) Begonja, S.; Rodenas, L. A. G.; Borghi, E. B.; Morando, P. J. Adsorption of Cysteine on TiO<sub>2</sub> at Different pH Values: Surface Complexes Characterization by FTIR-ATR and Langmuir Isotherms Analysis. *Colloids Surfaces A Physicochem. Eng. Asp.* **2012**, *403*, 114–120.
- (24) Young, A. G.; McQuillan, A. J. Adsorption/desorption Kinetics from ATR-IR Spectroscopy. Aqueous Oxalic Acid on Anatase TiO<sub>2</sub>. *Langmuir* **2009**, *25*, 3538–3548.
- (25) Mendive, C. B.; Bredow, T.; Blesa, M. A.; Bahnemann, D. W. ATR-FTIR Measurements and Quantum Chemical Calculations Concerning the Adsorption and Photoreaction of Oxalic Acid on TiO<sub>2</sub>. *Phys. Chem. Chem. Phys.* **2006**, *8*, 3232–3247.
- (26) Hug, S.; Sulzberger, B. In Situ Fourier Transform Infrared Spectroscopic Evidence for the Formation of Several Different Surface Complexes of Oxalate on TiO<sub>2</sub> in the Aqueous Phase. *Langmuir* **1994**, *18*, 3587–3597.



- (27) Atitar, M. F.; Belhadj, H.; Dillert, R.; Bahnem, D. W. The Relevance of ATR-FTIR Spectroscopy in Semiconductor Photocatalysis. In *Emerging Pollutants in the Environment - Current and Further Implications*; Marcelo L. Larramendy, Ed.; InTech, 2015.
- (28) House, J. E. *Inorganic Chemistry*; Academic Press; Academic Press/Elsevier, 2012.
- (29) Emeline, A. V.; Zhang, X.; Jin, M.; Murakami, T.; Fujishima, A. Application of A “black Body” like Reactor for Measurements of Quantum Yields of Photochemical Reactions in Heterogeneous Systems. *J. Phys. Chem. B* **2006**, *110*, 7409–7413.
- (30) Bahnemann, D.; Bockelmann, D.; Goslich, R. Mechanistic Studies of Water Detoxification in Illuminated TiO<sub>2</sub> Suspensions. *Sol. Energy Mater.* **1991**, *24*, 564–583.
- (31) Araujo, P. Z.; Mendive, C. B.; Rodenas, L. a. G.; Morando, P. J.; Regazzoni, A. E.; Blesa, M. a.; Bahnemann, D. FT-IR–ATR as a Tool to Probe Photocatalytic Interfaces. *Colloids Surfaces A Physicochem. Eng. Asp.* **2005**, *265*, 73–80.
- (32) Coates, J. Interpretation of Infrared Spectra , A Practical Approach. In *Encyclopedia of Analytical Chemistry*; R.A. Meyers, Ed.; John Wiley & Sons Ltd, Chichester, 2000; pp. 10815–10837.
- (33) Petrone, L.; McQuillan, A. J. Alginate Ion Adsorption on a TiO<sub>2</sub> Particle Film and Interactions of Adsorbed Alginate with Calcium Ions Investigated by Attenuated Total Reflection Infrared (ATR-IR) Spectroscopy. *Appl. Spectrosc.* **2011**, *65*, 1162–1169.
- (34) Jakobsen, R. J. Fourier Transform Infrared Spectra: Applications to Chemical Systems, Band 2. In; Ferraro, J. R.; Basile, L. J., Eds.; ACADEMIC PRESS, INC., 1979; pp. 165–191.
- (35) Beaussart, A.; Petrone, L.; Mierczynska-Vasilev, A.; McQuillan, a J.; Beattie, D. a. In Situ ATR FTIR Study of Dextrin Adsorption on Anatase TiO<sub>2</sub>. *Langmuir* **2012**, *28*, 4233–4240.
- (36) Chesalov, Y. A.; Chernobay, G. B.; Andrushkevich, T. V. FTIR Study of the Surface Complexes of  $\beta$ -Picoline, 3-Pyridine-Carbaldehyde and Nicotinic Acid on Sulfated TiO<sub>2</sub> (Anatase). *J. Mol. Catal. A Chem.* **2013**, *373*, 96–107.
- (37) Koczoń, P.; Dobrowolski, J. C.; Lewandowski, W.; Mazurek, a. P. Experimental and Theoretical IR and Raman Spectra of Picolinic, Nicotinic and Isonicotinic Acids. *J. Mol. Struct.* **2003**, *655*, 89–95.
- (38) Lewandowski, W.; Barańska, H.; Mościbroda, P. Vibrational Study of Nicotinic Acid Complexes with Different Central Ions. *J. Raman Spectrosc.* **1993**, *24*, 819–824.
- (39) Wang, F.; Berglund, K. a. Monitoring pH Swing Crystallization of Nicotinic Acid by the Use of Attenuated Total Reflection Fourier Transform Infrared Spectrometry. *Ind. Eng. Chem. Res.* **2000**, *39*, 2101–2104.
- (40) Kokaislova, A.; Parchansky, V.; Matejka, P. Surface-Enhanced Infrared Spectra of Nicotinic Acid and Pyridoxine on Copper Substrates: What Is the Effect of Temperature and Deposition Conditions? *J. Phys. Chem. C* **2015**, *119*, 26526–26539.
- (41) Church, F. M.; Cook, B. Y. G. L. Correlations of The Infrared Spectra of

- Some Pyridines. *J. Phys. Chem.* **1957**, *61*, 458–462.
- (42) Popova, G. Y.; Chesalov, Y. A.; Andrushkevich, T. V. In Situ FTIR Study of Pyridine-3-Carbaldehyde Adsorption on TiO<sub>2</sub> (Anatase) and V-Ti-O Catalyst. *React. Kinet. Catal. Lett.* **2004**, *83*, 353–360.
- (43) Chernobay, G. B.; Chesalov, Y. A.; Baltakhinov, V. P.; Popova, G. Y.; Andrushkevich, T. V. In Situ FTIR Study of  $\beta$ -Picoline Transformations on V-Ti-O Catalysts. *Catal. Today* **2011**, *164*, 58–61.
- (44) Zaki, M. I.; Hasan, M. a.; Al-Sagheer, F. a.; Pasupulety, L. In Situ FTIR Spectra of Pyridine Adsorbed on SiO<sub>2</sub>-Al<sub>2</sub>O<sub>3</sub>, TiO<sub>2</sub>, ZrO<sub>2</sub> and CeO<sub>2</sub>: General Considerations for the Identification of Acid Sites on Surfaces of Finely Divided Metal Oxides. *Colloids Surfaces A Physicochem. Eng. Asp.* **2001**, *190*, 261–274.
- (45) Bezrodna, T.; Puchkovska, G.; Shimanovska, V.; Chashechnikova, I.; Khalyavka, T.; Baran, J. Pyridine-TiO<sub>2</sub> Surface Interaction as a Probe for Surface Active Centers Analysis. *Appl. Surf. Sci.* **2003**, *214*, 222–231.
- (46) Nanayakkara, C. E.; Dillon, J. K.; Grassian, V. H. Surface Adsorption and Photochemistry of Gas-Phase Formic Acid on TiO<sub>2</sub> Nanoparticles: The Role of Adsorbed Water in Surface Coordination, Adsorption Kinetics, and Rate of Photoproduct Formation. *J. Phys. Chem. C* **2014**, *118*, 25487–25495.
- (47) Hug, S. J.; Bahnemann, D. Infrared Spectra of Oxalate, Malonate and Succinate Adsorbed on the Aqueous Surface of Rutile, Anatase and Lepidocrocite Measured with in Situ ATR-FTIR. *J. Electron Spectros. Relat. Phenomena* **2006**, *150*, 208–219.
- (48) Mudunkotuwa, I. A.; Grassian, V. H. Histidine Adsorption on TiO<sub>2</sub> Nanoparticles: An Integrated Spectroscopic, Thermodynamic, and Molecular-Based Approach toward Understanding Nano-Bio Interactions. *Langmuir* **2014**, *30*, 8751–8760.
- (49) Parikh, S. J.; Kubicki, J. D.; Jonsson, C. M.; Jonsson, C. L.; Hazen, R. M.; Sverjensky, D. a; Sparks, D. L. Evaluating Glutamate and Aspartate Binding Mechanisms to Rutile ( $\alpha$ -TiO<sub>2</sub>) via ATR-FTIR Spectroscopy and Quantum Chemical Calculations. *Langmuir* **2011**, *27*, 1778–1787.
- (50) Roddick-Lanzilotta, A.; Connor, P.; McQuillan, A. An in Situ Infrared Spectroscopic Study of the Adsorption of Lysine to TiO<sub>2</sub> from an Aqueous Solution. *Langmuir* **1998**, 6479–6484.
- (51) Roddick-Lanzilotta, A.; McQuillan, A. An in Situ Infrared Spectroscopic Study of Glutamic Acid and of Aspartic Acid Adsorbed on TiO<sub>2</sub>: Implications for the Biocompatibility of Titanium. *J. Colloid Interface Sci.* **2000**, *227*, 48–54.
- (52) Hay, M. B.; Myneni, S. C. B. Structural Environments of Carboxyl Groups in Natural Organic Molecules from Terrestrial Systems. Part 1: Infrared Spectroscopy. *Geochim. Cosmochim. Acta* **2007**, *71*, 3518–3532.
- (53) Max, J. J.; Chapados, C. Infrared Spectroscopy of Aqueous Carboxylic Acids: Comparison between Different Acids and Their Salts. *J. Phys. Chem. A* **2004**, *108*, 3324–3337.
- (54) Barth, A. The Infrared Absorption of Amino Acid Side Chains. *Prog. Biophys. Mol. Biol.* **2000**, *74*, 141–173.
- (55) Ilharco, L.; Garcia, A. Infrared Approach to the Study of Adsorption on

- Cellulose: Influence of Cellulose Crystallinity on the Adsorption of Benzophenone. *Langmuir* **1997**, *7463*, 4126–4132.
- (56) Lautié, A.; Lautié, M. F.; Gruger, A.; Fakhri, S. A. Etude Par Spectrométrie I.r. et Raman de L'indole et de L'indolizine. Liaison Hydrogène NH ... π. *Spectrochim. Acta Part A Mol. Spectrosc.* **1980**, *36*, 85–94.
- (57) Takeuchi, H.; Harada, I. Normal Coordinate Analysis of the Indole Ring. *Spectrochim. Acta Part A Mol. Spectrosc.* **1986**, *42*, 1069–1078.
- (58) Mudunkotuwa, I. A.; Grassian, V. H. Citric Acid Adsorption on TiO<sub>2</sub> Nanoparticles in Aqueous Suspensions at Acidic and Circumneutral pH: Surface Coverage, Surface Speciation, and Its Impact on Nanoparticle–Nanoparticle Interactions. *J. Am. Chem. Soc.* **2010**, *132*, 14986–14994.
- (59) Sathyanarayana, D. N.; Raja, S. V. K.; Shunmugam, R. Vibrational Spectra of Imidazoline-2-Thione and Imidazoline-2-One. *Spectrochim. Acta Part A Mol. Spectrosc.* **1987**, *43*, 501–506.
- (60) Bharti, B. *Adsorption, Aggregation and Structure Formation in Systems of Charged Particles*; Springer International Publishing, 2014.
- (61) Iwafuji, Y.; McNamee, C. E. Formation of Langmuir Monolayers of Titanium Dioxide Nanoparticles at Air/Aqueous Interfaces by the Addition of Ions to the Subphase: Effect of Ion Concentration and Type. *J. Phys. Chem. B* **2015**, *119*, 12308–12317.
- (62) Nakatsuji, H.; Yoshimoto, M.; Umemura, Y.; Takagi, S.; Hada, M. Theoretical Study of the Chemisorption and Surface Reaction of HCOOH on a ZnO(1010) Surface. *J. Phys. Chem.* **1996**, *100*, 694–700.
- (63) Montoya, J. F.; Bahnemann, D. W.; Peral, J.; Salvador, P. Catalytic Role of TiO<sub>2</sub> Terminal Oxygen Atoms in Liquid-Phase Photocatalytic Reactions: Oxidation of Aromatic Compounds in Anhydrous Acetonitrile. *Chemphyschem* **2014**, *15*, 2311–2320.
- (64) Ahmed, A. Y.; Oekermann, T.; Lindner, P.; Bahnemann, D. Comparison of the Photoelectrochemical Oxidation of Methanol on Rutile TiO<sub>2</sub> (001) and (100) Single Crystal Faces Studied by Intensity Modulated Photocurrent Spectroscopy. *Phys. Chem. Chem. Phys.* **2012**, *14*, 2774.

## 2.9. Supporting Information

1. Distribution of imazapyr species as a function of the pH value; 2. Details of the experimental ATR-FTIR set-up; 3. Plots of concentration vs. time for the photocatalytic degradation of imazapyr; 4. Typical ATR-FTIR spectra of aqueous 12 mmol L<sup>-1</sup> solutions of imazapyr, view of full spectral range.

1. The mathematical model proposed by Carrier *et al.*<sup>1</sup> has been used to calculate the distribution of imazapyr species (Figure 1 of the manuscript). The thus derived species distribution is summarized in Table 1 taking into account the pH values employed in this study.

**Table S2.1.** Distribution of Imazapyr Species as a Function of the pH Value.

Imazapyr species %	pH 3	pH 5	pH 7	pH 9
[II]	5.72	0.02	3E-07	3E-11
[III]	75.36	3.82	0.03	0.0003
[IV]	18.92	96.16	99.96	99.99

2. The experimental setup is described in detail in the experimental section, the solution compartment used in the study is depicted in (Figure S1).

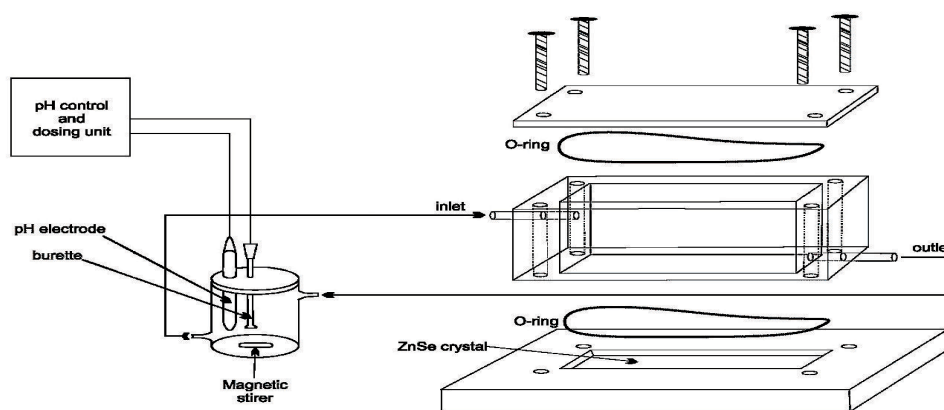


**Figure S2.1.** Details of the experimental set-up employed (ATR unit and solution compartment)

3.

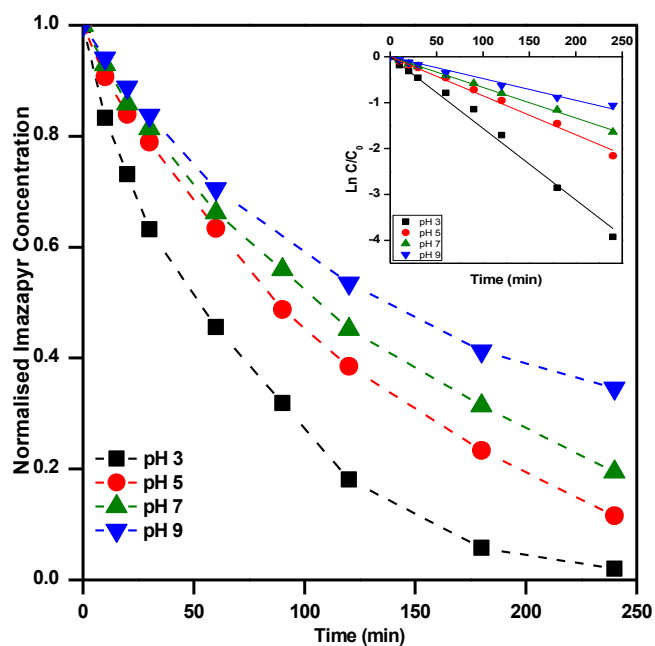


**Figure S2.2.** Plots of concentration vs. time for the photocatalytic degradation of imazapyr at different pH values. (Inset) first-order kinetic linear fitting of the photocatalytic degradation of imazapyr.

4.

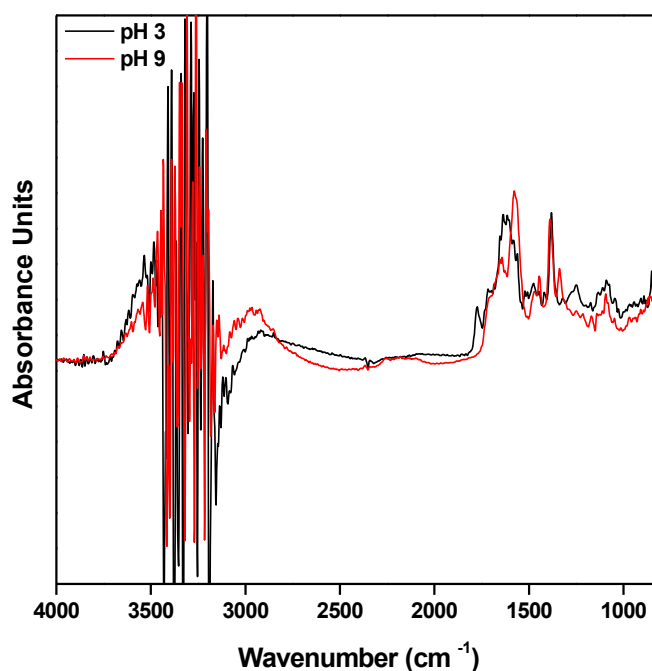


**Figure S2.3.** Typical ATR-FTIR spectra of aqueous 12 mmol L<sup>-1</sup> solutions of imazapyr in the absence of a TiO<sub>2</sub> film at pH 3 (black line) and at pH 9 (red line). These data correspond to the same experimental conditions of spectra plotted in

Figure 2.2. but are shown here for a view of the full spectral range extending from 4000 to 845 cm<sup>-1</sup>.

### References

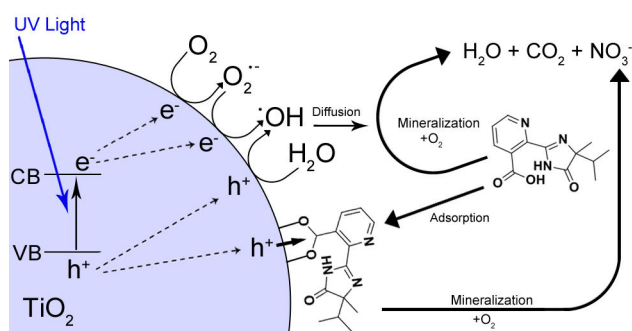
- (1) Carrier, M.; Perol, N.; Herrmann, J.-M.; Bordes, C.; Horikoshi, S.; Paise, J. O.; Baudot, R.; Guillard, C. Kinetics and Reactional Pathway of Imazapyr Photocatalytic Degradation Influence of pH and Metallic Ions. *Appl. Catal. B Environ.* **2006**, *65*, 11–20.

## Chapter 3

# Do The Initial Degradation Rates Correlate with The Adsorption Kinetics and Isotherms?

M. Faycal Atitar, Asmae Bouziani, Ralf Dillert, Mohamed El azzouzi and Detlef W. Bahnemann

Published in Catalysis Science & Technology, 2018, 8, 985-995.



### 3.1. Abstract

The objective of this work is to correlate the photocatalytic degradation of the herbicide imazapyr in aqueous suspensions of the commercially available Evonik Aeroxide TiO<sub>2</sub> P25 with the dark adsorption phenomena considering both the equilibrium state and the kinetics of adsorption. The results of this study show that the adsorption of imazapyr onto the TiO<sub>2</sub> surface is a second-order reaction and satisfies the criteria required by the Langmuir model. The adsorbed amount of imazapyr is found to be high at pH 3 and to decrease with increasing pH. The kinetics of the photocatalytic degradation of imazapyr were analysed taking into account the effect of the pH as well as of the catalyst mass concentration. However, special attention was focussed on the influence of the reactant concentration on the reaction rate. The Langmuir-Hinshelwood model fitting revealed that the apparent adsorption constant obtained under irradiation is significantly larger than the adsorption constant obtained in the dark. The initial reaction rates of the photocatalytic imazapyr degradation were larger than the initial adsorption rates of the probe molecule on the TiO<sub>2</sub> surface. It is therefore concluded, that the photocatalytic imazapyr degradation does not follow necessarily a Langmuir-Hinshelwood mechanism despite the fact that a rate law having the mathematical form of the Langmuir-Hinshelwood rate law was successfully used to describe the observed dependence of the initial reaction rates on the initial concentrations. A Langmuir-Hinshelwood mechanism for the photocatalytic imazapyr degradation is compatible only with the additional assumption that the rate constant of adsorption increases by irradiation with UV light.

### 3.2. Introduction

TiO<sub>2</sub> photocatalysts in their different forms and polymorphs have attracted considerable attention in the past decades because they are highly photo-reactive, cheap, non-toxic, chemically and biologically inert, and photo-stable. These properties allow possible applications for the purification of polluted water and air, the development of self-cleaning super-hydrophilic surfaces, and the conversion of energy.<sup>1-3</sup> In the past 25 years great advances have been made turning TiO<sub>2</sub> photocatalysis into an interesting issue not only for industrial applications but also



for fundamental research. However, there are still several issues, approaches, and mechanisms in the field of photocatalysis that remain unclear.

The photocatalytic reaction is assumed to occur on the surface of the photocatalyst, and therefore a large adsorption capacity is expected to favour the reaction kinetics.<sup>4</sup> Both the organic compound being degraded and the TiO<sub>2</sub> surface affect the adsorption process and the photocatalytic reaction. Furthermore, it was reported that a pre-adsorption of reactants onto the TiO<sub>2</sub> surface in the dark preceding the photocatalytic reaction results in a more efficient interfacial electron transfer process.<sup>5,6</sup> *Bahnemann et al.* have used laser flash photolysis experiments to investigate the kinetics of the interfacial electron transfer between an excited semiconductor and electron donor and/or acceptor molecules present in the surrounding aqueous phase. These authors found that the adsorption of the probe compounds dichloroacetate and thiocyanate on the TiO<sub>2</sub> surface prior to the band gap excitation was a prerequisite for efficient hole scavenging.<sup>7</sup>

Friedmann et al. have discussed the parameters affecting the kinetics and mechanisms of the photocatalytic process. These parameters can be subdivided into those that are intrinsic to the photocatalytic material and those that are extrinsic being influenced by the surrounding environment and conditions (e.g. pH, ionic strength, and the nature of the solvent). All these parameters mentioned before affect the adsorption rate and type, as well as the photocatalytic reaction rate. However, the specific mode of action of a given parameter on the photocatalytic performance of a TiO<sub>2</sub> sample is difficult to characterize since many of the before mentioned parameters are coupled.<sup>4</sup>

The assessment of the reaction kinetics is fundamental to evaluate and compare the performance of the catalyst. Furthermore, kinetic analysis can also be employed to prove the validity of a proposed mechanism.<sup>8,9</sup> The interpretation of the results of the kinetics studies of TiO<sub>2</sub> photocatalytic systems for water treatment and the elucidation of the underlying mechanisms have relied largely on the Langmuir–Hinshelwood (classical or modified) rate laws. Details of this kinetics with its underlying adsorption model (Langmuir-Hinshelwood mechanism) have been critically discussed in several publications.<sup>1,10–18</sup>

It seems that most authors suppose that a heterogeneous photocatalytic reaction is a bimolecular reaction between two species present on the surface of the photocatalyst. The substrate to be oxidized, of course, is one of the surface-bound species while

either a valence band hole or an OH radical on the surface of the semiconductor is the second species. For a batch system the rate law is then to be written as

$$\frac{dC_t}{dt} = \frac{k'_r n_{\text{ox}} n_{\text{os}}}{V} \quad (3.1)$$

with  $C_t$ ,  $t$ ,  $V$ ,  $k'_r$ ,  $n_{\text{ox}}$  and  $n_{\text{os}}$  being the concentration of the probe molecule dissolved in the aqueous phase, the irradiation time, the volume of the suspension, the reaction rate constant (in  $\text{mol}^{-1} \text{s}^{-1}$ ), the total amount of the oxidizing species in the whole reaction volume, and the total amount of adsorbed probe molecules (both in mol), respectively. Using a pseudo-steady state approach,<sup>11,12</sup> this rate law can be written as

$$\frac{dC_t}{dt} = k_r \frac{K_{\text{LH}} C_t}{1 + K_{\text{LH}} C_t} \quad (3.2)$$

with the parameter

$$K_{\text{LH}} = \frac{k_a}{k_d + k'_r n_{\text{ox}}} \quad (3.3)$$

and the maximum reaction rate  $k_r$ , the rate constant of adsorption  $k_a$ , and the rate constant of desorption  $k_d$  (see Chapter SI-3.1 in the ESI).

Eqn (3.2) with eqn (3.3) corresponds to the rate law as derived for a thermal catalytic reaction which proceeds according to the ‘‘Langmuir-Hinshelwood single-site mechanism’’.<sup>19</sup> At this point, it should be noted that in 1926 Hinshelwood, and later Schwab, interpreted this rate law in its mathematically equivalent form  $\frac{dp}{dt} = \frac{k \cdot p}{1 + b \cdot p}$

(derived for catalytic reactions of gases on surfaces) on the basis of the Langmuir adsorption isotherm.<sup>20-24</sup> In 1931, Schwab also pointed out that this rate law is also suitable to analyse the kinetics of catalytic reactions of organic compounds in colloidal solutions of metals.<sup>24</sup> In 1939, Gopala Rao expressly referred to the Langmuir adsorption isotherm to explain the experimentally observed photocatalytic oxidation kinetics of ammonia in irradiated  $\text{TiO}_2$  suspension.<sup>25</sup>

It is usually assumed that the photocatalytic process is a two-step process comprising a fast adsorption/desorption equilibrium and subsequently a slow surface step, i.e.,  $k_d \gg k'_r n_{\text{ox}}$ . Consequently, the kinetic parameter  $K_{\text{LH}}$  becomes equal to the Langmuir adsorption constant  $K_L = k_a/k_d$ , which is determined from the adsorption isotherms. However, eqn (3.3) shows that the parameter  $K_{\text{LH}}$  is less than or equal to

$K_L$ . Accordingly, only a few authors have reported experimental  $K_{LH}$  values being larger than the corresponding  $K_L$  values.<sup>26–35</sup>

It is understood that the derived equation assumes that the adsorption rate of the probe molecules is always larger than the reaction rate, i.e., the reaction is not inhibited by mass transfer.

Papers reporting about the correlation between the photocatalytic degradation rate of an organic substrate and both its adsorption isotherms and adsorption kinetics are rare.<sup>31,36–39</sup> Therefore, we have carried out respective investigations with imazapyr [2-(4-isopropyl-4-methyl-5-oxo-2-imidazolin-2-yl) nicotinic acid] as the probe molecule. Imazapyr is a non-selective herbicide used for the control of weeds.<sup>40</sup> Many researchers have investigated the photocatalytic degradation of imazapyr covering the influence of several operating parameters using commercial TiO<sub>2</sub> powders, mainly P25. The effect of the pH of the suspension, the temperature, the addition of electron acceptors such as potassium persulfate and hydrogen peroxide, as well as the presence of heavy metals on the imazapyr degradation kinetics have been studied.<sup>40–43</sup>

Recently *Atitar et al.* have investigated the adsorption of imazapyr onto the TiO<sub>2</sub> surface by means of ATR-FTIR spectroscopy. The authors have concluded that the favoured binding mode of imazapyr to the TiO<sub>2</sub> surface is the bridging mode via the carboxylic group. Besides of that, the authors proposed that the bridging oxygen in the neighbourhood of the adsorbed species serves as trap for a hole generated upon the absorption of UV light.<sup>44</sup> But it has been reported by *Carrier et al.* that also OH radicals play an important role in the photocatalytic degradation of imazapyr. The authors have determined the primary position for OH radical (being besides other properties an electrophilic species) attack on imazapyr by means of electron density calculations, and reported that this attack occurs preferably at the atoms with the largest electron density. Furthermore, these authors have presented a detailed degradation pathway of imazapyr.<sup>42</sup>

However, the importance of the adsorption for the overall photocatalytic process is still doubtful. No uniform information concerning the optimum pH for the photocatalytic degradation of imazapyr using TiO<sub>2</sub> could be extracted from the literature. The highest degradation rates have been reported to occur at pH 3<sup>44</sup>, and at pH 3.8<sup>42</sup>; other research groups have reported a maximum value at pH 4<sup>43</sup>, and at pH 4.3<sup>41</sup>, respectively.

The aim of this work is to find a possible correlation between the photocatalytic degradation rate and the adsorption behaviour of imazapyr at the TiO<sub>2</sub> surface. Therefore, the kinetics of the photocatalytic oxidation of imazapyr as well as the kinetics of the imazapyr adsorption in the dark have been investigated at different pH values to reveal the role of the adsorption of imazapyr onto the TiO<sub>2</sub> surface in the photocatalytic degradation process.

### 3.3. Experimental section

#### Materials

Imazapyr (Pestanal, purity > 99%) was purchased from Sigma-Aldrich (Germany). All solvents used for HPLC (High Performance Liquid Chromatography) analysis were chromatography grade and were also obtained from Sigma-Aldrich (Germany); all other chemicals were of analytical grade and used without any further purification. The water used in all experimental runs was deionized water (resistivity = 18.2 MΩ cm) collected from a Sartorius Arium 611 deionizer.

The commercial photocatalyst used in this study was Evonik Aeroxide P25 (mainly anatase with a rutile content of ca. 20%, a primary particle size of around 21 nm, and a BET surface area of 50 m<sup>2</sup> g<sup>-1</sup>).

#### Methods

**Photocatalytic degradation.** For the photocatalytic degradation studies 100 mL of aqueous imazapyr solutions containing varying initial concentrations of the probe molecule ( $20 \leq C_0 \leq 200 \mu\text{mol L}^{-1}$ ) and 0.01 mol L<sup>-1</sup> KClO<sub>4</sub> were irradiated in the presence of the desired amounts of TiO<sub>2</sub> after adjusting the initial pH by the addition of KOH or HNO<sub>3</sub>. Prior to the irradiation, the suspensions were shaken in the dark for at least 3 hours to achieve the adsorption equilibrium of the organic solute on the TiO<sub>2</sub> surface resulting in equilibrium imazapyr concentrations  $C_{e,0} < C_0$ .

All photocatalytic degradation experiments were performed using a Pyrex-Glass® cylindrical reactor irradiated from the top with an assembly of six UV-A lamps (Philips Cleo 15 W; emission,  $300 < \lambda < 400 \text{ nm}$ ;  $\lambda_{\text{max}} = 365 \text{ nm}$ ) under continuous stirring. A scheme of the experimental set-up is shown in Chapter SI-3.2 in the ESI. For the kinetic studies, samples were taken at regular time intervals and were analyzed after filtration by high performance liquid chromatography (HPLC). The temperature (21±1°C) remained constant during the experimental runs.

**Adsorption isotherms and kinetics.** Adsorption experiments were performed employing stock solutions of imazapyr in deionized water with the desired concentration of the probe molecule ( $100 \leq C_0 \leq 2000 \mu\text{mol L}^{-1}$ ). Known amounts of these stock solutions were added to 10 mL  $\text{TiO}_2$  P25 suspensions of different  $\text{TiO}_2$  mass concentrations  $C_c$  prepared in  $0.01 \text{ mol L}^{-1} \text{ KClO}_4$ . The suspensions were kept for 24 hours at constant temperature ( $21 \pm 1^\circ\text{C}$ ) in the dark under agitation. The pH of the suspensions was adjusted at the beginning and in regular time intervals by the addition of KOH or  $\text{HNO}_3$ . Samples were taken in appropriate time intervals, centrifuged for 5 minutes (4000 rpm) and filtered with a  $0.45 \mu\text{m}$  cellulose nitrate membrane filter (Macherey und Nagel) prior to HPLC analysis.

### **Analysis**

Samples were analyzed by HPLC using an ECOM spol. S.r.o. instrument fitted with a LCP 4100 pump, a LCD 2084 UV spectrophotometer, and a  $50 \mu\text{L}$  injection loop. A C-18 Inertsil ODS2  $150 \text{ \AA}$   $5 \mu\text{m}$   $250 \times 4.6 \text{ mm}$  column was used with a pre-column ( $10 \times 4.0 \text{ mm}$  Inertsil ODS2  $100 \text{ \AA}$   $5 \mu\text{m}$ ) in the cartridge holder. An isocratic acetonitrile/water mixture (60/40 vol. %) with phosphoric buffer (pH 3) was used as the mobile phase. The flow rate was adjusted at  $0.8 \text{ mL min}^{-1}$  and the detection wavelength at 254 nm. The calibration curves ( $R^2 \geq 0.999$ ) were prepared in the concentration range from 10 to  $50 \mu\text{mol L}^{-1}$ . The detection limit for imazapyr was found to be  $3 \mu\text{mol L}^{-1}$ .

All experimental runs to investigate the adsorption kinetics, the adsorption isotherms, and the photodegradation kinetics were performed in 2–3 replicates. This allows values to be obtained with an experimental error  $\leq 10\%$ . This error is considered to be the sum of all random experimental errors including the HPLC instrument error and the error intrinsic to mathematical calculations from the experimental concentration vs. time plots.

## **3.4. Results**

### **Photocatalytic degradation of imazapyr**

The photocatalytic degradation of imazapyr has been studied in a series of experimental runs at constant reaction volume, temperature, light intensity, and photocatalyst mass concentration, but varying the pH and the concentration of the probe molecule imazapyr in the suspension ( $20 \leq C_0 \leq 200 \mu\text{mol L}^{-1}$ ). The mass concentration of the  $\text{TiO}_2$  photocatalyst in these experimental runs was  $C_c = 2.5 \text{ g L}^{-1}$

because this concentration was found in preceding investigations to be the optimum catalyst mass concentration for the photocatalytic imazapyr degradation (see Chapter SI-3.3 in the ESI).

Fig. 3.1 shows a typical experimental dataset of the photocatalytic decomposition of imazapyr. The data points of all experimental runs were well fitted using an exponential decay model. Thus, the reaction rate  $r_t$  of the photocatalytic oxidation of imazapyr can obviously be described by a first order rate law,

$$r_t = \frac{dC_t}{dt} = k_{obs}C_t \quad (3.4)$$

where  $k_{obs}$  is the observed first-order rate constant,  $t$  is the irradiation time, and  $C_t$  is the actual concentration of the probe molecule in the aqueous suspension at time  $t$ . For each experimental run, the rate constant was determined from the plot of the natural logarithm of the pollutant concentration as a function of irradiation time employing the equation

$$\ln \frac{C_t}{C_{e,0}} = k_{obs}t \quad (3.5)$$

where  $C_{e,0}$  is the equilibrium concentration of the probe molecule in the suspension at the start of the UV(A) irradiation ( $t = 0$ ). The rate constants were found to decrease with increasing initial imazapyr concentrations  $C_{e,0}$  while the initial reaction rates  $r_{r,0}$  which were calculated employing  $r_{r,0} = k_{obs}C_{e,0}$  increased (*cf.* Table S3.1 in the ESI).

The influence of the initial concentration of the solute on the actual photocatalytic degradation rate of most organic compounds is usually rationalized employing a Langmuir–Hinshelwood type rate law

$$r_t = -\frac{dC_t}{dt} = k_r \frac{K_{LH}C_t}{1+K_{LH}C_t} \quad (3.6)$$

where the kinetic parameter  $k_r$  is the maximum photocatalytic reaction rate, and  $K_{LH}$  is the apparent adsorption constant of the probe molecule onto the  $\text{TiO}_2$  surface.<sup>10,45–47</sup>

Inserting the eqn (3.4) in (3.6) yields with  $C_t = C_{e,0}$  at  $t = 0$

$$r_{r,0} = k_{obs}C_{e,0} = k_r \frac{K_{LH}C_{e,0}}{1+K_{LH}C_{e,0}} \quad (3.7)$$

which yields after rearrangement the linear equation

$$\frac{1}{k_{obs}} = \frac{1}{k_r K_{LH}} + \frac{C_{e,0}}{k_r} \quad (3.8)$$

thus allowing the determination of the kinetic parameters  $k_r$  and  $K_{LH}$  from the slopes and the intercepts of the respective  $1/k_{obs}$  vs.  $C_{e,0}$  plots. Based on this equation, the

values of  $k_{\text{obs}}$  were plotted vs. the different initial imazapyr concentration  $C_{e,0}$  (Fig. 3.2). The kinetic parameters  $k_r$  and  $K_{\text{LH}}$  at pH 3, pH 5, and pH 7 obtained from these graphs are given in Table 3.1.

From a mathematical point of view the relation  $k_r \frac{K_{\text{LH}} C_t}{1 + K_{\text{LH}} C_t} \cong k_r K_{\text{LH}} C_t$  holds when the condition  $K_{\text{LH}} C_t \ll 1$  is fulfilled. With this boundary condition the Langmuir-Hinshelwood type rate law (eqn (3.6)) can be approximated by an apparent first-order rate law as it is given in eqn (3.4). With the  $K_{\text{LH}}$ -values given in Table 1 and the initial imazapyr concentrations employed in this study ( $C_{e,0} > 15 \mu\text{mol L}^{-1}$ ) the product  $K_{\text{LH}} C_t$  is calculated to be always larger than 0.55 at  $t = 0$ . The imazapyr concentration must therefore become considerably smaller until the condition for a first-order kinetics is fulfilled. The first-order kinetics observed here (Fig. 3.1) thus obviously do not correspond to the assumption of the limiting case of the Langmuir-Hinshelwood kinetics.

**Table 3.1.** Langmuir-Hinshelwood fitting parameters.

pH	3	5	7
$k_r / \mu\text{mol L}^{-1} \text{min}^{-1}$	2.97	2.95	1.24
$K_{\text{LH}} / 10^{-3} \text{L } \mu\text{mol}^{-1}$	56.5	38.3	129
$R^2$	0.987	0.982	0.971

Experimental conditions:  $20 \leq C_0 \leq 200 \mu\text{mol L}^{-1}$ ,  $\text{TiO}_2$  P25,  $C_c = 2.5 \text{ g L}^{-1}$ ,  $V = 100 \text{ mL}$ .

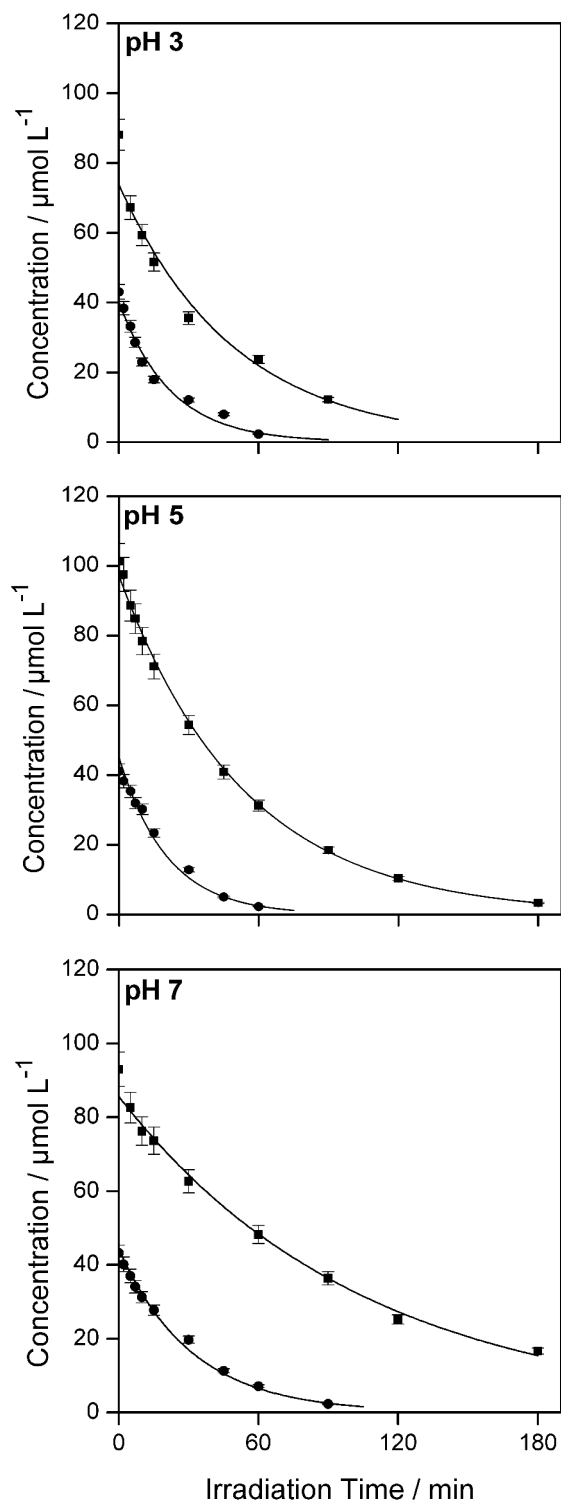


**Figure 3.1.** Typical plots of the imazapyr concentration  $C_t$  vs. irradiation time for the photocatalytic degradation at different pH values in the presence of Aeroxide  $\text{TiO}_2$  P25. The lines have been calculated assuming first-order kinetics. Experimental conditions:  $C_0 = 110$  and  $50 \mu\text{mol L}^{-1}$ ,  $C_c = 2.5 \text{ g L}^{-1}$ ,  $V = 100 \text{ mL}$ .



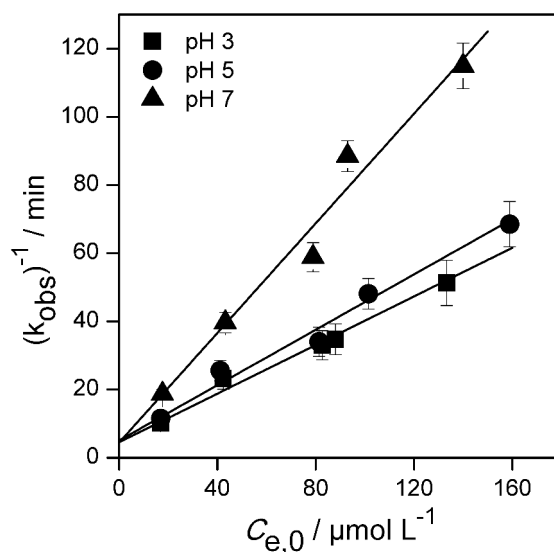


**Figure 3.2.** Langmuir-Hinshelwood plot of the reciprocal first order rate constant vs. the initial equilibrium imazapyr concentration. Experimental conditions:  $20 \leq C_0 \leq 200 \mu\text{mol L}^{-1}$ ,  $\text{TiO}_2$  P25,  $C_c = 2.5 \text{ g L}^{-1}$ ,  $V = 100 \text{ mL}$ .

### Adsorption isotherms

Adsorption isotherms have been measured at constant  $\text{TiO}_2$  catalyst mass concentration and constant suspension volume. However, the pH of the suspensions (pH 3, 5, and 7) and the initial concentration of imazapyr ( $100 \leq C_0 \leq 2000 \mu\text{mol L}^{-1}$ ) has been varied. The data are presented by the equilibrium isotherm value, which basically indicate the amount of substrate adsorbed (adsorbate) by a known mass of the adsorbent, i.e.,  $\text{TiO}_2$  P25, in the equilibrium. The adsorbed amount of imazapyr in the equilibrium was calculated employing

$$q_e = \frac{C_0 - C_e}{m} V \quad (3.9)$$

where  $C_0$  is the initial concentration,  $C_e$  is the equilibrium concentration of the adsorbate in the suspension,  $m$  is the catalyst mass, and  $V$  is the volume of the suspension. The parameters  $C_0$ ,  $m$ , and  $V$  are known quantities while  $C_e$  is determined by HPLC analysis after 24 hours shaking in the dark.

Fig. 3.3 shows the amount of imazapyr adsorbed at the  $\text{TiO}_2$  surface plotted *versus* the concentration of the probe molecule in the aqueous phase after the adsorption equilibrium has been established. Langmuir-Hinshelwood kinetics which has been employed above to describe the time course of the imazapyr concentration during photocatalytic degradation experiments are based on the assumption that the

absorption of the probe molecule can be described by the Langmuir adsorption isotherm

$$q_e = q_m \frac{K_L C_e}{1 + K_L C_e} \quad (3.10)$$

$q_m$  is the maximum monolayer capacity of adsorbent ( $\mu\text{mol g}^{-1}$ ) and can also be interpreted as the total number of binding sites that are available for sorption.  $K_L$  is the Langmuir adsorption constant ( $\text{L } \mu\text{mol}^{-1}$ ). Rearrangement of eqn (3.10) yields

$$\frac{1}{q_e} = \frac{1}{q_m K_L} \times \frac{1}{C_e} + \frac{1}{q_m} \quad (3.11)$$

thus allowing the determination of the parameters  $q_m$  and  $K_L$  from the slopes and the intercepts of the respective  $1/q_e$  vs.  $1/C_e$  (Fig. 3.4). The thus calculated values are tabulated in Table 3.2.

**Table 3.2.** Parameters for the Langmuir adsorption of imazapyr onto  $\text{TiO}_2$  at different pH values, and the ratio between  $K_{LH}$  and  $K_L$ .

pH	3	5	7
$q_m / \mu\text{mol g}^{-1}$	30.8	40.0	22.8
$K_L / 10^{-3} \text{ L } \mu\text{mol}^{-1}$	4.52	2.23	1.46
$R^2$	0.997	0.987	0.993
$K_{LH} / K_L$	12.5	17.1	88.4

Experimental conditions:  $100 \leq C_0 \leq 2000 \mu\text{mol L}^{-1}$ ,  $\text{TiO}_2$  P25,  $C_c = 5 \text{ g L}^{-1}$ ,  $V = 100 \text{ mL}$ .

The analysis of the experimental data employing the Freundlich model of adsorption resulted also in good fitting of the experimental data ( $0.915 \leq R^2 \leq 0.996$ , see Chapter SI-3.5). However, the Langmuir model was slightly better than the Freundlich model. The Langmuir isotherm model was found suitable to describe the imazapyr adsorption equilibrium ( $0.987 \leq R^2 \leq 0.997$ ). The maximum monolayer capacity of adsorbent  $q_m$  increased with increasing the pH value from pH 3 to pH 5, and decreased again at pH 7. The Langmuir adsorption constant  $K_L$  is a measure for the affinity between adsorbate and adsorbent with its reciprocal value yielding the concentration at which half of the maximum adsorption capacity of the adsorbent is reached.<sup>48</sup> The constant  $K_L$  decreased with increasing the pH from 3 to 7, indicating that the adsorption density was higher at a lower pH.

It becomes obvious that the values for  $K_{LH}$  which have been calculated from the concentration vs. time plots of the photocatalytic degradation experiments

(Table 3.1) are larger by a factor 10–100 than the values for the adsorption constant  $K_L$  at all pH values studied here (Table 3.2).

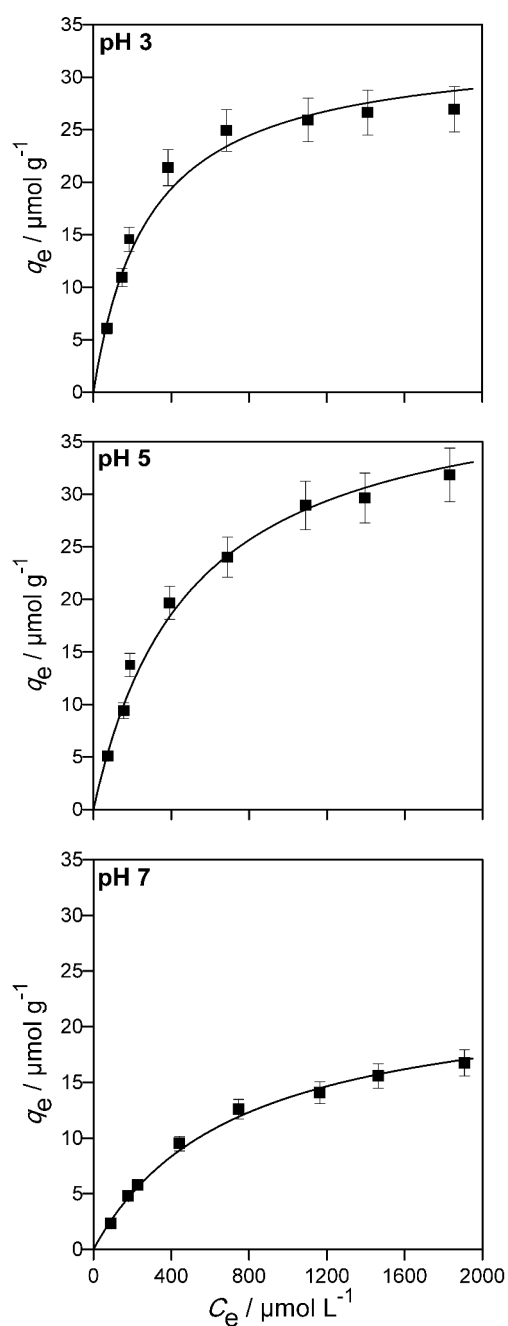


**Figure 3.3.** Adsorption isotherms of imazapyr onto Aeroxide  $\text{TiO}_2$  P25 at different pH values. The lines have been calculated employing eqn (3.10) and the data given in Table 3.2. Experimental conditions:  $100 \leq C_0 \leq 2000 \mu\text{mol L}^{-1}$ ,  $\text{TiO}_2$  P25,  $C_c = 5.0 \text{ g L}^{-1}$ ,  $V = 100 \text{ mL}$ .

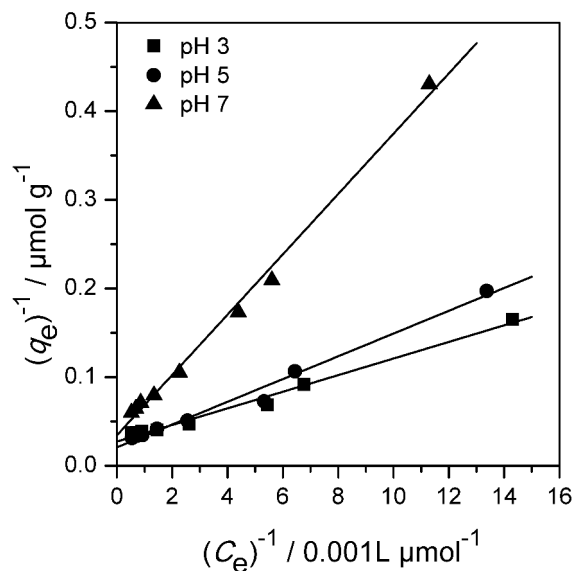


**Figure 3.4.** Langmuir plot of the reciprocal equilibrium loading vs. the reciprocal equilibrium imazapyr concentration. Experimental conditions:  $100 \leq C_0 \leq 2000 \mu mol L^{-1}$ , TiO<sub>2</sub> P25,  $C_c = 5.0 g L^{-1}$ ,  $V = 100 mL$ .

With the values for the maximum capacity of the adsorbent,  $q_m$ , given in Table 2 and the known surface area of the photocatalyst ( $50 m^2 g^{-1}$ ), the amount of adsorbed molecules per unit area is calculated as  $0.616 \mu mol m^{-2}$  ( $0.37 molecule nm^{-2}$ ),  $0.800 \mu mol m^{-2}$  ( $0.48 molecule nm^{-2}$ ) and  $0.456 \mu mol m^{-2}$  ( $0.27 molecule nm^{-2}$ ) at pH 3, pH 5 and pH 7, respectively. With the surface area and the density of the photocatalyst ( $\rho = 3.8 \times 10^6 g m^{-3}$  for anatase), a radius of 15.8 nm is calculated for a single photocatalyst particle. Consequently, a single photocatalyst particle with a surface area of approximately  $3100 nm^2$  will be fully covered by 1162, 1509 and 860 imazapyr molecules at pH 3, pH 5 and pH 7, respectively. One imazapyr molecule on the surface thus demands an area between 2.1 and  $3.2 nm^2$ . These values are in reasonable agreement with the values calculated from the geometry of an imazapyr molecule.

**Adsorption kinetics.** The kinetics of imazapyr adsorption onto Evonik Aeroxide TiO<sub>2</sub> P25 were studied at three different pH values. The respective concentration vs. time plots are presented in Fig. 3.5. The data given in this Fig. 3.5 clearly show that the adsorption of imazapyr reaches the equilibrium concentration in the liquid phase after about 120 min. The equilibrium seems to be established within 3 hours at all pH values investigated in this study. The highest adsorbed amount of imazapyr is obtained at pH 3, while this amount decreases with the increase of the pH from pH 3 to pH 7.

The obtained experimental data have been analysed using a pseudo-second order kinetic model. The pseudo second order equation based on adsorption equilibrium capacity is expressed by

$$\frac{dq_t}{dt} = k'_a(q_e - q_t)^2 \quad (3.12)$$

where  $k'_a$  is the pseudo-second-order rate constant ( $\text{g } \mu\text{mol}^{-1} \text{min}^{-1}$ ).<sup>49–51</sup> Integration with the initial condition  $q_t = 0$  at  $t = 0$  results in

$$q_t = \frac{q_e^2 k'_a t}{1 + q_e k'_a t} \quad (3.13)$$

The plots of the fitted experimental data are presented in Fig. 3.6. The calculated values of  $q_e$  and  $k'_a$  as well as the correlation coefficients are summarized in Table 3.3. Based on the obtained correlation coefficient values, it is concluded that pseudo-second order model describes well the adsorption kinetics of imazapyr onto  $\text{TiO}_2$ . The Lagergreen pseudo-first order model<sup>50,52,53</sup> was also used for the analysis of the experimental data (see Chapter SI-3.6), but the best accordance between the experimental and the calculated values were obtained with the pseudo-second-order kinetic model.

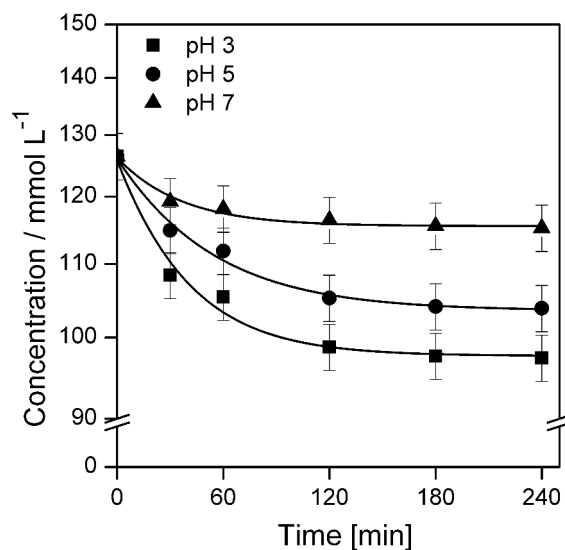


**Figure 3.5.** Plot of imazapyr concentration vs. time during the adsorption onto  $\text{TiO}_2$  P25 at different pH values. Experimental conditions:  $C_0 = 126.5 \mu\text{mol L}^{-1}$ ,  $C_c = 5 \text{ g L}^{-1}$ ,  $V = 20 \text{ mL}$ .

**Table 3.3.** Fitting parameters of the adsorption kinetics obtained at different pH values.

pH	3	5	7
$q_e / \mu\text{mol g}^{-1}$	6.52	5.41	2.41
$k_a / 10^{-3} \text{ g } \mu\text{mol}^{-1} \text{ min}^{-1}$	5.82	4.42	15.6
$R^2$	0.997	0.993	0.998

Experimental conditions:  $C_0 = 126.5 \mu\text{mol L}^{-1}$ ,  $\text{TiO}_2 \text{ P25}$ ,  $C_c = 5 \text{ g L}^{-1}$ ,  $V = 20 \text{ mL}$ .

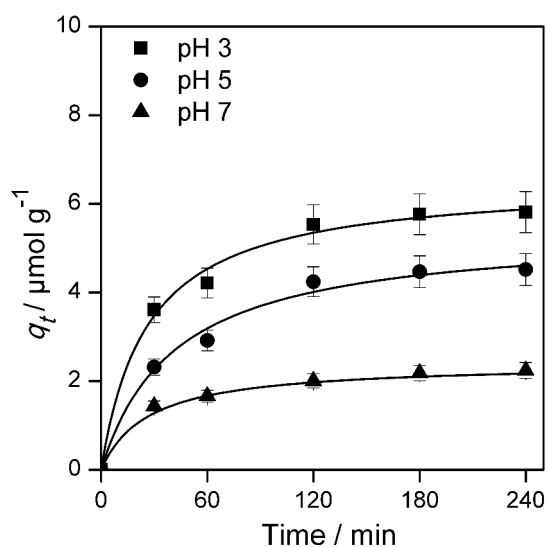


**Figure 3.6.** Plot of the amount of adsorbed species ( $q_t$ ) vs. contact time at different pH values fitted to the pseudo-second order rate law given in eqn (3.13). Experimental conditions:  $C_0 = 126.5 \mu\text{mol L}^{-1}$ ,  $\text{TiO}_2 \text{ P25}$ ,  $C_c = 5 \text{ g L}^{-1}$ ,  $V = 20 \text{ mL}$ .

### 3.5. Discussion

It has been assumed that the dark adsorption as well as the structure of the adsorbate play an important role for the photocatalytic degradation of imazapyr.<sup>42,44</sup> The favoured mode of adsorption as a bridged surface complex<sup>44</sup> followed by the direct hole oxidation of the carboxyl moiety by means of the photo-Kolbe reaction is one of the degradation pathways where adsorption is assumed to play an important role.<sup>42,44</sup> However, the latter is not the main pathway in the overall photocatalytic process. *Carrier et al.* have reported that OH radicals can attack the atoms directly at the position of the largest electron density in the imazapyr molecule.<sup>42</sup> These species (i.e., OH radicals) can be generated through the oxidative pathway by the reaction of valence band holes with  $\text{H}_2\text{O}/\text{OH}^-$  being present at the photocatalyst surface, and/or through the reductive pathway by the reaction of conduction band electrons with

adsorbed molecular oxygen. The latter is usually neglected in the photocatalytic degradation of organic pollutants and is considered to play an important role in case of imazapyr photodegradation.

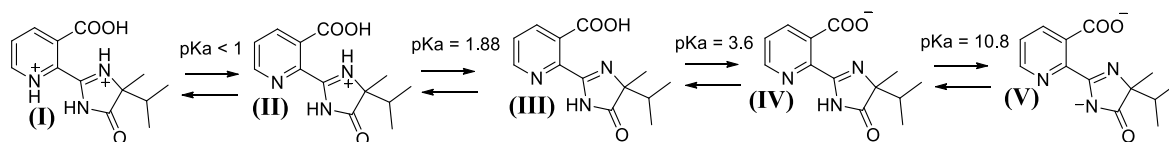
In this work, the reaction rates, the adsorption rates and the adsorption isotherms were determined at three different pH values with the aim of obtaining further insights into the mechanism underlying the photocatalytic degradation of imazapyr. The inorganic ions  $H^+$ ,  $K^+$ ,  $NO_3^-$ , and  $ClO_4^-$  have been added to the aqueous  $TiO_2$  suspensions to establish the desired pH value and to keep constant the ionic strength. It is known that inorganic ions might interact with the photocatalyst surface, thus, affecting the adsorption and the photocatalytic degradation of organic probe molecules.<sup>54-58</sup> It is, therefore, understood that the quantitative results presented here may be particularly dependent on the kind and concentration of the added anions. However, it has been reported that  $NO_3^-$  and  $ClO_4^-$  interact only weakly with the  $TiO_2$  surface and have only little effect on the rate of the photocatalytic degradation.<sup>55-58</sup> In the following discussion, it is therefore assumed that the abovementioned ions do not significantly influence the kinetics of the photocatalytic degradation or the adsorption kinetics and the adsorption equilibrium.

The photodegradation kinetics of imazapyr in  $TiO_2$  suspensions have been modeled employing a Langmuir-Hinshelwood type rate law (eqn (3.2)) which is a manifestation of the general case of saturation-type kinetics. The plots of the reciprocal rate constants vs. the reciprocal initial equilibrium concentrations  $C_{e,0}$  are shown in Fig. 3.2. The linear relationships indicate that the degradation kinetics under UV irradiation can be described by a Langmuir-Hinshelwood type rate law. The fitting parameters  $k_r$  and  $K_{LH}$  derived from this Fig. 3.2 are summarized in Table 3.1.

The analysis of the adsorption data obtained in the dark, using the Langmuir adsorption isotherms, shows a good accordance between the experimental and the calculated data. This implies that the  $TiO_2$  and the imazapyr are strongly interacting. It is worth to note that the Langmuir model assumes the adsorption energy to be uniform over the whole surface and that there is no interaction between the adsorbed species. Furthermore, only chemical interactions are considered. Thus only monolayers of the adsorbate can be formed on the surface of the adsorbent. The results of the adsorption experiments indicate that the maximum monolayer capacity

of the adsorbent  $q_m$  is  $30 \mu\text{mol g}^{-1}$  at pH 3, and increases to reach  $40 \mu\text{mol g}^{-1}$  at pH 5. Moreover, it decreases to  $23 \mu\text{mol g}^{-1}$  at pH 7.

With the data given in Table 3.2 and assuming an initial equilibrium imazapyr concentration of  $100 \mu\text{mol L}^{-1}$  in the liquid phase it is calculated that the amount of imazapyr adsorbed at the  $\text{TiO}_2$  surface in the dark is decreasing from  $9.6 \mu\text{mol g}^{-1}$  at pH 3 to  $2.9 \mu\text{mol g}^{-1}$  at pH 7. If the amount of the organic molecules (imazapyr) adsorbed on the surface of the photocatalyst is decisive for the rate of the photocatalytic degradation, it is expected that the photocatalytic degradation rate as well as the rate of imazapyr adsorption follows the same trend: at pH 3, the rates should therefore be the highest and the rates should decrease with increasing pH. In fact, this decrease of the rates with increasing pH was observed for both, the photocatalytic degradation and the adsorption, in the experimental runs performed here (Table S3.1 and Figure S3.2).



**Scheme 3.1.** Different forms of the herbicide imazapyr and the associated acid-base dissociation constants. Reprinted with permission from M. Faycal Atitar, Ralf Dillert, and Detlef W. Bahnemann. Surface Interactions between Imazapyr and the  $\text{TiO}_2$  Surface: An in Situ ATR-FTIR Study. *Journal of Physical Chemistry C*; 121:4293-4303. Copyright (2017) American Chemical Society.

Taking into account that the probe molecule imazapyr exhibits five distinct species with three  $pK_a$  values (1.88, 3.60 and 10.80) (cf. Scheme 3.1) and  $\text{TiO}_2$  has a pH dependent surface charge, any interaction between the probe molecule and the photocatalyst surface can be explained assuming attractive and repulsive forces between these species. In the range between pH 2 and pH 4 the neutral imazapyr molecule is interacting with the positively charged  $\text{TiO}_2$  surface possibly via the  $\text{COOH}$  group by dissociative adsorption. Moderate acidic conditions between pH 4 and pH 6 lead to a strong electrostatic interaction between the positively charged  $\text{TiO}_2$  surface and the organic solutes that mainly exist in their deprotonated negatively charged form (cf. Scheme 3.1). However, at a  $\text{pH} > \text{pH}_{\text{zpc}} = 6.9$  ( $\text{TiO}_2$  P25)<sup>59</sup> both imazapyr as well as the  $\text{TiO}_2$  surface are negatively charged resulting in a substantial repulsion between these species retarding adsorption which in turn will significantly negatively affect the photocatalytic degradation. Carrier *et al.* as well as Osajima *et al.* have concluded that the dependence of the degradation rate on the pH



of the suspension is due to these interactions between imazapyr species and the TiO<sub>2</sub> surface.<sup>40,42</sup> Additionally, the interaction is found to be more favourable between the deprotonated imazapyr molecule IV in Scheme 1 and the protonated TiO<sub>2</sub> surface as TiOH<sub>2</sub><sup>+</sup>.<sup>40,44</sup>

Thus, the pH dependence of the determined rates for the adsorption and the photocatalytic degradation on the basis of electrostatic interactions between imazapyr and the TiO<sub>2</sub> surface can be explained. This explanation does not contradict the assumption that the probe molecule is photocatalytically degraded by a Langmuir-Hinshelwood mechanism. However, this mechanism presupposes that the rate of the photocatalytic reaction rate is smaller than or equal to the rate of imazapyr adsorption ( $r_r \leq r_a$ , cf. eqn (3.2) in combination with eqn (3.3)). But the adsorption equilibria in the dark were only established after more than two hours (Fig. 3.5).

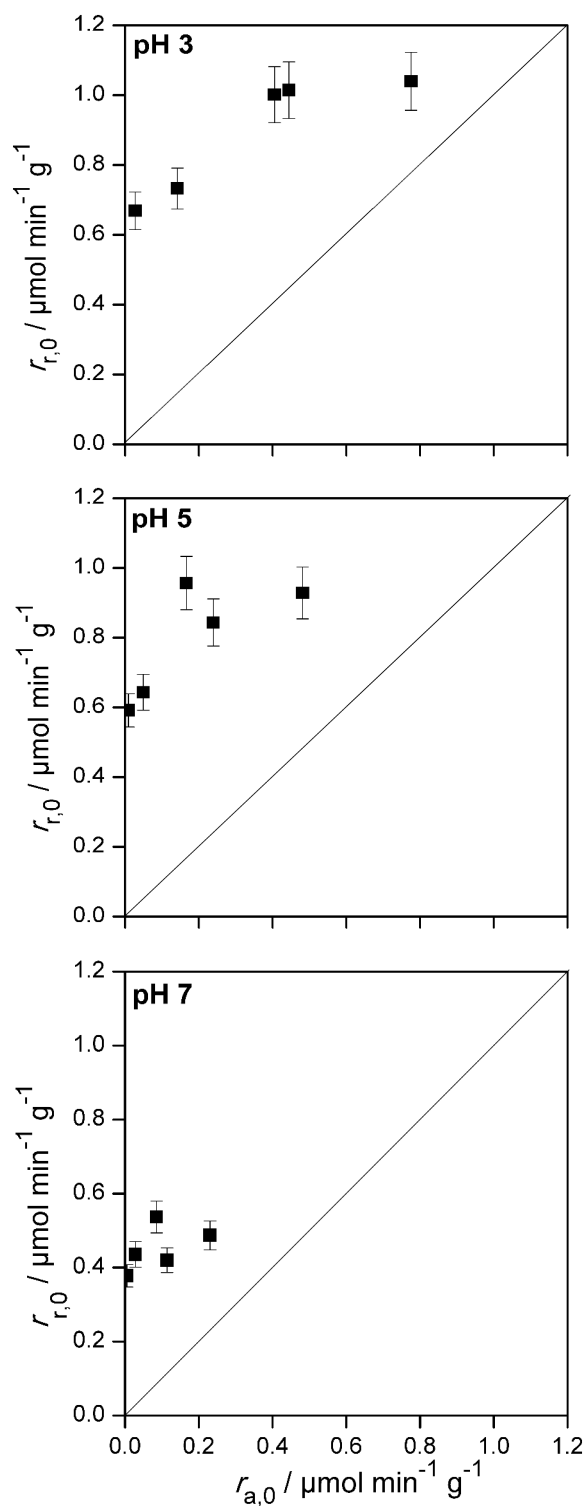


**Figure 3.7.** Initial photocatalytic degradation rate vs. initial adsorption rate of imazapyr at different pH values.

To perform the comparison between these rates, the initial reaction rates,  $r_{r,0}$ , of the imazapyr degradation have been calculated considering the concentration of the photocatalyst in the aqueous suspension (Table S3.4). The initial adsorption rates of imazapyr,  $r_{a,0}$ , have been calculated using the pseudo-second order equation

(eqn (3.12)) with the initial condition  $q_t = 0$  at  $t = 0$ . The amount of the adsorbed substrate  $q_e$  in the initial equilibrium was calculated employing eqn (3.10) and the parameters of the Langmuir isotherm (Table 3.2):

$$r_{a,0} = k'_a \left( q_m \frac{K_L C_0}{1 + K_L C_0} \right)^2 \quad (3.14)$$

The calculation of the initial adsorption rates has been performed for different initial imazapyr concentrations (Chapter SI-3.8) to reveal the correlation to the initial degradation rate, as well as the effect of the initial concentration of imazapyr. However, the comparison of the initial imazapyr degradation rates with the initial imazapyr dark adsorption rates at different pH values (Fig. 3.7) show that the initial photocatalytic reactions are always faster than the dark adsorption. In other words, the initial photocatalytic degradation rate of imazapyr was found to be 2–3 times larger than its initial adsorption rate obtained in the dark.

If one does not want to abandon the idea, that the photocatalytic degradation reaction occurs according to an Langmuir-Hinshelwood mechanism, one must demand that the rate constant of the adsorption under irradiation with UV light is drastically increasing. This would inevitably also result in a value for  $K_{LH}$  determined experimentally under exposure to UV light being greater than the value of  $K_L$  determined from adsorption isotherms in the dark.

In fact, it was found here that the kinetic parameters  $K_{LH}$  are significantly greater than the adsorption constants  $K_L$  for all investigated pH values ( $K_{LH} / K_L \geq 12.5$ , cf. Table 3.2). A ratio  $K_{LH} / K_L > 1$  (i.e.,  $K_{LH} > K_L$ ) has also been observed for other probe molecules such as salicylic acid and other substituted benzoic acids,<sup>26,31</sup> phenol,<sup>27</sup> 4-chlorophenol,<sup>28,33,34</sup> di- and tri-substituted phenols,<sup>32,34,35</sup> acetophenone,<sup>30</sup> and eosin.<sup>29</sup>

Matthews has explained the observation of  $K_{LH} > K_L$  suggesting that reactions between freely diffusing OH radicals and the organic substrate occur in the suspension in addition to the surface reaction.<sup>27</sup> Some authors have suggested this discrepancy to be due to photoadsorption followed by a fast photoreaction of the probe molecule on the TiO<sub>2</sub> surface.<sup>26,29</sup> Other authors have attributed this observation to a redistribution of the electrons under irradiation possibly altering the adsorption sites and thus the substrate-surface interaction.<sup>30,35</sup> Ollis has assumed that sites associated with the photocatalytic reaction are different to those where dark adsorption occurs. Possibly, the reactive adsorption sites are only produced under

irradiation.<sup>12</sup> The possibility that these new adsorption sites are formed by deaggregation of titanium dioxide clusters which are known to be present in aqueous suspensions should not be excluded. Deaggregation is decreasing the cluster size and increasing the available surface area of the photocatalyst,<sup>60,61</sup> and possibly yields new high-energy surfaces. It has been shown for very small particles that the dark adsorption constant depends on the particle diameter.<sup>62-64</sup> This has been rationalized with a driving force to decrease the total free energy by adsorption of molecules from the surrounding environment.<sup>62</sup> The experimental results presented here can only be reconciled with a Langmuir-Hinshelwood mechanism by assuming light-induced changes of the photocatalyst surface which have a significant effect on the adsorption of the probe molecule.

### 3.6. Conclusion

The adsorption kinetics and the adsorption-desorption equilibrium of imazapyr in TiO<sub>2</sub> aqueous suspensions have been studied in the dark. Adsorption equilibria were only established after more than two hours in the dark. The dark adsorption of imazapyr has been successfully described by a Langmuir adsorption isotherm; the maximum coverage of the surface was found to be pH-dependent. The kinetics of the adsorption in the dark was described employing a pseudo-second order rate law.

The rate of the photocatalytic degradation of imazapyr in the presence of TiO<sub>2</sub> was also found to be pH-dependent. The observed decrease of the imazapyr concentration during irradiation could be described by a first-order kinetics. The dependence of the initial reaction rate on the initial equilibrium concentration of the probe molecule in the aqueous phase could be described by a Langmuir-Hinshelwood type rate law. However, the Langmuir adsorption constants determined from the adsorption isotherms of imazapyr in the presence of TiO<sub>2</sub> in the dark were smaller than the adsorption constant determined from the analysis of the Langmuir-Hinshelwood type kinetics of the photocatalytic degradation of the probe molecule. Under the experimental conditions of this study the rate of the photocatalytic reactions were found to be always higher than the rate of the adsorption of imazapyr in the dark. In other words, the overall rate of the photocatalytic oxidation of imazapyr is not determined by the dark adsorption of the probe molecule onto the TiO<sub>2</sub> surface.

Consequently, it can be concluded that imazapyr degradation does not follow necessarily a Langmuir-Hinshelwood mechanism despite the fact that a rate law

having the mathematical form of the Langmuir-Hinshelwood rate law can be used successfully to describe the observed dependence of the initial reaction rate on the initial concentration. A Langmuir-Hinshelwood mechanism for the photocatalytic imazapyr degradation is compatible only with the additional assumption that the adsorption-desorption kinetics are also affected by irradiation with UV light, and in particular that the adsorption rate increases significantly.

### **3.7. Acknowledgments**

Mohamed Faycal Atitar gratefully acknowledges a scholarship from the DAAD in the frame of the Sandwich-Program. Financial support of the BMBF in the framework of an international collaboration between Morocco and Germany is gratefully acknowledged (FKZ: 01DH12028).

### 3.8. References

- 1 M. R. Hoffmann, S. T. Martin, W. Choi and D. W. Bahnemann, *Chem. Rev.*, 1995, **95**, 69–96.
- 2 J. Schneider, M. Matsuoka, M. Takeuchi, J. Zhang, Y. Horiuchi, M. Anpo and D. W. Bahnemann, *Chem. Rev.*, 2014, **114**, 9919–9986.
- 3 M. Grätzel, *Nature*, 2001, **414**, 338–344.
- 4 D. Friedmann, C. Mendive and D. Bahnemann, *Appl. Catal. B Environ.*, 2010, **99**, 398–406.
- 5 R. W. Matthews, *Chem. Ind.*, 1988, **4**, 28–30.
- 6 T. Tachikawa, M. Fujitsuka and T. Majima, *J. Phys. Chem. C*, 2007, **111**, 5259–5275.
- 7 D. W. Bahnemann, M. Hilgendorff and R. Memming, *J. Phys. Chem. B*, 1997, **101**, 4265–4275.
- 8 G. Camera-Roda, V. Augugliaro, A. G. Cardillo, V. Loddo, L. Palmisano, F. Parrino and F. Santarelli, *Catal. Today*, 2016, **259**, 87–96.
- 9 G. Camera-Roda, V. Loddo, L. Palmisano and F. Parrino, *Catal. Today*, 2017, **281**, 221–230.
- 10 C. S. Turchi and D. F. Ollis, *J. Catal.*, 1990, **122**, 178–192.
- 11 D. F. Ollis, *Top. Catal.*, 2005, **35**, 217–223.
- 12 D. F. Ollis, *J. Phys. Chem. B*, 2005, **109**, 2439–2444.
- 13 A. Mills and S. Le Hunte, *J. Photochem. Photobiol. A Chem.*, 1997, **108**, 1–35.
- 14 A. V Emeline, V. K. Ryabchuk and N. Serpone, *J. Phys. Chem. B*, 2005, **109**, 18515–18521.
- 15 D. Monllor-Satoca, R. Gómez, M. González-Hidalgo and P. Salvador, *Catal. Today*, 2007, **129**, 247–255.
- 16 B. Ohtani, *Chem. Lett.*, 2008, **37**, 216–229.
- 17 B. Ohtani, *J. Photochem. Photobiol. C Photochem. Rev.*, 2010, **11**, 157–178.
- 18 B. OHTANI, *Electrochemistry*, 2014, **82**, 414–425.
- 19 H. S. Fogler, *Elements of chemical reaction engineering*, Prentice Hall international series in the physical and chemical engineering sciences; Pearson Education Internat: Upple Saddle River, NJ, 4th edn., 2011.
- 20 C. N. Hinshelwood, *The kinetics of chemical change in gaseous systems*, Clarendon Press: Oxford, 1st edn., 1926.
- 21 G.-M. Schwab, in *Ergebnisse der Exakten Naturwissenschaften*, Springer Berlin Heidelberg, Berlin, Heidelberg, 1928, pp. 276–341.
- 22 G.-M. Schwab and E. Pietsch, *Zeitschrift für Phys. Chemie*, 1928, **1B**, 385.
- 23 G.-M. Schwab and E. Pietsch, *Zeitschrift für Elektrochemie und Angew. Phys. Chemie*, 1929, **35**, 135–141.
- 24 G.-M. Schwab, *Katalyse vom Standpunkt der Chemischen Kinetik*, Springer Berlin Heidelberg, Berlin, Heidelberg, 1931.
- 25 G. GopalaRao, *Zeitschrift für Phys. Chemie*, 1939, **184-A**, 377–384.
- 26 J. Cunningham and G. Al-Sayyed, *J. Chem. Soc., Faraday Trans.*, 1990, **86**, 3935–3941.
- 27 R. W. Matthews and S. R. McEvoy, *J. Photochem. Photobiol. A Chem.*, 1992, **64**, 231–246.
- 28 A. Mills and S. Morris, *J. Photochem. Photobiol. A Chem.*, 1993, **71**, 75–83.
- 29 F. Zhang, J. Zhao, T. Shen, H. Hidaka, E. Pelizzetti and N. Serpone, *Appl. Catal. B Environ.*, 1998, **15**, 147–156.
- 30 Y. Xu and C. H. Langford, *J. Photochem. Photobiol. A Chem.*, 2000, **133**, 67–

- 71.
- 31 S. M. Ould-Mame, O. Zahraa and M. Bouchy, *Int. J. Photoenergy*, 2000, **2**, 59–66.
- 32 E. Kusvuran, A. Samil, O. M. Atanur and O. Erbatur, *Appl. Catal. B Environ.*, 2005, **58**, 211–216.
- 33 A. Mills, J. Wang and D. F. Ollis, *J. Phys. Chem. B*, 2006, **110**, 14386–14390.
- 34 E. Pino and M. V. Encinas, *J. Photochem. Photobiol. A Chem.*, 2012, **242**, 20–27.
- 35 E. P. Melián, O. G. Díaz, J. M. D. Rodríguez, J. Araña and J. P. Peña, *Appl. Catal. A Gen.*, 2013, **455**, 227–233.
- 36 H. Y. Chen, O. Zahraa, M. Bouchy, F. Thomas and J. Y. Bottero, *J. Photochem. Photobiol. A Chem.*, 1995, **85**, 179–186.
- 37 D. Chakraborty and S. Sen Gupta, *J. Environ. Sci. (China)*, 2013, **25**, 1034–1043.
- 38 D. Chakraborty and S. Sen Gupta, *Indian J. Chem. Technol.*, 2015, **22**, 34–41.
- 39 N. Haddou, M. R. Ghezzar, F. Abdelmalek, S. Ognier and A. Addou, *Plasma Sci. Technol.*, 2013, **15**, 915–922.
- 40 J. A. Osajima, H. M. Ishiki and K. Takashima, *Monatshefte für Chemie - Chem. Mon.*, 2008, **139**, 7–11.
- 41 P. Pizarro, C. Guillard, N. Perol and J. M. Herrmann, in *Catalysis Today*, 2005, vol. 101, pp. 211–218.
- 42 M. Carrier, N. Perol, J.-M. Herrmann, C. Bordes, S. Horikoshi, J. O. Paise, R. Baudot and C. Guillard, *Appl. Catal. B Environ.*, 2006, **65**, 11–20.
- 43 G. Kaichouh, N. Oturan, M. A. Oturan, A. El Hourch and K. El Kacemi, *Environ. Technol.*, 2008, **29**, 489–496.
- 44 M. F. Atitar, R. Dillert and D. W. Bahnemann, *J. Phys. Chem. C*, 2017, **121**, 4293–4303.
- 45 H. Al-Ekabi and N. Serpone, *J. Phys. Chem.*, 1988, **92**, 5726–5731.
- 46 G. Mills and M. R. Hoffmann, *Environ. Sci. Technol.*, 1993, **27**, 1681–1689.
- 47 J. Cunningham, G. Al-Sayyed, P. Sedlak and J. Caffrey, *Catal. Today*, 1999, **53**, 145–158.
- 48 A. F. Alkaim, T. A. Kandiel, F. H. Hussein, R. Dillert and D. W. Bahnemann, *Catal. Sci. Technol.*, 2013, **3**, 3216.
- 49 Y. . Ho and G. McKay, *Process Biochem.*, 1999, **34**, 451–465.
- 50 H. Qiu, L. Lv, B. Pan, Q. Q. Zhang, W. Zhang and Q. Q. Zhang, *J. Zhejiang Univ. Sci. A*, 2009, **10**, 716–724.
- 51 Y. S. Ho, J. C. Y. Ng and G. McKay, *Sep. Purif. Methods*, 2000, **29**, 189–232.
- 52 S. Lagergren, *K. Sven. Vetenskaps-Akademiens Handl. Bih.*, 1898, **24**, 1–39.
- 53 Y. S. Ho, *Scientometrics*, 2004, **59**, 171–177.
- 54 M. Lindner, D. W. Bahnemann, B. Hirthe and W.-D. Griebler, *J. Sol. Energy Eng.*, 1997, **119**, 120–125.
- 55 M. Abdullah, G. K. C. Low and R. W. Matthews, *J. Phys. Chem.*, 1990, **94**, 6820–6825.
- 56 V. Subramanian, V. G. Pangarkar and A. A. C. M. Beenackers, *Clean Prod. Process.*, 2000, **2**, 0149–0156.
- 57 S. Bendjabeur, R. Zouaghi, O. N. . Kaabeche and T. Sehili, *Int. J. Chem. React. Eng.*, 2017, **15**, 4.
- 58 J. Farner Budarz, A. Turolla, A. F. Piasecki, J.-Y. Bottero, M. Antonelli and M. R. Wiesner, *Langmuir*, 2017, **33**, 2770–2779.
- 59 P. K. Dutta, A. K. Ray, V. K. Sharma and F. J. Millero, *J. Colloid Interface Sci.*, 2004, **278**, 270–275.

- 60 C. Wang, R. Pagel, D. W. Bahnemann and J. K. Dohrmann, *J. Phys. Chem. B*, 2004, **108**, 14082–14092.
- 61 C.-Y. Wang, R. Pagel, J. K. Dohrmann and D. W. Bahnemann, *Comptes Rendus Chim.*, 2006, **9**, 761–773.
- 62 H. Zhang, R. L. Penn, R. J. Hamers and J. F. Banfield, *J. Phys. Chem. B*, 1999, **103**, 4656–4662.
- 63 J. M. Pettibone, D. M. Cwiertny, M. Scherer and V. H. Grassian, *Langmuir*, 2008, **24**, 6659–6667.
- 64 H. M. Lu, Z. Wen and Q. Jiang, *Chem. Phys.*, 2005, **309**, 303–307.



### 3.9. Supporting Information

#### SI-3.1 Derivation of Equation 3.2

In the following, the derivation of the Langmuir-Hinshelwood rate law, as given by Ollis,<sup>1,2</sup> is summarized. The following nomenclature is used:

---

$C_t$	mol L <sup>-1</sup>	amount concentration of the dissolved (non-adsorbed) probe molecule in the suspension
$k_a$	L mol <sup>-1</sup> s <sup>-1</sup>	rate constant of adsorption
$k_d$	s <sup>-1</sup>	rate constant of desorption
$k'_r$	mol <sup>-1</sup> s <sup>-1</sup>	rate constant of the photocatalytic reaction
$k_r$	mol L <sup>-1</sup> s <sup>-1</sup>	maximum rate of the photocatalytic reaction
$K_L$	mol <sup>-1</sup>	Langmuir adsorption constant
$K_{LH}$	mol <sup>-1</sup>	constant in Langmuir-Hinshelwood rate law
$n_{os}$	mol	amount of occupied sites
$n_{ox}$	mol	amount of oxidizing species at the photocatalyst surface
$n_{ts}$	mol	total amount of surface sites
$t$	min	time
$V$	L	total volume of suspension

---

The Langmuir-Hinshelwood rate law is derived employing the amount balance of sites at the photocatalyst surface occupied by the probe molecule during the photocatalytic reaction:

$$\frac{dn_{os}}{dt} = +k_a(n_{ts} - n_{os})C_t - k_d n_{os} - k'_r n_{ox} n_{os} \quad (S3.1)$$

Under steady state conditions, i.e.,  $\frac{dn_{os}}{dt} = 0$  and  $\frac{dn_{ox}}{dt} = 0$ , it can be written

$$+k_a n_{ts} C_t - k_a n_{os} C_t - k_d n_{os} - k'_r n_{ox} n_{os} = k_a (n_{ts} C_t - n_{os} k_a C_t + k_d + k'_r n_{ox}) = 0 \quad (S3.2)$$

and after rearrangement

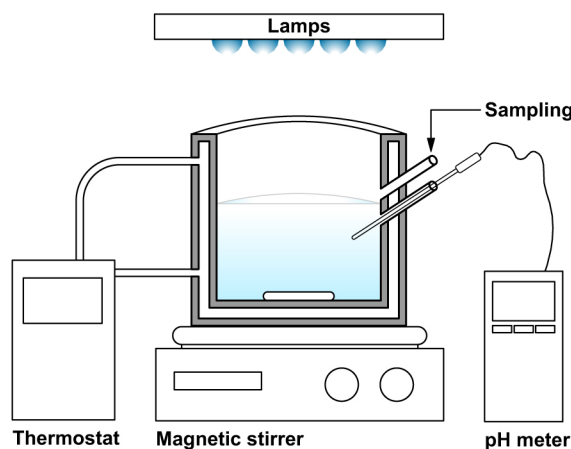
$$n_{os} = \frac{k_a n_{ts} C_t}{k_a C_t + k_d + k'_r n_{ox}} \quad (S3.3)$$

Inserting Equation (S3.3) into the Equation (3.1) yields

$$\frac{dC_t}{dt} = \frac{k'_r n_{ox} n_{ts}}{V} \times \frac{k_a C_t}{k_a C_t + k_d + k'_r n_{ox}} = \frac{k'_r n_{ox} n_{ts}}{V} \times \frac{\frac{k_a}{k_d + k'_r n_{ox}} C_t}{1 + \frac{k_a}{k_d + k'_r n_{ox}} C_t} \quad (S3.4)$$

With the abbreviations  $k_r = \frac{k'_r n_{ox} n_{ts}}{V}$  and  $K_{LH} = \frac{k_a}{k_d + k'_r n_{ox}}$  Equation (S3.4) yields Equation (3.2).

### SI-3.2 Scheme of the experimental setup used for the photocatalytic degradation experiments



### SI-3.3 Effect of the photocatalyst concentration on the photocatalytic degradation rate

The photocatalytic degradation of imazapyr employing different mass concentrations  $C_c$  of  $\text{TiO}_2$  P25 powder was studied in order to determine the optimum concentration of the photocatalyst. As can be seen from the Figure S3.1, the initial photodegradation rate increases slowly as the photocatalyst mass concentration is increased from  $0.5$  to  $2.5 \text{ g L}^{-1}$ , then it decreases when the catalyst concentration is beyond  $2.5 \text{ g L}^{-1}$ , indicating an overload by the photocatalyst at higher concentrations.

From Figure S3.1a, it can be concluded that screening effects of the irradiation, due to an excess of  $\text{TiO}_2$ , became dominant. An important fraction of  $\text{TiO}_2$  nanoparticles are not excited by the photons emitted by the lamp resulting in a reduction of the photocatalytic activity as reported previously.<sup>3,4</sup> It has also been reported that excessive photocatalyst concentration may reduce the photocatalytic efficiency by formation of the particle agglomerates, which produces light scattering and screening effect. Several works have shown that increasing the photocatalyst concentration beyond an optimum value is accompanied by a decrease of the photocatalytic degradation efficiency of the target substance.<sup>5-7</sup>

The normalization of the initial degradation rate to the catalyst mass concentration and volume (Figure S3.1b) shows a different behavior than the initial rate in its classical form, whereas the normalized initial degradation rate decreases with the increase of the catalyst mass concentration, this result can also be explained by the fact that the normalization in this case have been performed to the increasing amount

of the catalyst (i.e., 0.5 to 5 g L<sup>-1</sup>) which results in the decrease of the initial degradation rate. Furthermore increasing the amount of photocatalyst over the so-called optimum concentration induces the formation of particle agglomerates in the solution. Consequently penetration depth is reduced and the scattering of the incident light beam is increased.<sup>8</sup> Similar results have been presented by Pizarro et al., who have also investigated the influence of the photocatalyst mass concentration in the range 0–2.5 g L<sup>-1</sup> on the photodegradation of imazapyr. They have assumed that the maximum absorption of light is already achieved with the lowest mass of the photocatalyst, and that the screening effects of the irradiation due to an excess of TiO<sub>2</sub> becomes dominant.<sup>4</sup>

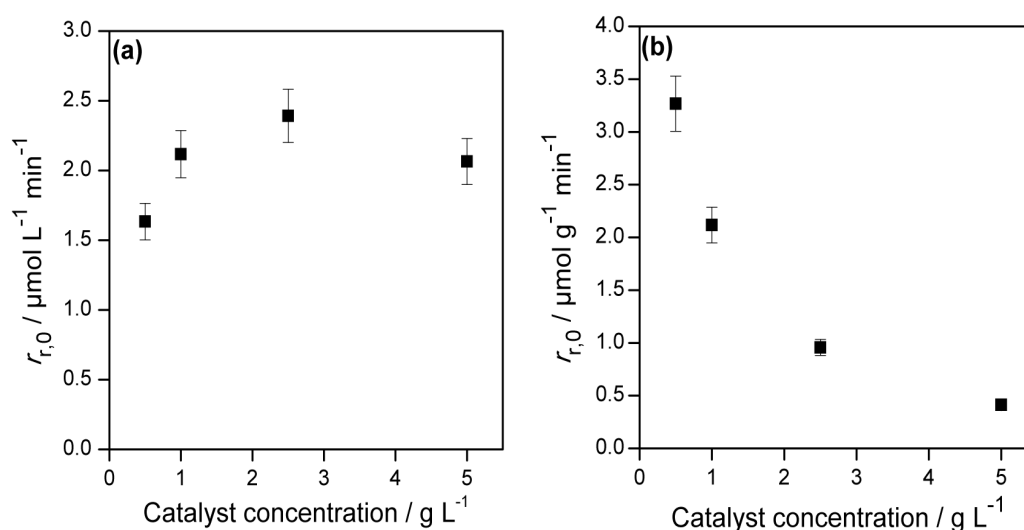


**Figure S3.1.** (a) Initial degradation rate of the imazapyr as a function of the photocatalyst mass concentration  $C_c$  using Aeroxide TiO<sub>2</sub> P25. (b) Initial degradation rate of the imazapyr normalized to the catalyst mass concentration and volume. Experimental conditions:  $C_0 = 80 \mu\text{mol L}^{-1}$ ,  $V = 100 \text{ mL}$ , pH 5.

**SI-3.4 Initial reaction rates****Table S3.1.** Initial equilibrium concentrations, observed photocatalytic first-order rate constants and calculated initial photocatalytic reaction rates.

pH	$C_{e,0} / \mu\text{mol L}^{-1}$	$k_{\text{obs}} / \text{min}^{-1}$	$r_{r,0} = k_{\text{obs}}C_{e,0} / \mu\text{mol L}^{-1} \text{min}^{-1}$	$r_{r,0} = k_r K_{\text{LH}} C_{e,0} / (1 + K_{\text{LH}} C_{e,0}) / \mu\text{mol L}^{-1} \text{min}^{-1}$
3	16.9	0.098	1.66	1.45
	42.4	0.043	1.82	2.10
	82.6	0.030	2.48	2.45
	88.0	0.028	2.46	2.47
	133	0.019	2.53	2.62
5	17.0	0.087	1.48	1.16
	41.1	0.039	1.60	1.80
	81.4	0.029	2.36	2.23
	101	0.021	2.12	2.34
	159	0.015	2.39	2.53
7	17.7	0.054	0.96	0.86
	43.2	0.025	1.08	1.05
	78.9	0.017	1.34	1.13
	92.9	0.011	1.02	1.14
	140	0.010	1.40	1.18

Experimental conditions:  $20 \leq C_0 \leq 200 \mu\text{mol L}^{-1}$ ,  $\text{TiO}_2$  P25,  $C_c = 2.5 \text{ g L}^{-1}$ ,  $V = 100 \text{ mL}$ .

Note: The values of  $k_r$  and  $K_{\text{LH}}$  have been taken from Table (3.1).

**SI-3.5 Freundlich adsorption isotherms**

The Freundlich isotherm equation is given as

$$q_e = kC_e^{\frac{1}{n}} \quad (\text{S3.5})$$

$k$  and  $n$  are the constants of adsorption density and adsorption intensity, respectively.

Equation S5 can be linearized:

$$\ln q_e = \ln k + \frac{1}{n} \ln C_e \quad (\text{S3.6})$$

The value of  $k$  and  $n$  can be estimated from the intercept and slope of the linear plot of experimental data of  $\ln q_e$  versus  $\ln C_e$ . The Freundlich isotherm provides no information on the monolayer adsorption density in comparison with the Langmuir model. The values of  $k$  and  $n$  from the linearized plots are shown in Table S2 following with the regression correlation coefficients. The parameter  $k$  related to the adsorption density increased with increasing pH. The meaning of  $n > 1.0$  indicates that imazapyr was adsorbed favorably onto the TiO<sub>2</sub> surface at different pH values.

**Table S3.2.** Fitting parameters of the Freundlich adsorption isotherm of imazapyr onto TiO<sub>2</sub> at different pH values.

Substrate	TiO <sub>2</sub> P 25			
	pH	3	5	7
Freundlich isotherm constants				
$n$		3.60	2.023	1.71
$k$		323.27	367.9	553.18
$R^2$		0.996	0.967	0.915

Experimental conditions:  $100 \leq C_0 \leq 2000 \mu\text{mol L}^{-1}$ , TiO<sub>2</sub> P25,  $C_c = 5 \text{ g L}^{-1}$ ,  $V = 100 \text{ mL}$ .

### SI-3.6 Lagergren adsorption kinetics

The Lagergren pseudo-first order model is believed to be the earliest model pertaining to the adsorption rate based on the adsorption capacity.<sup>9,10</sup> It can be presented as follows:

$$\frac{dq_t}{dt} = k_1(q_e - q_t) \quad (\text{S3.7})$$

where  $q_t$  (in  $\mu\text{mol/g}$ ) is the amount of adsorbate adsorbed at time  $t$ ,  $q_e$  (in  $\mu\text{mol/g}$ ) is the adsorption capacity in the equilibrium,  $k_1$  (in  $\text{min}^{-1}$ ) is the pseudo-first-order rate constant, and  $t$  is the contact time (in min).<sup>11</sup> The Lagergren equation represents the pseudo-first order kinetics for the whole adsorption reaction, with a one-partial order with respect to the free concentration sites, and a zero-partial order with respect to the solute in the solution. Integrating the Equation (S3.7) with the boundary conditions of  $q_t=0$  at  $t=0$  and  $q_t=q_t$  at  $t=t$ , yields:

$$\ln\left(\frac{q_e - q_t}{q_e}\right) = k_1 t \quad (\text{S3.8})$$

**Table S3.3.** The parameters of adsorption kinetics model fitting obtained at different pH values. The initial imazapyr concentration is  $126.5 \mu\text{mol L}^{-1}$  and the catalyst amount is  $5 \text{ g L}^{-1}$ .

Substrate	TiO <sub>2</sub> P 25			
	pH	3	5	7
Lagergren kinetic constants				
$q_e$ ( $\mu\text{mol g}^{-1}$ )		5.82	4.52	2.24
$k_1$ ( $\text{min}^{-1}$ )		0.026	0.0241	0.0202
$R^2$		0.991	0.984	0.969

Experimental conditions:  $C_0 = 126.5 \mu\text{mol L}^{-1}$ , TiO<sub>2</sub> P 25,  $C_c = 5 \text{ g L}^{-1}$ ,  $V = 20 \text{ mL}$ .

**SI-3.7 Initial adsorption rate**

The initial adsorption rates (calculated employing Equation 3.12) as function of the pH, and as function of the mass concentration of the photocatalyst are presented in the Figure S3.2.

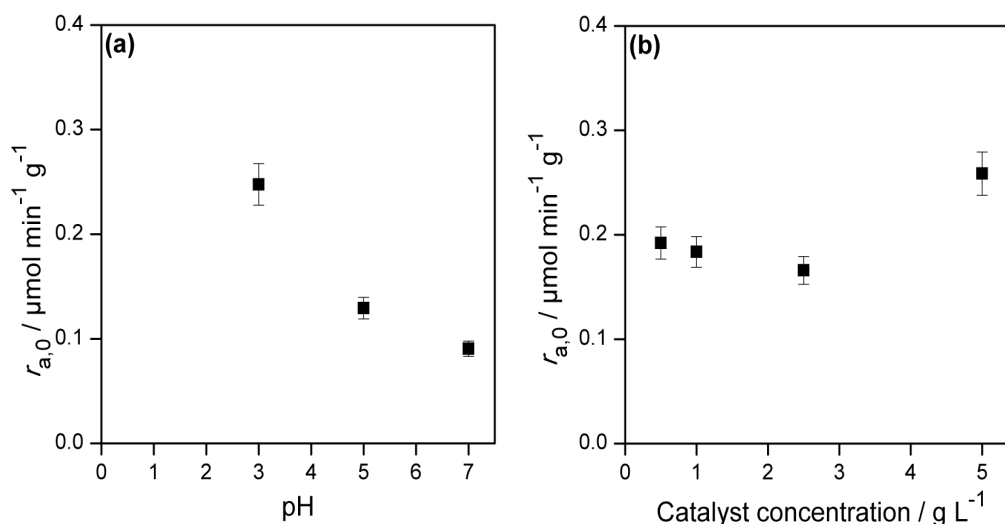


**Figure S3.2.** (a) Initial adsorption rates vs. pH, and (b) initial adsorption rates vs. catalyst concentration. Experimental conditions: (a)  $C_0 = 80 \mu\text{mol L}^{-1}$ ,  $\text{TiO}_2$  P25,  $C_c = 2.5 \text{ g L}^{-1}$ ,  $V = 20 \text{ mL}$ , (b)  $C_0 = 80 \mu\text{mol L}^{-1}$ ,  $\text{TiO}_2$  P25, pH 5,  $V = 20 \text{ mL}$ .

The initial adsorption rate decreases with the increase of the pH value from pH 3 to pH 7 (Figure S3.2a). The same behavior has been observed for the initial photocatalytic degradation rate, and explained to be due to the interactions between imazapyr species and the  $\text{TiO}_2$  surface. Furthermore the Figure (S3.2b) shows the variation of the initial adsorption rate as function of the photocatalyst concentration. The initial adsorption rate decreases with the increase of the catalyst loading from  $0.5 \text{ g L}^{-1}$  to  $2.5 \text{ g L}^{-1}$ , and increases with increasing the catalyst concentration from  $2.5 \text{ g L}^{-1}$  to  $5 \text{ g L}^{-1}$ . The increase of the initial adsorption rate can be explained by the fact that in the presence of high catalyst amounts, more adsorption sites are available. However the values of the initial adsorption rate are almost comparable when taking the experimental error into account.



### SI-3.8 Comparison between the initial adsorption rates and the initial photocatalytic reaction rates

**Table S3.4.** Calculated initial adsorption and reaction rates at different pH values and initial equilibrium concentrations.

pH	$C_{e,0}$ $\mu\text{mol L}^{-1}$	$r_{a,0} = k'_a \left( \frac{q_m K_L C_{e,0}}{1 + K_L C_{e,0}} \right)^2$ $\mu\text{mol g}^{-1} \text{min}^{-1}$	$r_{r,0} = \frac{V k_r K_{LH} C_{e,0}}{m(1 + K_{LH} C_{e,0})}$ $\mu\text{mol g}^{-1} \text{min}^{-1}$
3	16.9	0.03	0.58
	42.4	0.14	0.84
	82.6	0.41	0.98
	88.0	0.45	0.99
	133	0.79	1.05
5	17.0	0.01	0.47
	41.1	0.05	0.72
	81.4	0.17	0.89
	101	0.24	0.94
	159	0.48	1.01
7	17.7	0.01	0.35
	43.2	0.03	0.42
	78.9	0.09	0.45
	92.9	0.12	0.46
	140	0.23	0.47

Note: The values of  $k'_a$ ,  $q_m$ ,  $K_L$ ,  $k_r$  and  $K_{LH}$  have been taken from the Table 3.2 and Table 3.1.  $V/m$  is the reciprocal value of the mass concentration of the photocatalyst in the suspension.

## References

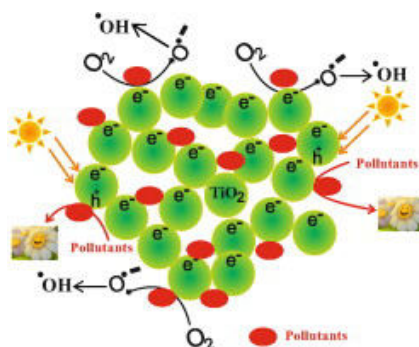
- 1 D. F. Ollis, *Top. Catal.*, 2005, **35**, 217–223.
- 2 D. F. Ollis, *J. Phys. Chem. B*, 2005, **109**, 2439–2444.
- 3 M. A. Rahman and M. Muneer, *Desalination*, 2005, **181**, 161–172.
- 4 P. Pizarro, C. Guillard, N. Perol and J. M. Herrmann, in *Catalysis Today*, 2005, **101**, 211–218.
- 5 J. C. Garcia and K. Takashima, *J. Photochem. Photobiol. A Chem.*, 2003, **155**, 215–222.
- 6 M. Muneer, M. Qamar, M. Saquib and D. W. Bahnemann, *Chemosphere*, 2005, **61**, 457–468.
- 7 M. Carrier, N. Perol, J.-M. Herrmann, C. Bordes, S. Horikoshi, J. O. Paise, R. Baudot and C. Guillard, *Appl. Catal. B Environ.*, 2006, **65**, 11–20.
- 8 H. Kisch and D. Bahnemann, *J. Phys. Chem. Lett.*, 2015, **6**, 1907–1910.
- 9 S. Lagergren, *K. Sven. Vetenskaps-Akademiens Handl. Bih.*, 1898, **24**, 1–39.
- 10 Y. S. Ho, *Scientometrics*, 2004, **59**, 171–177.
- 11 H. Qiu, L. Lv, B. Pan, Q. Q. Zhang, W. Zhang and Q. Q. Zhang, *J. Zhejiang Univ. Sci. A*, 2009, **10**, 716–724.

## Chapter 4

# Mesoporous TiO<sub>2</sub> Nanocrystals as Efficient Photocatalysts: Impact of Calcination Temperature and Phase Transformation on Photocatalytic Performance

M. Faycal Atitar, Adel. A. Ismail, S. A. Al-Sayari, Detlef. W. Bahnemann, D. Afanasev, A.V. Emeline

Published in Chemical Engineering Journal, 2015, 264, pp 417-424



#### 4.1. Abstract

Mesoporous TiO<sub>2</sub> nanocrystals have been synthesized through sol gel method in presence of triblock copolymer as the structure directing agent. The as-prepared TiO<sub>2</sub> nanocrystals have been calcined at different temperatures, i.e., at 400°C, 500°C, 600°C, 700°C, and 800°C to demonstrate how their structural properties (morphology, mesoporosity, crystallite phases and sizes) affect the photocatalytic performance. The TEM images indicate that TiO<sub>2</sub> nanocrystals calcined at 500 °C have a mesoporous structure with particle sizes of approximately 10–15 nm. However, the TiO<sub>2</sub> calcined at 800 °C shows a lower mesoporosity and particle sizes of ~ 75 nm. The photocatalytic performance of the newly synthesized photocatalysts has been evaluated through the photodegradation of two different pollutants, i.e., the herbicide imazapyr and phenol, and has been compared to that of the commercially available nonporous Aeroxide TiO<sub>2</sub> P25. For the imazapyr photodegradation, the newly synthesized mesoporous TiO<sub>2</sub> nanocrystals show an initial degradation rate around 2 times higher than the rate observed with the non-porous Aeroxide TiO<sub>2</sub> P25. The highest photocatalytic activity is observed for the samples calcined at 500 °C followed by those calcined at 800 °C. In contrast to that, a different behavior is found for the photodegradation of phenol. The results indicate that the TiO<sub>2</sub> samples calcined at 500 °C show the highest photocatalytic activity for phenol photodegradation. It is proposed that the behavior of the photocatalysts in term of their photocatalytic efficiency and rate constants varies based on the pollutant type. TiO<sub>2</sub> calcined at 500 °C can be considered as economically more efficient by saving energy through the lower temperature required in the calcination process.

**Keywords:** Mesoporous TiO<sub>2</sub>; Calcination temperatures; Photodegradation; Herbicide imazapyr; Phenol.

#### 4.2. Introduction

Pesticides and phenols are considered to be the most common type of water and soil pollutants. Imazapyr is a herbicide belonging to the imidazolinone family, which has the ability to damage the plants even at low concentrations [1]. Moreover, imazapyr is a persistent herbicide with a high mobility in soils. The half-life of imazapyr is found to vary from 21 days to 49 months as observed in field studies. Since imazapyr is considered to be groundwater contaminant [1]. Various attempts have been made to remove it from the polluted water using Ozone. However, this

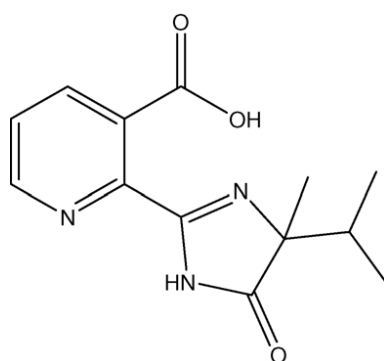
process is ineffective since an important amount of imazapyr still remains in the water [2]. Phenols are also highly toxic organic compounds, found in wastewater and effluents coming from the petroleum and chemical industries. Up to now, several studies on the decomposition of imazapyr and phenol using Fenton, photo-Fenton and electro-Fenton processes have been performed [3-6]. This has led to the consideration of heterogeneous photocatalysis as one of the most promising advanced oxidation processes. The interest in this scientific field has increased during the last decades, since photocatalysis is assumed to be a powerful tool for the degradation and remediation of highly toxic pollutants such as imazapyr and phenols.

The photocatalytic oxidation of imazapyr has been performed in the aqueous phase using commercially available Aeroxide TiO<sub>2</sub> P-25, Crystal Global PC-500 [7-9], and PC-500 coated on natural cellulose [10]. However, experimental evidence indicates that mixed phases, such as anatase/rutile [11-13], brookite/rutile [14,15], and brookite/anatase [16-20], exhibit synergistic effects, thus enhancing the photocatalytic activity. The photodegradation of phenol has been extensively studied using TiO<sub>2</sub> [21-23]. Therefore, it is of great importance to develop methods to synthesize TiO<sub>2</sub> with particular properties such as crystal sizes and phases, mesoporous structures and high surface areas and study their influence on the photocatalytic performance. In general, the phase composition and particle size of TiO<sub>2</sub> prepared by wet processes are dependent on the temperature, the pH, as well as on the type and the concentration of the reactants employed in the synthetic reaction [11,24-29]. Mesoporous TiO<sub>2</sub> nanocrystals are promising materials for photocatalytic applications. They have the ability to significantly improve the photocatalytic performance compared to the commercially available P-25 [24-29]. In this work, we report about the synthesis of mesoporous TiO<sub>2</sub> samples and the determination of their respective photocatalytic activity with the respect to the degradation of the two pollutants imazapyr and phenol. We focus on the relationship between the effect of calcination temperature, the phase transformation, and the surface area of the synthesized mesoporous photocatalysts.

### 4.3. Experimental section

**Materials.** Ti(OC(CH<sub>3</sub>)<sub>3</sub>)<sub>4</sub> (TBOT), HCl, CH<sub>3</sub>OH, C<sub>2</sub>H<sub>5</sub>OH, CH<sub>3</sub>COOH, the block copolymer surfactant EO<sub>106</sub>-PO<sub>70</sub>EO<sub>106</sub> (F-127, EO—CH<sub>2</sub>CH<sub>2</sub>—O—,PO—CH<sub>2</sub>(CH<sub>3</sub>))

CHO-, MW 12600 g/mol), phenol, and Imazapyr (C<sub>13</sub>H<sub>15</sub>N<sub>3</sub>O<sub>3</sub> > 99%) were purchased from Sigma-Aldrich. Scheme 4.1. shows the chemical structure of the herbicide imazapyr. H<sub>3</sub>PO<sub>4</sub> and HCl were purchased from Neva Reactifs Russia, KNO<sub>3</sub> from VEKTON Russia and Methanol from Merck. Aeroxide TiO<sub>2</sub> P-25 from Evonik, (mainly anatase, with a rutile content of ca. 20 %, primary particle size of around 30 nm, and BET surface area of this non-porous material of 50 m<sup>2</sup> g<sup>-1</sup>) was used as received. Water was purified in a Millipore Mill-Q system (resistivity ≥ 18 MΩ cm).



**Scheme 4.1.** Chemical Structure of Imazapyr

**Preparation of mesoporous TiO<sub>2</sub>.** Mesoporous TiO<sub>2</sub> nanocrystals were synthesized through a simple one-step sol-gel process in the presence of the F127 triblock copolymer as the structure directing agent [25-26,30]. In a typical synthesis procedure, 1.6 g of F127 was dissolved in 30 ml of ethanol for 60 min and then added to 2.3 ml of CH<sub>3</sub>COOH and 0.74 ml of HCl. Afterwards 3.5 ml of TBOT was gradually added to the mixture. The mixture was stirred vigorously for additional 60 min and transferred into a Petri dish. Ethanol was subsequently evaporated at 40 °C and a relative humidity of 40 % for 12 h followed by the transfer of the sample into a 65 °C oven, and the aging for additional 24 h. The as-made hybrid materials were calcined at 400 °C, 500 °C, 600 °C, 700 °C, and 800 °C in air for 4h with a heating rate of 1 °C/min and a cooling rate of 2 °C/min to remove the surfactant and to obtain mesoporous TiO<sub>2</sub> nanocrystals denoted as T-400, T-500, T-600, T-700, and T-800 according to the calcination temperatures.

**Characterization.** X-ray diffraction data were acquired on a Bruker AXS D4 Endeavour X diffractometer using Cu Kα<sub>1/2</sub>, λ<sub>α1</sub>=154.060 pm, λ<sub>α2</sub> = 154.439 pm radiation. Transmission electron microscopy (TEM) was performed at 200 kV with a JEOL JEM-2100F-UHR field-emission instrument equipped with a Gatan GIF 2001 energy filter and a 1k-CCD camera in order to obtain EEL spectra. The nitrogen

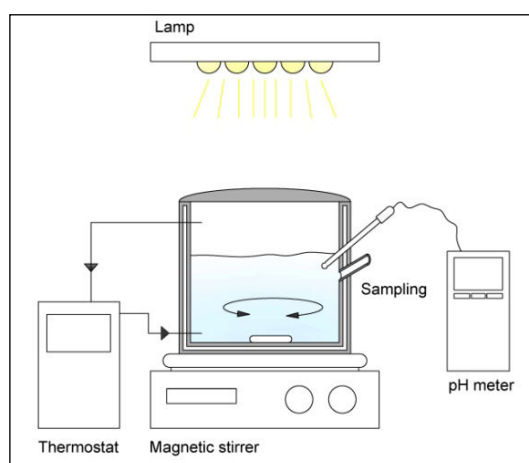
adsorption and desorption isotherms at  $-196\text{ }^{\circ}\text{C}$  were determined using a Quantachrome Autosorb 3B. All the samples were vacuum-dried at  $200\text{ }^{\circ}\text{C}$  overnight before the measurement. The Barrett-Joyner-Halenda (BJH) model with Halsey equation was employed to analyze the sorption data. Raman spectroscopy was carried out using a Bruker Senterra dispersive Raman microscope. The spectra were taken to the powder samples exposed to air in the range from  $0$  to  $1555\text{ cm}^{-1}$  using a laser excitation wavelength of  $532\text{ nm}$  and laser power of  $2\text{ mW}$ . Diffuse reflectance spectroscopy (DRS) was employed to measure the bandgap energy of the prepared photocatalysts. A Varian Cary 100 Scan UV-vis system equipped with a Labsphere integrating sphere diffuse reflectance accessory was employed to record the reflectance spectra of the samples at  $200\text{--}800\text{ nm}$  [31]. The diffuse reflectance mode ( $R$ ) was transformed to the Kubelka-Munk function  $F(R)$  to separate the extent of light absorption from scattering. Furthermore, the band gap values were calculated based on the modified Kubelka–Munk function  $(F(R)E)^{1/2}$  and the energy of the absorbed light  $E$  as follows in Eq. (4.1) [32].

$$F(R)E^{1/2} = \left( \frac{(1-R)^2}{2R} \times hv \right)^{1/2} \quad (4.1)$$

The band gap energy was determined from the intersection of the tangent through the point of inflexion in the absorption band and the photon energy axis (Fig. 5b).

**Photocatalytic activity tests.** Mesoporous TiO<sub>2</sub> nanocrystals were dispersed in  $50\text{ ml}$  of water ( $C_{\text{cat}}=1\text{ g l}^{-1}$ ) in addition to  $10\text{ mmol l}^{-1}$  KNO<sub>3</sub>, by sonication and shaking in an ultrasonic bath for  $15\text{ min}$ . KNO<sub>3</sub> was added to keep the ionic strength of the solution constant throughout the experiment. An aliquot of a stock solution of the organic substrate  $21.25\text{ mmol l}^{-1}$  in case of phenol, and  $7.65\text{ mmol l}^{-1}$  in case of imazapyr was added to the suspension to establish the desired initial concentration of  $0.27\text{ mmol l}^{-1}$  phenol and  $0.08\text{ mmol l}^{-1}$  imazapyr. The pH value of the suspension was adjusted to pH 3 using HCl standard solution. The suspensions were stirred at  $300\text{ rpm}$  overnight in a closed borosilicate glass beaker to reach adsorption equilibrium. Irradiation experiments were conducted under top illumination of a borosilicate glass beaker with a setup consisting of a  $1000\text{ W}$  Hg-Xe lamp (Newport 6295NS) equipped with a  $10\text{ cm}$  water filter outlet and dichroic Beam Turning Mirror (66232 Newport Technology) (Scheme 4.2.). Before illumination,  $1\text{ ml}$  of the previously equilibrated suspensions was analyzed, being considered as the initial equilibrium concentration. The photoreactor was filled with  $50\text{ ml}$  of the equilibrated

suspension and magnetically stirred at 300 rpm while being air-bubbled. Afterward, a shutter was removed and the reactor was illuminated under continuous stirring. The temperature of the liquid phase, periodically monitored during the experiment, was  $25 \pm 1$  °C. For kinetic studies, samples were taken at regular time intervals and were analyzed directly using the High Performance Liquid Chromatography (HPLC) analysis. The analysis of phenol and imazapyr concentrations was performed with a HPLC system from Agilent Technologies 1260 Infinity composed of a G1311C-1260 Quat pump and a G1365D-1260 MWD UV detector adjusted to 270 nm in case of phenol and 254 nm in case of imazapyr. An Agilent Eclipse plus C18 column (100 mm Long  $\times$  4.6 mm i.d., 3.5  $\mu$ m particles) working at room temperature was employed as the stationary phase, and a mixture of methanol and water (30:70 %v/v) operating at pH 3 by adding H<sub>3</sub>PO<sub>4</sub> as the mobile phase. The flow rate was kept constant at 0.8 ml/min. A peak attributed to phenol was observed at a retention time of 4.80 min and to imazapyr at 4.60 min. Calibration curves ( $R^2 > 0.999$ ) of aqueous solution of phenol and imazapyr were obtained by measuring 6 different concentrations in the range between 0 and 0.27 mmol l<sup>-1</sup>, and 0 and 0.08 mmol l<sup>-1</sup>, respectively. It is worth noting that, the photodegradation experiments and the HPLC analysis were performed 2-3 replicates, allowing initial reaction rates to be obtained with a mean experimental error of about  $\pm 5\%$  to 10%. This error is considered to be the sum of the HPLC instrument error and the error intrinsic to mathematical calculations from the experimental concentration vs. time plots.



**Scheme 4.2.** Schematic of the experimental setup.



#### 4.4. Results and Discussion

**Structural Investigations.** Mesoporous TiO<sub>2</sub> has been synthesized through a simple one-step sol-gel process in the presence of F127 as the structure directing agent followed by the calcinations of the samples at 400 °C, 500 °C, 600 °C, 700 °C, and 800 °C. Fig. 1 shows the XRD patterns of the mesoporous TiO<sub>2</sub> nanocrystals at different calcination temperatures. The diffraction patterns can be indexed to the anatase and rutile phases for all prepared samples. The XRD data show that a biphasial anatase and rutile mixture (53.86 %/46.14 %) is formed at 400 °C (Figure 4.1. and Table 4.1). Furthermore, (73.25 %/16.75 %) anatase/rutile mixed phase is obtained in the sample T-500. The increase of the calcination temperature is accompanied with a decrease in the intensity of the peaks assigned to the anatase phase, whereas, the additional rutile phase is formed to reach a rutile/anatase ratio of (81.90%/18.10%) in the T-800 sample (Fig 4.1 and Table 4.1.). These results indicate that the phase transformation from anatase to rutile nanoparticles is associated to the increase of the calcination temperature.

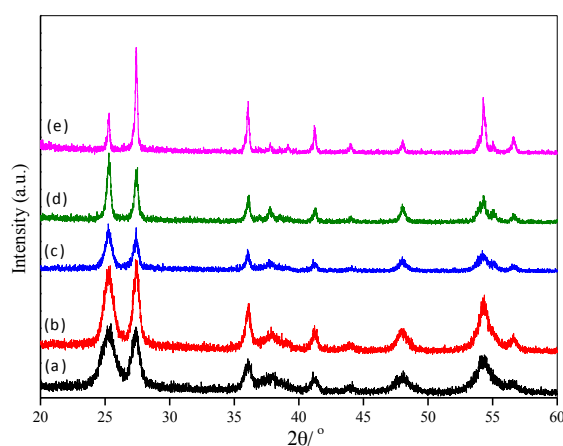


**Figure 4.1.** XRD patterns of mesoporous TiO<sub>2</sub> calcined at 400 °C (a), 500 °C (b), 600 °C (c), 700 °C (d), and 800 °C (e) for 4 h. Shifted for sake of clarity.

The crystallinity of the TiO<sub>2</sub> samples and their phase transformation during calcination are also confirmed by Raman spectroscopy (Figure 4.2.). For the T-400 and the T-500 samples, five of the six Raman active modes at 148 cm<sup>-1</sup> (Eg), 197.5 cm<sup>-1</sup> (Eg), 396.9 cm<sup>-1</sup> (B1g), 517.0 cm<sup>-1</sup> (B1g), and 639.9 cm<sup>-1</sup> (Eg) are assigned to correspond to the anatase phase with only a weak rutile phase contribution [33]. However, with increasing calcination temperatures from 500 to

800 °C, the peak, which is referred to the TiO<sub>2</sub> anatase phase at 148 cm<sup>-1</sup>, is slightly blue shifted to 143.7 cm<sup>-1</sup> as a result of the crystal growth and the phase transformation of the TiO<sub>2</sub> nanocrystals from the anatase to the rutile phase thus increasing the ratio. For the T-800 sample, the rutile phase yields typical bands, with the three Raman active modes being assigned at 143 cm<sup>-1</sup> (B1g), 435.7 cm<sup>-1</sup> (Eg), and 611.1 cm<sup>-1</sup> (A1g), respectively [34]. However, even at the highest calcination temperature employed here, i.e., at 800 °C, the anatase phase is still found to co-exist with the rutile phase. The Raman spectra are in good agreement with the result obtained from the XRD analysis.

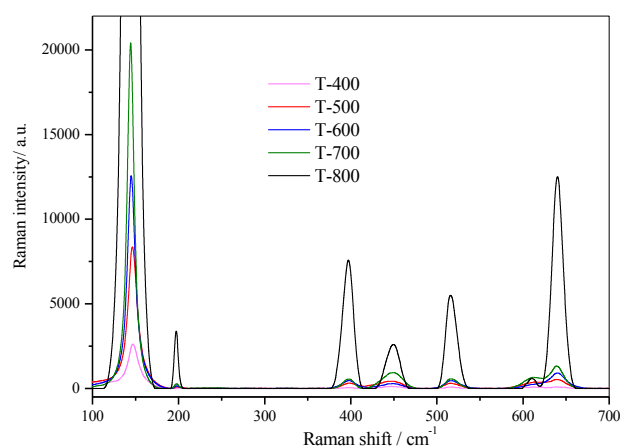


**Figure 4.2.** Raman spectra of mesoporous TiO<sub>2</sub> calcined at 400 °C, 500 °C, 600 °C, 700 °C, and 800 °C for 4 h.

N<sub>2</sub> adsorption isotherms and pore size distributions (inset) of all prepared photocatalysts are shown in Figure 4.3. The results show a typical type IV adsorption behavior and a H<sub>2</sub> hysteresis loop of the adsorption/desorption branches as characteristics of the isotherms of the T-400, T-500, T-600, and T-700 samples. At the low calcination temperatures (400 °C and 500 °C), the relative pressures  $p/p_0$  between 0.45 and 0.9 are characteristic for the regularity and the uniformity of the prepared photocatalysts. The mesoporous TiO<sub>2</sub> T-400 has a surface area of 165 m<sup>2</sup>g<sup>-1</sup> and pore volume of 0.441 cm<sup>3</sup>g<sup>-1</sup>. As the calcinations temperature increases from 400 °C to 700 °C, the specific surface area and pore volume decrease, whereas the mean pore size increases (Table 4.1.). This is related to the transformation in the morphology, which is presumably driven by the growth of the nanocrystallites inside the pores. Some of the formed large TiO<sub>2</sub> nanocrystals can thrust into the channels

and block the mesopores [35]. For the T-800 sample, the absence of the hysteresis loop shows that this sample exhibits the behavior that the packing of rather large (nano)particles can be regarded as irregular voids [25]. However, some mesoporosity is particularly evident from the TEM images (Figure 4.4e.).

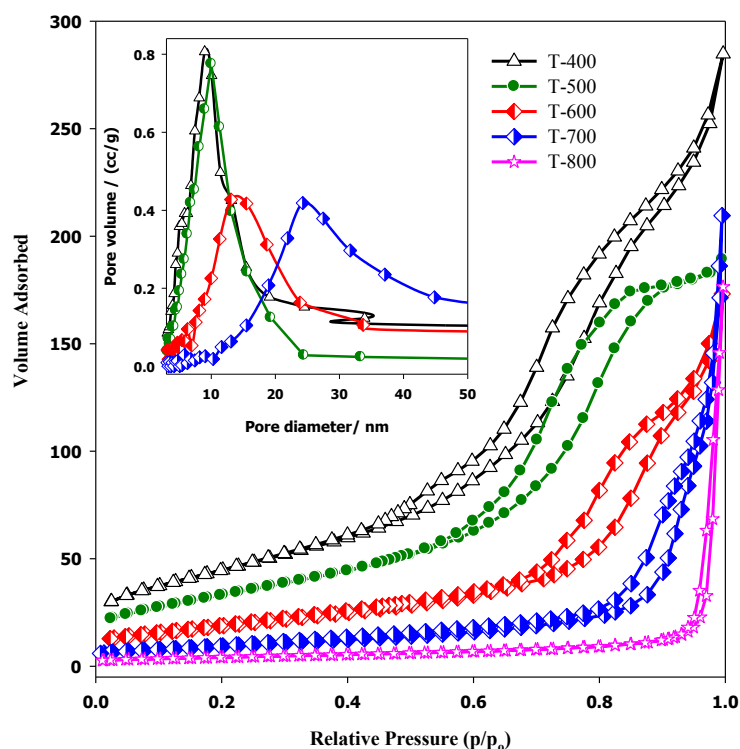


**Figure 4.3.** N<sub>2</sub> sorption isotherms and pore size distribution (inset) of the mesoporous TiO<sub>2</sub> calcined at 400 °C (a), 500 °C (b), 600 °C (c), 700 °C (d), and 800 °C for 4 h.

The TEM images of the mesoporous TiO<sub>2</sub> nanocrystals calcined at 500 °C and 800 °C are shown in Fig. 4. For the T-500 sample, an interparticulate mesoporous structure is clearly visible (Figure 4.4a). The TiO<sub>2</sub> nanoparticles have a size of approximately 10-15 nm and form agglomerates of approximately 1-3 μm in size. The dark-field TEM image of the TiO<sub>2</sub> sample calcined at 500 °C shows the mesoporous structure of TiO<sub>2</sub> nanoparticles (Figure 4.4b). HRTEM images of the lattice fringes show the typical distances for the anatase phase, i.e., TiO<sub>2</sub> (101) (3.52 Å) (Figure 4.4c). The selected area electron diffraction (SAED) patterns additionally emphasize that the anatase nanocrystals are composed (Figures 4.4c, inset). In contrast to that, in the T-800 sample, the TiO<sub>2</sub> nanoparticles have a size of approximately 50-75 nm and form agglomerates of approximately 1-5 μm in size (Figure 4.4d). The packing of TiO<sub>2</sub> nanoparticles in agglomerates shows some

mesoporosity (Figure 4.4e). The high-resolution TEM micrograph (Figure 4.4f) shows the rutile and anatase lattice. The corresponding Fourier transform (Figure 4.4f, Inset) confirms the orientation of the anatase and the rutile nanoparticles. Thus exhibit mainly (101) and (110)-type facets, respectively (Figure 4.4f).

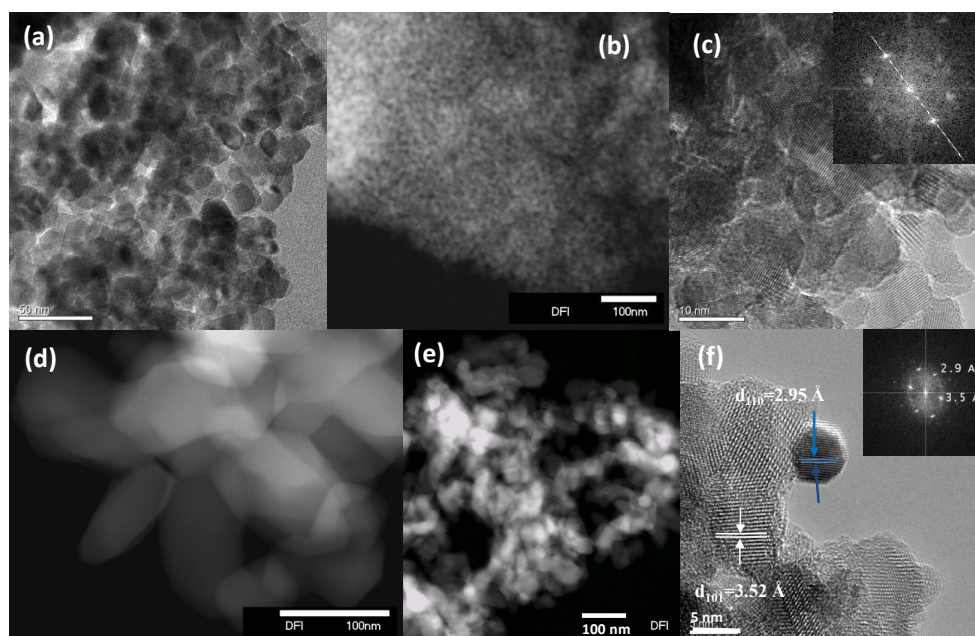


**Figure 4.4.** TEM image of mesoporous TiO<sub>2</sub> calcined at 500 °C (a), the dark-field TEM image of mesoporous TiO<sub>2</sub> calcined at 500 °C (b), HRTEM image of mesoporous TiO<sub>2</sub> calcined at 500 °C (c), The insets show the SAED patterns for the anatase phase (c), The dark-field TEM image of mesoporous TiO<sub>2</sub> calcined at 800 °C (d and e), HRTEM image of mesoporous TiO<sub>2</sub> calcined at 800 °C.

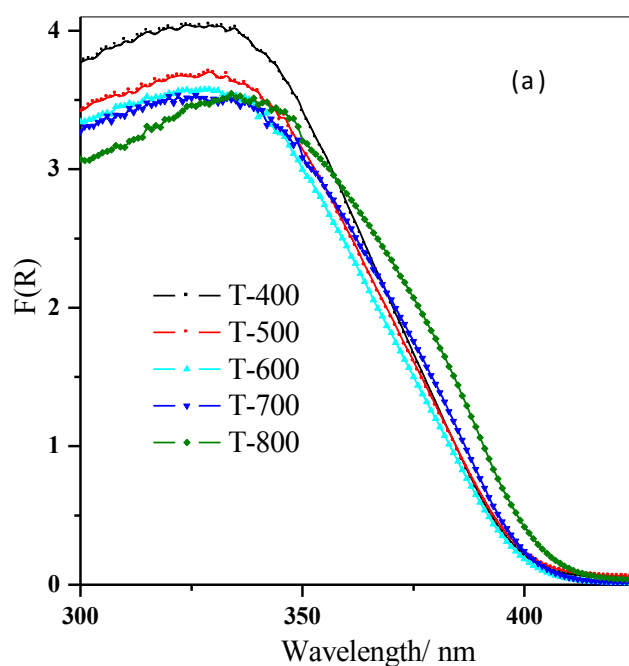
**Table 4.1.** Textural properties of mesoporous TiO<sub>2</sub> calcined at 400°C, 500°C, 600°C, 700 °C, and 800 °C and commercial P-25 and their photocatalytic performances.

Samples	$S_{BET}$ $m^2 g^{-1}$	Anatase %	Rutile %	Cs anatase nm	Cs Rutile nm	Band gap/ eV	$V_p$ , $cm^3/g$	$D_p$ (nm)	$K$ ( $min^{-1}$ ) Imazpyr	$K$ ( $min^{-1}$ ) Phenol
T-400	165	53.86	46.14	15.6	16.8	3.14	0.441	8.15	0.0134	0.0136
T-500	120	73.25	16.75	20.6	21.4	3.13	0.293	9.10	0.0344	0.0199
T-600	70	51.77	48.23	24.1	28.8	3.13	0.268	10.49	0.024	0.0148
T-700	35	47.32	52.68	43.60	41.0	3.11	0.273	18.50	0.0313	0.0182
T-800	15	18.10	81.90	91.1	75.1	3.00	-	-	0.0335	0.0152
P-25	50	80	20	-	-	3.20	-	-	0.0136	0.017

$S_{BET}$  Surface area;  $V_p$  pore volume;  $D_p$  pore diameter;  $K$  Rate constant.

Diffuse reflectance UV-Vis spectra of the prepared TiO<sub>2</sub> calcined at 400 °C, 500 °C, 600 °C, 700 °C, and 800 °C are given in Fig. 5. As shown in Fig. 5a, as the calcination temperature increases, the absorption edge is gradually shifted from 398 nm to 408 nm, revealing that the band gap energy values of the obtained mesoporous TiO<sub>2</sub> decrease as a result of the increase in the rutile/anatase ratio. The band gap energies of T-400, T-500, T-600, T-700, and T-800 photocatalysts estimated from the tangents are 3.06, 3.03, 3.01, 3.0 and 2.94 eV, respectively. The light absorption of T-800 is obviously lower than that of the prepared samples calcined at low temperature, in the range from 250 to 400 nm.

**Photocatalytic Degradation of Imazapyr and Phenol.** The photocatalytic performance of the prepared mesoporous TiO<sub>2</sub> nanocrystals calcined at the above mentioned temperatures for the photodegradation of both pollutants imazapyr and phenol were compared to that of the commercial P-25 (Figures 4.6. and 4.7.).



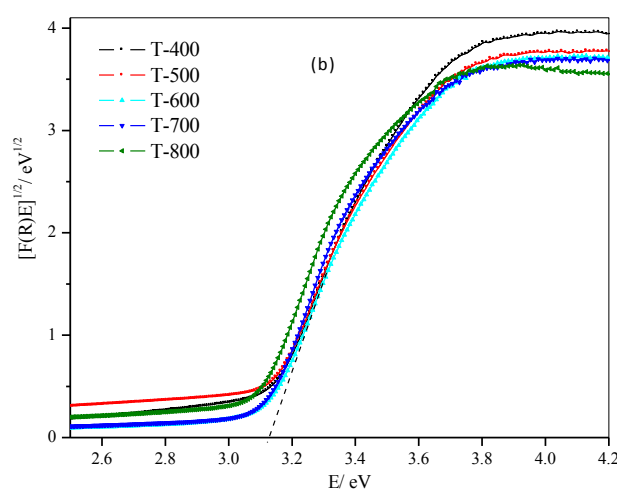


**Figure 4.5.** Diffuse reflectance spectra of mesoporous TiO<sub>2</sub> calcined at 400 °C, 500 °C, 600 °C, 700 °C, and 800 °C for 4 h (a). Plot of transferred Kubelka–Munk vs. energy of the light absorbed (b).

At first, the discussion will focus on the photocatalytic degradation of imazapyr (Figure 4.6). The photodegradation of imazapyr was performed in an aqueous solution by photolysis using UV light without photocatalyst. The results indicate that the degradation of imazapyr is negligible without photocatalyst, which indicates that imazapyr cannot easily be degraded by UV illumination. The initial concentration of the imazapyr has also been calculated before and after the dark adsorption. The adsorbed amount of imazapyr onto the surface and pores of TiO<sub>2</sub> nanocrystals for all the prepared samples is found to be around 7 %. Figure 4.6. shows the change in the imazapyr concentration as a function of the illumination time using T-400, T-500, T-600, T-700, T-800, and P-25 photocatalysts. All the prepared photocatalysts exhibit a promising behavior under UV illumination. However, the synthesized mesoporous TiO<sub>2</sub> nanocrystals calcined at different temperatures have shown a better photocatalytic activity than the commercial P-25. From the results, it is obvious that the imazapyr's percentage of photodegradation using the T-500 photocatalyst is 100 % whereas only 74 % of the photodegradation has been reached in presence of the commercial P-25 after 120 minutes, indicating a higher photocatalytic activity of the mesoporous T-500 photocatalyst in case of imazapyr (Figure 4.6a). With the help of a linear regression, the rate constants for the performed experiments are calculated on the basis of the natural logarithm (ln) of the imazapyr concentration and the illumination time, i.e., first-order degradation kinetics. This rate constant is employed

to calculate the initial photodegradation rates for the photooxidation of imazapyr using the formula:  $-d[A]/dt = kc^n$  where  $k$  is the rate constant,  $c$  the concentration of the imazapyr, and  $n$  the order of the reaction.

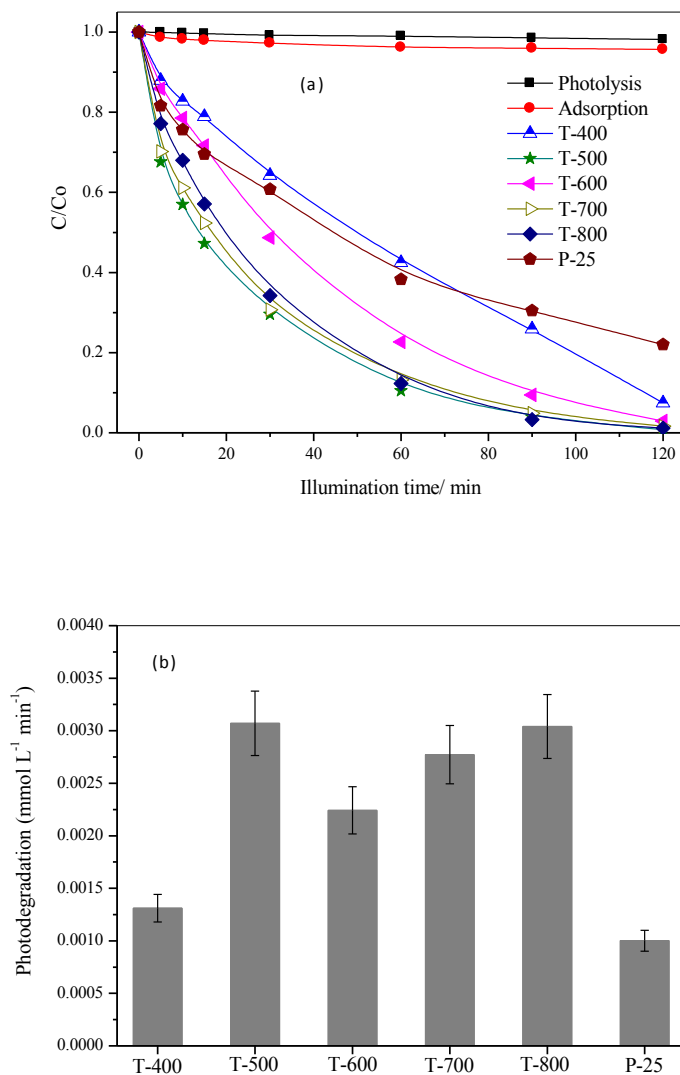


**Figure 4.6.** Change of the imazapyr concentration as a function of the illumination time using T-400, T-500, T-600, T-700, T-800, and P-25 photocatalysts (a), comparison of the initial degradation rate of imazapyr in the presence of commercial P-25, T-400, T-500, T-600, T-700, and T-800 photocatalysts (b). Photocatalyst loading,  $1 \text{ g l}^{-1}$ ;  $0.08 \text{ mmol l}^{-1}$  aqueous solution of imazapyr ( $\text{O}_2$  saturated,  $\text{pH} = 3$ ;  $T = 25 \pm 1 \text{ }^\circ\text{C}$ ); reaction volume 50 ml.

The initial degradation rate of imazapyr using the synthesized mesoporous TiO<sub>2</sub> increases from  $0.0013 \text{ mmol l}^{-1} \text{min}^{-1}$  to  $0.0029 \text{ mmol l}^{-1} \text{min}^{-1}$  with an increase of the calcination temperature from 400 to 500  $^\circ\text{C}$ , then a decrease to reach 0.0023

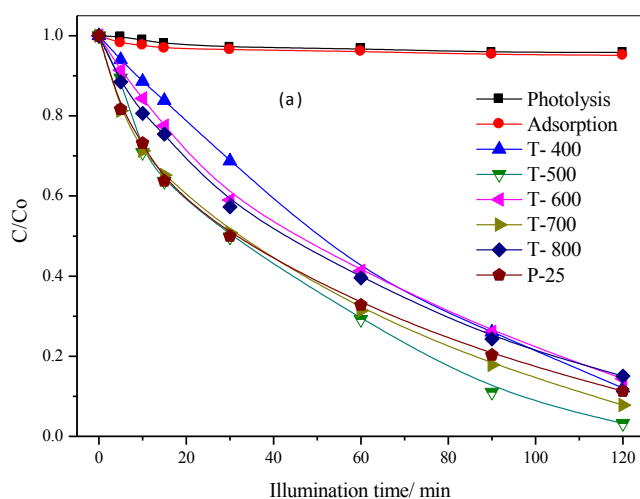
mmol l<sup>-1</sup> min<sup>-1</sup> at 600 °C. Again, the initial rate increases with the increase of the calcination temperature from 700 to 800 °C. The initial photodegradation rate of imazapyr using both, the T-500 and the T-800 samples, is similar. The results indicate that the initial rate using T-500 and T-800 is around 3 times higher than in case of the Aeroxide P-25.

The difference in the photocatalytic activity of the mesoporous samples prepared at different calcination temperatures compared to P-25 can be explained by several effects, such as a lower light scattering effect of the mesopores and higher cumulative •OH inside the pores [26, 36]. This effect can be attributed to the high dispersion of mesoporous TiO<sub>2</sub> nanocrystals in aqueous solution due to the smaller particle size compared to the nonporous P-25. Also, the imazapyr molecule is easily transported and diffused to the active sites of the mesoporous TiO<sub>2</sub>. However, it is hindered in the case of the nonporous P-25 photocatalyst. In addition, the results reveal that the surface area of the material is not the reason for the enhancement of the photocatalytic activity in the present system. This, due to the fact that the activities of the T-500 and T-800 samples are almost similar, in spite of the surface area of the T-500 (120 m<sup>2</sup> g<sup>-1</sup>) being 8 times higher than that of the T-800 sample (15 m<sup>2</sup> g<sup>-1</sup>). It can be concluded that the phase transformation, in this case the anatase/rutile ratio is playing the major role for improving the photocatalytic performance of the prepared samples. As can be seen in Table 1 and as the results of the structural investigations have already shown, the percentage of the anatase phase increases starting from 53.86% for the T-400 to reach 73.25% for the T-500 sample, then it gradually decreases as result of the transformation to the rutile phase which itself increases in percentage to reach 81.9% for the T-800 sample. However in the T-800 sample, the surface area is decreased while the rutile to anatase ratio is increased. This crystalline rutile/anatase ratio (81.9%/18.1%) in the T-800 sample is the responsible for the production of reactive •OH radicals. Under such conditions, the probability of formation of these active species should be much higher compared to the results obtained using the T-600 and T-700 samples which have shown a slight downtrend in the photodegradation of imazapyr. This can be explained by the difference in the anatase/rutile ratios, implying that in this system, the appropriate rutile/anatase ratio is essential for a complete reaction. Based on the result above we suggest that the following has occurred: The T-800 sample has a lower surface area and lost its mesoporous structure, however, due to the high crystalline rutile/anatase



mixed phase formation, it has a synergetic effect. This leads to a better charge separation, and an increase of the photocatalytic activity, by transferring the excited electrons from one phase to the other, which decreases the probability of the charge carriers recombination [37]. However, the T-500 sample must be considered as efficient due to its structure and ordered morphology.

Furthermore, it was expected that the behavior of the prepared photocatalysts for the phenol photodegradation is similar to imazapyr features. However, the results indicate that the photodegradation rate of phenol significantly increases at the beginning, and then shows a downward trend when the calcination temperature increases (Figure 4.7a). The photocatalytic efficiency of phenol using the T-500 sample is 100 % within 2 hours, however, the photocatalytic efficiency decreases to 80% using the T-800 sample (Figure 4.7b). The initial degradation rate of the T-500 sample is approximately twice as high compared to the rate of the commercial P-25. The photocatalytic degradation of phenol could be significantly increased using the T-500 sample (73.25 % anatase/16.75 % rutile), compared to the T-800 sample with a rutile/anatase ratio of (81.9%/18.1%) (Figure 4.7). The higher surface area, the crystallinity, and the mesoporous structure of the T-500 sample led to improve the adsorption capacity, indicating high active sites on the surface. This is assumed to be the main feature responsible for the higher photocatalytic activity of the T-500. In general, it is concluded that the behavior of the photocatalyst in term of photocatalytic efficiency and degradation rate is different according to the type of pollutant.



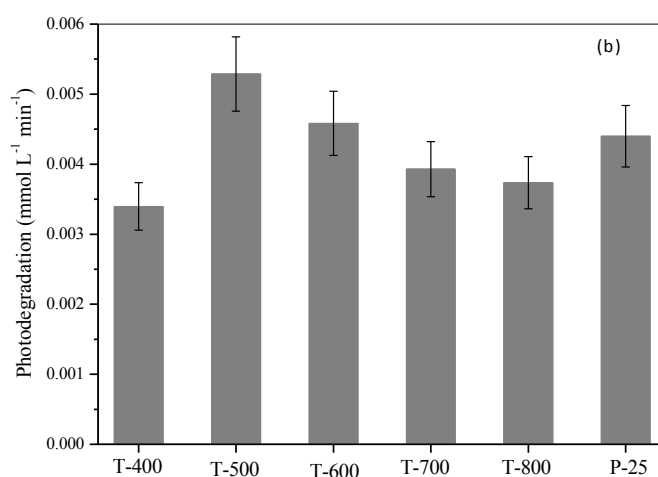


**Fig. 4.7.** Change of the phenol concentration as a function of the illumination time using T-400, T-500, T-600, T-700, T-800, and P-25 photocatalysts (a), comparison of the initial degradation rate of phenol in the presence of commercial P-25, T-400, T-500, T-600, T-700, and T-800 photocatalysts (b). Photocatalyst loading, 1 g l<sup>-1</sup>; 0.27 mmol l<sup>-1</sup> aqueous solution of phenol (O<sub>2</sub> saturated, pH = 3, T = 25 ± 1 °C); reaction volume 50 ml.

#### 4.5. Conclusions

TiO<sub>2</sub> nanocrystals have been synthesized through a facile method using the F127 tri-block copolymer as a template. The as-prepared hybrid meso-structures have been calcined at different temperatures to study their structural influence on the photocatalytic properties. The mesoporous TiO<sub>2</sub> photocatalysts are photocatalytically active, and show a higher activity for the decomposition of both pollutants, imazapyr and phenol, compared to the commercially available Aeroxide TiO<sub>2</sub> P-25. Also, the initial degradation rate of T-500 and T-800 is 3 times higher than P-25 for the photodegradation of imazapyr. In contrast to that, the initial degradation rate of T-500 sample is approximately twice the rate of the P-25 for photodegradation of phenol. The mesoporous structure, the morphology, the crystal growth, the phase transformation, and the surface area of the synthesized materials influence on the photocatalytic activity. Therefore, It is concluded that the behavior of the photocatalyst in term of initial degradation rate is different based on the pollutant type. In addition, the low calcination temperature leads to the homogeneity, the regularity and the uniformity of the pores. However, higher calcination temperature leads to higher crystallinity of the synthesized materials. Based on the results, mesoporous TiO<sub>2</sub> T-500 is an efficient material for the depollution of water from the

organic contaminants. Furthermore, the T-500 is considered to be a more viable photocatalyst as compared to the T-800 since for their preparation energy can be saved in the calcination process.

#### **4.6. Acknowledgments**

M. Faycal Atitar gratefully acknowledges a scholarship from the German Academic Exchange Service (DAAD) in the Frame of a Sandwich-Program. A. A. Ismail acknowledges the Alexander von Humboldt (AvH) Foundation for granting him a renewed research fellowship. Financial support from the Russian Foundation for Basic Research (13-03-90917 mol\_in\_nr) and the grant of the government of Russian Federation N 14.Z50.310016 are also gratefully acknowledged. Special thanks are due to Ms. Natalja Wendt of the Institut für Anorganische Chemie, Uni-Hannover, for her kind help in N<sub>2</sub> sorption measurements. TEM measurements performed by Prof. Dr. Armin Feldhoff of the Institut für Physikalische Chemie-Hannover are also gratefully acknowledged. The authors also thank Johannes Melcher and Imme Kretschmer from the Institut für Technische Chemie, Uni-Hannover, for Raman and XRD measurements, respectively.

#### 4.7. References

- [1] C. Cox, Nonyl phenol and related compounds, *J. Pesticide Reform* 16 (1996) 15-20.
- [2] K. Ikehata, M. Gamal El-Din, Aqueous Pesticide Degradation by Ozonation and Ozone-Based Advanced Oxidation Processes: A Review (Part II), *The Journal of the International Ozone Association*, 27 (2005)173-202.
- [3] N. M. Mallipudi, S.J. Stout, A.R. daCunha, A.-H. Lee, Photolysis of imazapyr (AC 243997) herbicide in aqueous media, *J. Agric. Food Chem.* 39 (1991) 412-417.
- [4] A. Santoro, M. Mansour, M. Tropea, A. Scopa, S. A. Bufo, Residue analysis of imazapyr and chlozolate in water using sunlight, *Bull. Environ. Contam. Toxicol.* 63(1999) 33-38.
- [5] G. Kaichouh, N. Oturan, M. A. Oturan, A. El Hourch, K. El Kacemi, Mineralization of herbicides imazapyr and imazaquin in aqueous by, fenton, photo-fenton and electro-fenton processes, *Environmental Technology*, 29(2008) 489-496.
- [6] S. Ahmed, M.G. Rasul, R. Brown, M.A. Hashib, Influence of parameters on the heterogeneous photocatalytic degradation of pesticides and phenolic contaminants in wastewater: A short review, *J. Environmental Management* 92(2011)311-330.
- [7] P. Pizarro, C. Guillard, N. Perol, J.-M. Herrmann, Photocatalytic degradation of imazapyr in water: Comparison of activities of different supported and unsupported TiO<sub>2</sub>-based catalysts, *Catalysis Today* 101(2005)211-218.
- [8] R. R. Ishiki, H. M. Ishiki, K. Takashima, Photocatalytic degradation of imazethapyr herbicide at TiO<sub>2</sub>/H<sub>2</sub>O interface, *Chemosphere* 58 (2005)1461-1469.
- [9] J. A. Osajima H. M. Ishiki, K. Takashima, The Photocatalytic degradation of imazapyr, *Monatshefte fur Chemie*, 139 (2008)7-11.
- [10] L. Lhomme, S. Brosillon, D. Wolbert, Photocatalytic degradation of pesticides in pure water and a commercial agricultural solution on TiO<sub>2</sub> coated media, *Chemosphere* 70 (2008)381-386.
- [11] X. Shen, J. Zhang, B. Tian, Microemulsion-mediated solvothermal synthesis and photocatalytic properties of crystalline titania with controllable phases of anatase and rutile, *J. Hazard. Mater.* 192 (2011) 651- 657.
- [12] J. H. Zhang, X. Xiao, J.M. Nan, Hydrothermal-hydrolysis synthesis and photocatalytic properties of nano-TiO<sub>2</sub> with an adjustable crystalline structure, *J. Hazard. Mater.* 176 (2010) 617-622.
- [13] M.C. Yan, F. Chen, J.L. Zhang, M. Anpo, Preparation of controllable crystalline titania and study on the photocatalytic properties, *J. Phys. Chem. B* 109 (2005)8673-8678.
- [14] H. Xu, L.Z. Zhang, Controllable one-pot synthesis and enhanced photocatalytic activity of mixed-phase TiO<sub>2</sub> nanocrystals with tunable brookite/rutile ratios, *J. Phys. Chem. C* 113(2009)1785-1790.
- [15] J.P. Wei, J.F. Yao, X.Y. Zhang, W. Zhu, H. Wang, M.J. Rhodes, Hydrothermal growth of titania nanostructures with tunable phase and shape, *Mater. Lett.* 61 (2007) 4610-4613.
- [16] J.C. Yu, L. Zhang, J.G. Yu, Direct Sonochemical Preparation and Characterization of Highly Active Mesoporous TiO<sub>2</sub> with a Bicrystalline Framework, *Chem. Mater.* 14 (2002) 4647-4653.

- [17] J.C. Yu, J.G. Yu, W.K. Ho, L.Z. Zhang, Preparation of highly photocatalytic active nano-sized TiO<sub>2</sub> particles *via* ultrasonic irradiation, *Chem. Commun.* 19 (2001) 1942-1943.
- [18] G. Zhang, Y. Zhang, M. Nadagouda, C. Han, K. O'Shea, S. M. El-Sheikh, A. A. Ismail, D. D. Dionysiou, Visible light-sensitized S, N and C co-doped polymorphic TiO<sub>2</sub> for photocatalytic destruction of microcystin-LR, *Applied Catalysis B: Environmental* 144 (2014) 614-621.
- [19] G. Zhang, M. Nadagouda, K. O'Shea, S. M. El-Sheikh, A. A. Ismail, D. D. Dionysiou, V. Likodimos, P. Falaras, Degradation of cylindrospermopsin by using polymorphic titanium dioxide under UV-Vis irradiation, *Catalysis Today* 224(2014) 49-55.
- [20] A. A. Ismail, T. A. Kandiel, D. W. Bahnemann, Novel (and better?) titania-based photocatalysts: brookite nanorods and mesoporous structures, *J. Photochemistry & Photobiology: A Chemistry* 216 (2010)183-193.
- [21] E. Grabowska, J. Reszczynska, A. Zaleska, Mechanism of phenol photodegradation in the presence of pure and modified-TiO<sub>2</sub>: A review, *Water research* 46 (2012) 5453-5471.
- [22] T. Luenloi, B. Chalermssinsuwana, T. Sreethawong, N. Hinchiranan, Photodegradation of phenol catalyzed by TiO<sub>2</sub> coated on acrylic sheets: Kinetics and factorial design analysis, *Desalination* 274 (2011) 192-199.
- [23] N. Guo, Y. Liang, S. Lan, L. Liu, G. Jia, S. Gan, H. Zou, X. Xu, Uniform TiO<sub>2</sub>-SiO<sub>2</sub> hollow nanospheres: Synthesis, characterization and enhanced adsorption-photodegradation of azo dyes and phenol, *Applied Surface Science* 305 (2014) 562-574.
- [24] A. A. Ismail, Facile synthesis of mesoporous Ag-loaded TiO<sub>2</sub> thin film and its photocatalytic properties, *Microporous & Mesoporous Materials*, 159 (2012)69-75.
- [25] L. Robben, A. A. Ismail, S. J. Lohmeier, A. Feldhoff, D. W. Bahnemann, J-C. Buhl, Facile synthesis of highly ordered mesoporous and well crystalline TiO<sub>2</sub>: Impact of different gas atmosphere and calcinations temperature on structural properties, *Chem. Mater.* 24(2012)1268-1275.
- [26] A. A. Ismail, D. W. Bahnemann, L. Robben, M. Wark, Palladium doped porous titania photocatalysts: Impact of mesoporous order and crystallinity, *Chem. Mater.*, 22 (2010)108-116.
- [27] A. A. Ismail, D. W. Bahnemann, I. Bannat, M.Wark, Gold nanoparticles on mesoporous interparticle networks of titanium dioxide nanocrystals for enhanced photonic efficiencies, *J. Phys. Chem. C*, 113 (2009) 7429-7435.
- [28] A. A. Ismail and D. W. Bahnemann, One-step synthesis of mesoporous platinum/titania nanocomposites as photocatalyst with enhanced its photocatalytic activity for methanol oxidation, *Green Chemistry* 13 (2011) 428- 435.
- [29] A. A. Ismail and D. W. Bahnemann, Mesoporous Pt/TiO<sub>2</sub> nanocomposites as highly active photocatalysts for the photooxidation of dichloroacetic acid, *J. Phys. Chem. C* 115(2011) 5784-5791.
- [30] J. Fan, S. W. Boettcher, G. D. Stucky, Nanoparticle assembly of ordered multicomponent mesostructured metal oxides via a versatile sol-gel process, *Chem. Mater.* 18 (2006) 6391-6396.
- [31] M. Grätzel, *Heterogeneous Photochemical Electron Transfer*; CRC Press: Baton Rouge, LA, 1988.

- [32] J. Tauc, R. Grigorovici, A. Vanuc, Optical properties and electronic structure of amorphous germanium, *Phys. Stat. Sol.* (1966) 15627-15637.
- [33] Y. Gao, H. Wang, J. Wu, R. Zhao, Y. Lu, B. Xin, Controlled facile synthesis and photocatalytic activity of ultrafine high crystallinity TiO<sub>2</sub> nanocrystals with tunable anatase/rutile ratios, *Applied Surface Science* 294 (2014) 36-41.
- [34] L. Miao, S. Tanemura, S. Toh, K. Kaneko, M. Tanemura, Fabrication, characterization and Raman study of anatase-TiO<sub>2</sub> nanorods by a heating-sol-gel template process, *Journal of Crystal Growth*, 264 (2004) 246-252.
- [35] R. Liu, Y. Ren, Y. Shi, F. Zhang, L. Zhang, B. Tu, D. Zhao, Controlled synthesis of ordered mesoporous C-TiO<sub>2</sub> nanocomposites with crystalline titania frameworks from organic-inorganic-amphiphilic coassembly, *Chem. Mater.* 20 (2008) 1140-1146.
- [36] S. Tojo, T. Tachikawa, M. Fujitsuka, T. Majima, Oxidation processes of aromatic sulfides by hydroxyl radicals in colloidal solution of TiO<sub>2</sub> during pulse radiolysis, *Chem. Phys. Lett.* 384 (2004) 312-316.
- [37] D. Sukkim, S-Y. Kwak, Photocatalytic inactivation of *E. coli* with a mesoporous TiO<sub>2</sub> coated film using the film adhesion method, *Environ. Sci. Technol.* 43 (2009) 148-151.

## Chapter 5

### Summarizing Discussion

This chapter begins with the discussion of the insight on the surface interactions between the model compound (i.e., imazapyr) and the TiO<sub>2</sub> surface obtained by an ATR-FTIR adsorption study, followed by the interpretation of the formed surface complexes. The role that these surface complexes may specifically play under illumination and the role that the adsorption generally plays in the overall photocatalytic process will be the focus of the discussion based on the results obtained by ATR-FTIR and the photocatalytic degradation studies. Finally, the design and synthesis of new materials being efficient for the photocatalytic degradation of imazapyr are also discussed.

As mentioned before, it is important to investigate the adsorption of organic compounds on the catalyst surface to reveal the importance of this process for the photocatalytic degradation. Nevertheless, the influence of diverse parameters on the adsorption behaviour has to be considered. Several parameters are known to influence the adsorption of organic molecules on TiO<sub>2</sub> surfaces, such as, the specific surface area, and the reaction pH (i.e., surface charge, and ionic forms of the organic molecule). Moreover, the surface shape of the material (i.e., the exposed faces and the presence of surface defects) as well as the presence of contaminant molecules on the surface should also be taken into account.

The adsorption on the TiO<sub>2</sub> surface is affected by electrostatic interactions. The organic compound employed here, i.e., imazapyr dissolved in water presents five distinct species with different charge depending on the pH of the solution (Figure 5.1a). Furthermore, the TiO<sub>2</sub> surface is predominantly positively charged at pH values below the p*H*<sub>zpc</sub>, neutral at p*H*<sub>zpc</sub>, and negatively charged at pH values above the p*H*<sub>zpc</sub> (Figure 5.1b) (i.e., Evonik Aeroxide TiO<sub>2</sub> P25 has p*H*<sub>zpc</sub> in the range 6.25-6.9). Thus, electrostatic attraction or repulsion between the semiconductor surface and the organic species should be considered depending on the pH of the solution. When the adsorption is electro-neutral, it may proceed simply just via the exchange of a basic OH surface group with the corresponding organic ligand to form inner sphere complexes.

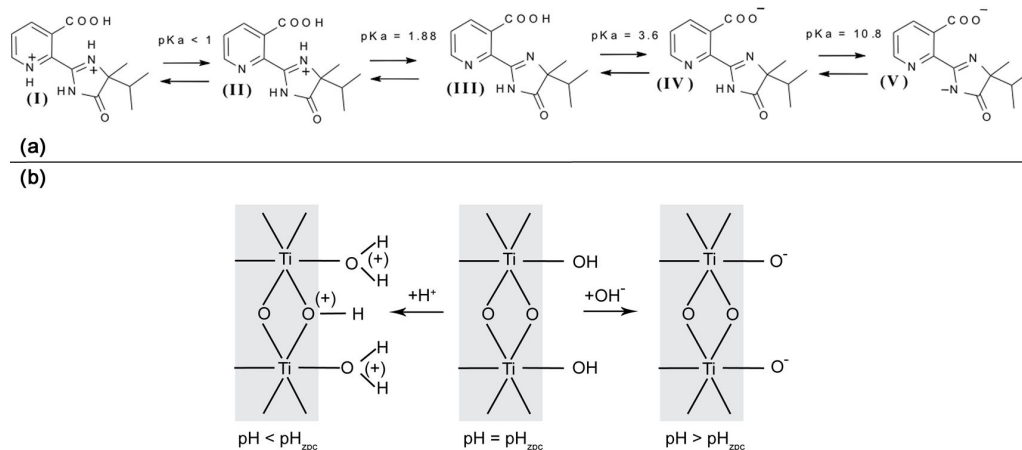


**Figure 5.1.** Different forms of imazapyr (a) (Reprinted with permission from M. Faycal Atitar, Ralf Dillert, and Detlef W. Bahnemann. Surface Interactions between Imazapyr and the  $\text{TiO}_2$  Surface: An *in Situ* ATR-FTIR Study. *Journal of Physical Chemistry C*; 121:4293-4303. Copyright (2017) American Chemical Society), and scheme of the protonation and deprotonation of hydroxylated  $\text{TiO}_2$  surface leading to positive and negative charges at the surface (b) (adapted from [1]), depending respectively on the pH.

The adsorption of imazapyr onto a  $\text{TiO}_2$  film has been investigated in-situ using attenuated total reflection Fourier transform infrared spectroscopy (ATR-FTIR) to disclose the nature of the binding mode of imazapyr at the  $\text{TiO}_2$  surface. The change in spectra of imazapyr as a function of the pH indicates that this interaction is pH dependent. This could be attributed to the pH dependent protonation and deprotonation of the imazapyr molecule as is evident from the spectra of homogeneous imazapyr solutions. However, this pH dependency in the presence of a  $\text{TiO}_2$  layer is associated to different interaction modes between the imazapyr species present in the solution and at the  $\text{TiO}_2$  surface.

The identification as well as the interpretation of different bands assigned to the main functional groups of the probe molecule was performed with the help of previously published works presenting IR studies of adsorbed molecules having similar functional groups as imazapyr. The respective analysis of the spectra indicated that imazapyr is covering the  $\text{TiO}_2$  surface as a bidentate and/or bridging ligand over the investigated pH range. Additional information concerning the structure of the adsorbates has been obtained from previously published work [2]. These are based on the calculated charge densities of the different imazapyr species



in the aqueous phase and a dihedral angle equivalent to N3(imidazol)–C2(imidazol)–C2(pyridine)–N1(pyridine) given as  $212^\circ$ . It has been concluded that the adsorption occurs mainly through the carboxylic oxygen. Furthermore, the interaction is more favourable between the deprotonated imazapyr molecule (Figure 5.2) and the protonated  $\text{TiO}_2$  surface as  $\text{TiOH}^{2+}$ .

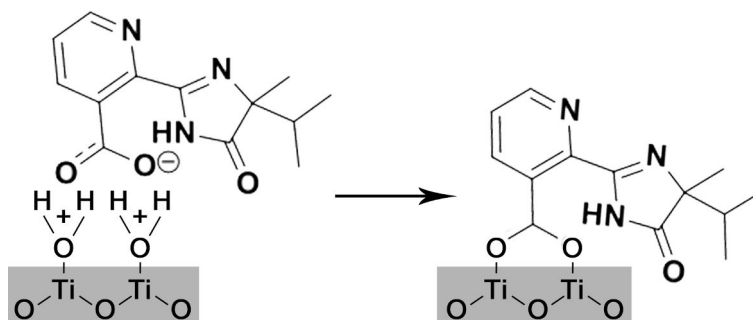


**Figure 5.2.** Favoured mode of interaction between deprotonated imazapyr species and the positively charged  $\text{TiO}_2$  surface leading to the bridging ligand.

Hence, from this spectral evidence the adsorption of imazapyr at the  $\text{TiO}_2$  surface results in different surface-adsorbed species as depicted in Figure 5.3. The adsorption of imazapyr onto the  $\text{TiO}_2$  surface is favoured at pH values below the point of zero charge of  $\text{TiO}_2$ . Upon adsorption, the carboxylic acid group of imazapyr binds at surface Ti(IV) centers mainly as a bridging ligand at acidic pH (i.e.,  $\text{pH} < \text{pH}_{\text{zpc}}$ ). With increasing pH values (in alkaline medium) the binding of imazapyr to the surface becomes less favourable, this is due to the fact that both imazapyr as well as the  $\text{TiO}_2$  surface are negatively charged leading to electrostatic repulsion. Presumably, imazapyr dissociatively adsorbs through the contribution of the pyridine ring and the N–C=O moiety of the imidazole ring.

From the above discussion, two important points should be taken into account. The first issue concerns the pH effects on the adsorption. The influence of electrostatic interactions was mentioned to be the cause of decreasing adsorption with increasing pH. This is not only the result of changing the pH of the solution, but may also be affected by the ionic strength of the electrolyte solution. The Debye length determines the length scale at which electrostatic interactions between charged particles are screened. Furthermore, it has been suggested that the charging behaviour of nanostructured surfaces may have important consequences for adsorption processes as well as for surface interactions.

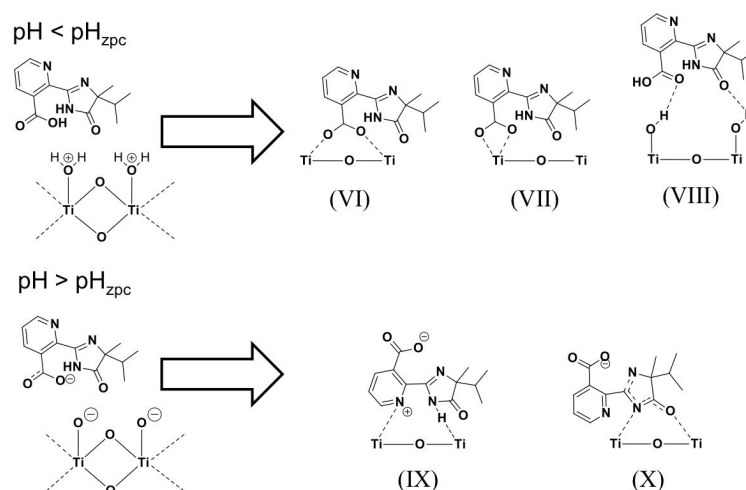


**Figure 5.3.** Proposed structures of adsorbed imazapyr species on the  $\text{TiO}_2$  surface at different pH values. (Reprinted with permission from M. Faycal Atitar, Ralf Dillert, and Detlef W. Bahnemann. Surface Interactions between Imazapyr and the  $\text{TiO}_2$  Surface: An *in Situ* ATR-FTIR Study. *Journal of Physical Chemistry C*; 121:4293-4303. Copyright (2017) American Chemical Society).

The electrolyte used in all experiments is  $10 \text{ mmol L}^{-1}$  (0.01 M salt) which results in a Debye length of 3.1 nm at pH 5 and 7 and 2.9 nm at pH 3 and 9. Since the presented data have been obtained at nearly constant Debye lengths, the possible effect of the ionic strength cannot be considered to play a significant role for the interpretation of the pH effect presented here. However, the probability of screening of electrostatic repulsions between the negatively charged imazapyr and the negatively charged  $\text{TiO}_2$  surface, or the formation of surface species due to the adsorption of the electrolyte, cannot be excluded.

The second issue concerns the allocation of the adsorbed species onto the surface, the presence of the bidentate surface complex as well as that of hydrogen-bonded and other inner- or outer-sphere surface species (which are not proposed in the interpretation) is not excluded in the overall interaction. The probability that the different adsorbates coexist at the  $\text{TiO}_2$  surface is also concluded from the spectral analysis. The predominance of the above-mentioned adsorbed imazapyr species at acidic pH was based on the intensity of the bands assigned to these species. However, no specific spectral evidence exists concerning the amount of adsorbed species per square nanometer ( $\text{nm}^2$ ) at the  $\text{TiO}_2$  surface. Several studies have reported an adequate parameter to compare the adsorption efficiency of different powders, that is the number of sites per  $\text{nm}^2$  (sites/ $\text{nm}^2$ ). This parameter provides the

information required to determine the number of exchangeable OH groups at the surface of the TiO<sub>2</sub> sample. Furthermore, the number of sites/nm<sup>2</sup> is experimentally usually determined from the fluoride adsorption isotherm, since fluoride is considered to adsorb onto the TiO<sub>2</sub> through a maximal exchange of OH groups. For Evonik Aeroxide TiO<sub>2</sub> P25 the number of exchangeable OH groups has been given in the range [1.7-2.4]/nm<sup>2</sup> [3,4]. However this value should be used with care when comparing different adsorbed molecules and/or different TiO<sub>2</sub> samples. The values for the maximum capacity of the adsorbent,  $q_m$ , and the known surface area of the photocatalyst (50 m<sup>2</sup> g<sup>-1</sup>), have been used to calculate the amount of adsorbed molecules per unit area for imazapyr. This is found to be 0.616 μmol m<sup>-2</sup> (0.37 molecule nm<sup>-2</sup>), 0.800 μmol m<sup>-2</sup> (0.48 molecule nm<sup>-2</sup>) and 0.456 μmol m<sup>-2</sup> (0.27 molecule nm<sup>-2</sup>) at pH 3, pH 5 and pH 7, respectively. With the surface area and the density of the photocatalyst (3.8×10<sup>6</sup> g m<sup>-3</sup> for anatase), a radius of 15.8 nm is calculated for a single photocatalyst particle. Consequently, a single photocatalyst particle with a surface area of approximately 3100 nm<sup>2</sup> will be fully covered by 1162, 1509 and 860 imazapyr molecules at pH 3, pH 5 and pH 7, respectively. One imazapyr molecule on the surface thus demands an area between 2.1 and 3.2 nm<sup>2</sup>. These values are in reasonable agreement with the values calculated from the geometry of an imazapyr molecule.

The results of the ATR-FTIR investigations performed here can be taken as experimental confirmation for the results of semi-empirical calculations that have been performed earlier by another research group [2]. These researchers have reported that the preferential mode of adsorption of imazapyr is the bridging binding of the carboxylic group to the TiO<sub>2</sub> surface. Moreover, the main product of the photocatalytic imazapyr degradation is formed by the direct hole oxidation of the carboxyl moiety attached to the pyridine ring followed by subsequent decarboxylation (Photo-Kolbe reaction).

The combination of the experimental results and the theoretical calculations published previously allowed a better understanding of some aspects of the adsorption as well as of the photocatalytic degradation mechanism of imazapyr. The explanation for the mechanism of the photocatalytic degradation of imazapyr adsorbed in a bridging form at acidic pH is that the TiO<sub>2</sub> surface oxygen atoms located directly underneath the adsorbed imazapyr species serve as traps for the holes generated by the absorption of UV light. This leads to the generation of oxygen-

centered radicals in the direct neighbourhood to the target molecule enabling a facile interfacial electron transfer from the carboxylate group to these hole traps (Figure 5.4).

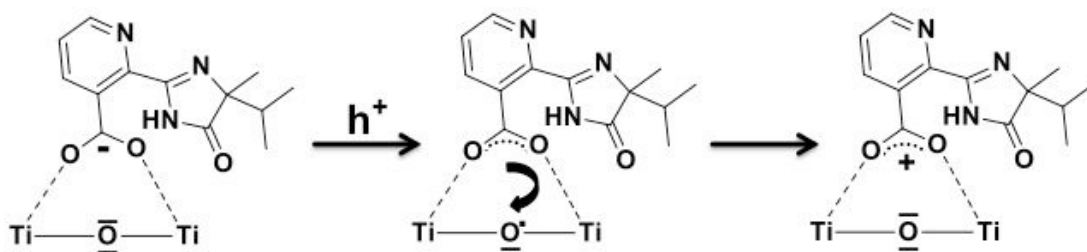


**Figure 5.4.** Proposed mechanism of the interaction of imazapyr with a terminal oxygen radical formed on the  $\text{TiO}_2$  surface upon light absorption. (Reprinted with permission from M. Faycal Atitar, Ralf Dillert, and Detlef W. Bahnemann. Surface Interactions between Imazapyr and the  $\text{TiO}_2$  Surface: An *in Situ* ATR-FTIR Study. Journal of Physical Chemistry C; 121:4293-4303. Copyright (2017) American Chemical Society).

The importance of the above-proposed mechanism for the overall photocatalytic degradation process still remains unclear. For deeper understanding of the mechanism, the approach is to correlate the photocatalytic degradation with the adsorption phenomena, taking both the equilibrium and the kinetics into consideration. The kinetics of the photocatalytic imazapyr degradation were analyzed taking into account the effect of the pH as well as the catalyst loading. However, special attention was given to the influence of the reactant concentration. The adsorption of imazapyr onto the  $\text{TiO}_2$  surface has been quantified by isotherms which basically indicate the mass of substrate adsorbed (adsorbate) per known mass of adsorbent being  $\text{TiO}_2$  P25 in our case. Furthermore, adsorption kinetics are of great significance to evaluate the performance of a given adsorbent and to gain insight into the underlying mechanisms. On the other hand, it describes the rate of adsorbate uptake by an adsorbent, and controls the equilibration time.

For this purpose, The photocatalytic degradation of imazapyr was studied in a series of experimental runs at constant volume, temperature, light intensity, and photocatalyst loading. The effect of the initial imazapyr concentration was investigated in the presence of  $2.5 \text{ g L}^{-1}$  of  $\text{TiO}_2$ , being the optimum catalyst loading for the photocatalytic imazapyr degradation. The initial substrate (i.e., imzapyr) concentration was varied in the range of 15–200  $\mu\text{M}$ . The photocatalytic oxidation of

imazapyr obeys first order rate law, and the rate constants was determined from the plot of natural logarithm of pollutant concentration as a function of irradiation time. The photodegradation kinetics of imazapyr in TiO<sub>2</sub> P25 dispersion has been modelled to the simple Langmuir-Hinshelwood (L-H) model. The linear relationship indicate that the degradation kinetics under UV illumination apparently follow the L-H model which is a manifestation of the general case of saturation-type kinetics.

The adsorption of imazapyr onto TiO<sub>2</sub> nanoparticles (i.e., Evonik Aeroxide TiO<sub>2</sub> P25) was studied at different pH values. The results show that the dark adsorption of imazapyr is rather fast at initial times but reaches the equilibrium concentration only after about 120 min. The final equilibrium seems to be established within 3 hours. The highest adsorbed amount of imazapyr is obtained at pH 3, while this amount decreases with an increase of the pH value.

The analysis of the adsorption equilibrium data, using Langmuir and Freundlich models, has shown good fits to both models, and that a strong interaction between TiO<sub>2</sub> and imazapyr can be expected. It is worth to note that the Langmuir model assumes the adsorption energy to be uniform across the entire surface without any interaction between the adsorbed species. Furthermore, only chemical interactions are considered. Thus, only monolayers of the adsorbate can be formed on the surface of the adsorbent. In contrast, the Freundlich model does not assume energetic equivalence among the adsorption centres. On the other hand, The experimental data of the adsorption kinetics have been analyzed using two different models. From the values of the correlation coefficient it has been concluded that pseudo-second order model describes the adsorption kinetics of imazapyr onto TiO<sub>2</sub> rather well.

The results of the adsorption experiments indicate that the maximum monolayer capacity of adsorbent is 30  $\mu\text{mol g}^{-1}$  at pH 3, and increases to 40  $\mu\text{mol g}^{-1}$  at pH 5, whereas it decreases to 23  $\mu\text{mol g}^{-1}$  at pH 7. On the other hand, the different values determined for the Langmuir constant  $K_L$  indicate that the adsorption density is higher at pH 3 because of limitations of the TiO<sub>2</sub> adsorption capacity whereas the value of the Langmuir adsorption constant decreases with increasing pH. Assuming an initial equilibrium imazapyr concentration of 100  $\mu\text{mol L}^{-1}$  in the liquid phase, it is calculated that the amount of imazapyr adsorbed at the TiO<sub>2</sub> surface in the dark is decreasing from 9.6  $\mu\text{mol g}^{-1}$  at pH 3 to 2.9  $\mu\text{mol g}^{-1}$  at pH 7. If the amount of the organic molecules (imazapyr) adsorbed on the surface of the photocatalyst is decisive for the rate of the photocatalytic degradation, it is expected that the photocatalytic

degradation rate as well as the rate of imazapyr adsorption follows the same trend: at pH 3, the rates should therefore be the highest and the rates should decrease with increasing pH. In fact, this decrease of the rates with increasing pH was observed for both, the photocatalytic degradation and the adsorption, in the experimental runs performed here. The pH dependence of the determined rates for the adsorption and the photocatalytic degradation on the basis of electrostatic interactions between imazapyr and the TiO<sub>2</sub> surface can be explained. This explanation does not contradict the assumption that the probe molecule is photocatalytically degraded by a Langmuir-Hinshelwood mechanism. However, this mechanism presupposes that the rate of the photocatalytic reaction rate is smaller than or equal to the rate of imazapyr adsorption ( $r_r \leq r_a$ ). But the adsorption equilibria in the dark were only established after more than two hours.

To compare between these rates, the initial reaction rates,  $r_{r,0}$ , of the imazapyr degradation have been calculated considering the concentration of the photocatalyst in the aqueous suspension. The initial adsorption rates of imazapyr,  $r_{a,0}$ , have been calculated using the pseudo-second order model equation with the initial condition  $q_t = 0$  at  $t = 0$ . The amount of the adsorbed substrate  $q_e$  in the initial equilibrium was calculated employing the parameters of the Langmuir isotherm.

The calculation of the initial adsorption rates has been performed for different initial imazapyr concentrations to reveal the correlation to the initial degradation rate, as well as the effect of the initial concentration of imazapyr. However, the comparison of the initial imazapyr degradation rates with the initial imazapyr dark adsorption rates at different pH values show that the initial photocatalytic reactions are always faster than the dark adsorption. In other words, the initial photocatalytic degradation rate of imazapyr was found to be 2–3 times larger than its initial adsorption rate obtained in the dark.

If it is assumed that the photocatalytic degradation reaction occurs according to an Langmuir-Hinshelwood mechanism, one must demand that the rate constant of the adsorption under irradiation with UV light is drastically increasing. This would inevitably also result in a value for  $K_{LH}$  determined experimentally under exposure to UV light being greater than the value of  $K_L$  determined from adsorption isotherms in the dark. In fact, it was found here that the kinetic parameters  $K_{LH}$  are significantly greater than the adsorption constants  $K_L$  for all investigated pH values ( $K_{LH} / K_L \geq 12.5$ ). Such a ratio between these constants has also been observed for other probe

molecules as reported by several authors [5,6]. This has been explained by the fact that reactions between freely diffusing  $\bullet\text{OH}$  radicals and the organic substrate occur in the suspension in addition to the surface reaction. Another assumption is that sites associated with the photocatalytic reaction are different to those where dark adsorption occurs. Possibly, the reactive adsorption sites are only produced under irradiation. The possibility that these new adsorption sites are formed by deaggregation of titanium dioxide clusters which are known to be present in aqueous suspensions should not be excluded. It has been shown for very small particles that the dark adsorption constant depends on the particle diameter. This has been rationalized with a driving force to decrease the total free energy by adsorption of molecules from the surrounding environment.

The experimental results presented here can only be reconciled with a Langmuir-Hinshelwood mechanism by assuming light-induced changes of the photocatalyst surface which have a significant effect on the adsorption of the probe molecule. In other words, a Langmuir-Hinshelwood mechanism for the photocatalytic imazapyr degradation is compatible only with the additional assumption that the adsorption-desorption kinetics are also affected by irradiation with UV light, and in particular that the adsorption rate increases significantly

The photocatalytic reaction of imazapyr occurs not only at the  $\text{TiO}_2$  surface involving adsorbed imazapyr species, but also in the aqueous suspension involving freely diffusing  $\bullet\text{OH}$  radicals and the dissolved organic reactant. These species (i.e.,  $\bullet\text{OH}$  radicals) can be generated through the oxidative pathway by the reaction of valence band holes with  $\text{H}_2\text{O}/\text{OH}^-$  being present at the photocatalyst surface, and/or through the reductive pathway by the reaction of conduction band electrons with adsorbed molecular oxygen. Hence, it is concluded that the photocatalytic degradation of imazapyr involves combination of mechanisms, the direct transfer mechanism via holes, and the indirect transfer mechanism via  $\bullet\text{OH}$  radicals (Figure 5.5).

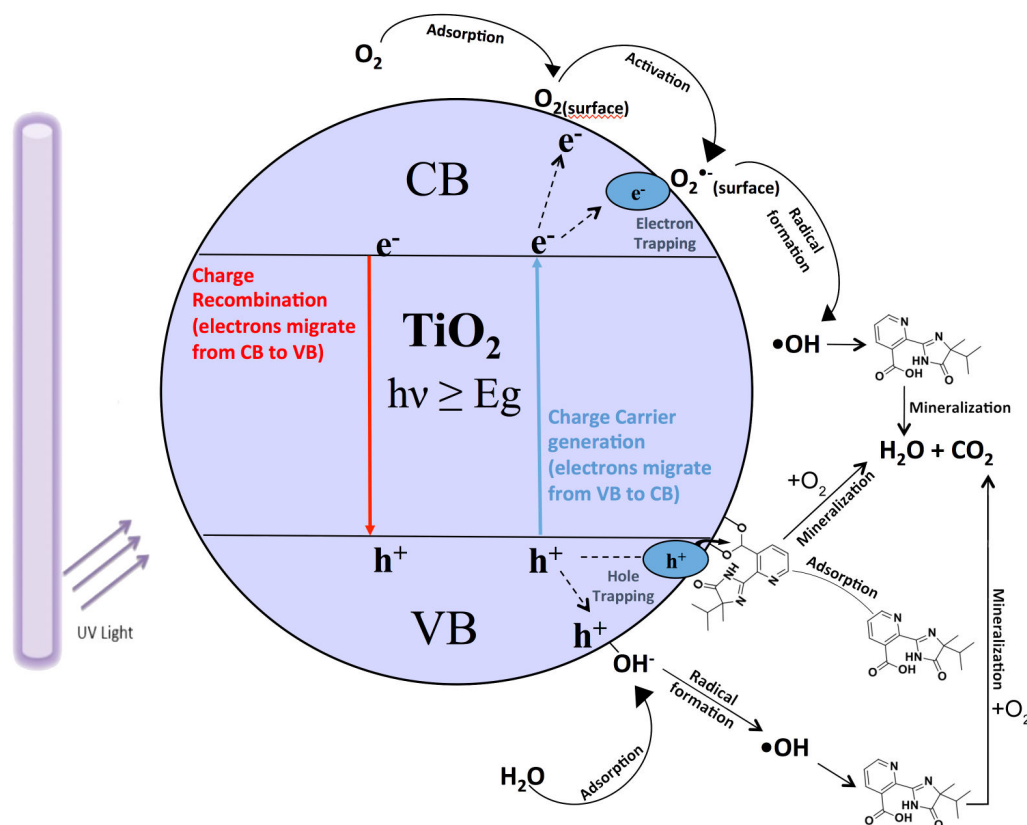


**Figure 5.5.** Mechanism of the photocatalytic degradation of imazapyr

It has already been mentioned earlier (in the introduction) that several parameters affect the kinetics and mechanisms of the photocatalytic process. These parameters can be subdivided into those that are intrinsic to the photocatalytic material and those that are extrinsic being influenced by the surrounding environment and conditions (e.g. pH, ionic strength, and the nature of the solvent). Therefore, the synthesis of mesoporous TiO<sub>2</sub> nanomaterials was expected to yield new insights into the photocatalytic degradation mechanism of imazapyr from the photocatalytic material point of view. The focus of this study was the relationship between the effect of calcination temperature, the phase transformation, and the surface area of the synthesized mesoporous TiO<sub>2</sub> photocatalysts with respect to the photocatalytic activity using imazapyr as the organic model compound.



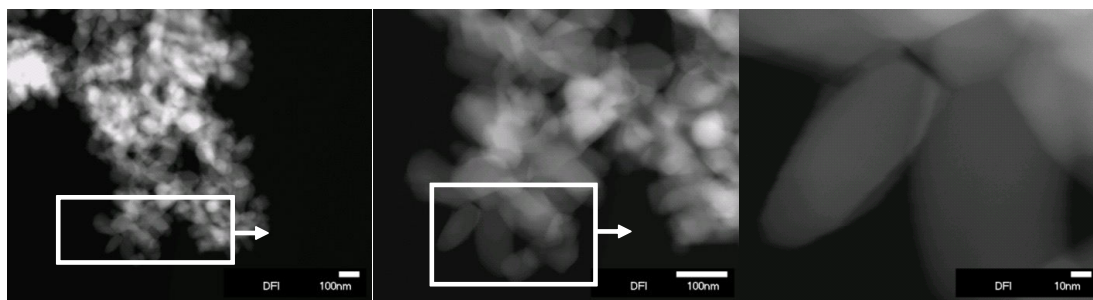


**Figure 5.6.** HRTEM images of the T-800 sample calcined at 800°C

Mesoporous TiO<sub>2</sub> has been synthesized through a simple one-step sol-gel process in the presence of the tri-block copolymer F127 as the structure templating agent followed by calcination of the samples at 400 °C, 500 °C, 600 °C, 700 °C, and 800 °C. The physical characterization of the newly prepared photocatalysts was carried out using X-ray diffraction (XRD), transmission electron microscopy (TEM), N<sub>2</sub> adsorption isotherm, Raman spectroscopy, as well as diffuse reflectance spectroscopy (DRS).

The XRD patterns as well as the Raman spectra revealed that all synthesized materials are mixed phase TiO<sub>2</sub> (i.e., anatase/rutile). On the other hand, the sample T-400 shows very low crystallinity indicating an incomplete transition from amorphous to the anatase/rutile structural mixture. Calcination at low temperature frequently results in amorphous or poorly crystallized titania with a high surface area. For the other samples, the increase of the rutile content was found to be associated with the increase in the calcination temperature, *i.e.*, the rutile content varies from 17 to 82 % when the calcination temperature is increased from 500 to 800°C, respectively. Furthermore, the BET surface area of the thus prepared TiO<sub>2</sub> nanocrystals was found to be in the range from 50-165 m<sup>2</sup> g<sup>-1</sup> and their pore diameter ranging from 8.15 to 18.50 nm. For the samples calcined at 800°C the results show that the samples are non-porous, where the agglomeration of the large (nano) particles leads to irregular voids between the particles. However, some mesoporosity is evident from the TEM images (Figure 5.6).

The photocatalytic performance of these newly prepared mesoporous TiO<sub>2</sub> nanocrystals calcined at the above mentioned temperatures for the photodegradation of the model pollutants imazapyr and phenol was compared to that of the commercial material Aeroxide TiO<sub>2</sub> P-25. All newly prepared photocatalysts were found to be

photocatalytically active. Moreover, the initial degradation rate of T-500 (sample calcined at 500°C) and T-800 (sample calcined at 800°C) is found to be 3 times higher than P-25 for the photodegradation of imazapyr. This is explained by several effects such as lower light scattering effect of the mesopores and a higher cumulative •OH radical concentration inside the pores. This effect can be attributed to the high dispersion of mesoporous TiO<sub>2</sub> nanocrystals in aqueous solution due to the smaller particle size compared to that of the nonporous P-25. Moreover, the imazapyr molecule can easily be transported to the active sites of the mesoporous TiO<sub>2</sub> whereas these processes are hindered in the case of the nonporous P-25 photocatalyst. Additionally, the results reveal that the surface area of the material cannot be regarded as the main reason for the enhancement of the photocatalytic activity in the present system. The activities of T-500 and T-800 samples are almost similar, in spite of the surface area of the T-500 (120 m<sup>2</sup> g<sup>-1</sup>) being 8 times higher than that of the T-800 sample (15 m<sup>2</sup> g<sup>-1</sup>).

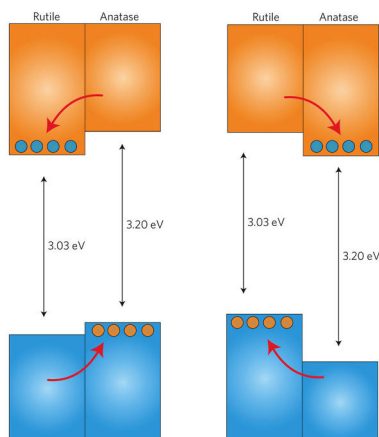


**Figure 5.7.** Two proposed valence and conduction band alignment mechanisms for the anatase/rutile interface. the arrows indicate the flow of electrons (holes) in the conduction band (valence band). Blue and orange dots represent electrons and holes, respectively. Adapted by permission from Macmillan Publishers Ltd: [Nature Materials] (David O. Scanlon, Charles W. Dunnill, John Buckeridge, Stephen A. Shevlin, Andrew J. Logsdail, Scott M. Woodley. Band alignment of rutile and anatase TiO<sub>2</sub>. 12(9): 798-801), copyright (2013).

It could be concluded that the phase transformation, in this case the anatase/rutile ratio, is playing a major role for improving the photocatalytic performance of the prepared samples. The T-800 sample has a lower surface area and has lost its mesoporous structure, however, the high crystalline rutile/anatase mixed phase

formation apparently leads to a better charge separation and hence an increase in photocatalytic activity, by transferring the excited electrons from one phase to the other (Figure 5.7), which decreases the probability of charge carrier recombination. However, the T-500 sample showed similar efficiency due to its uniform structure and its ordered morphology.

**References:**

- [1] R. Beranek, (Photo)electrochemical methods for the determination of the band edge positions of TiO<sub>2</sub>-based nanomaterials, *Adv. Phys. Chem.* 2011 (2011) 1–20. doi:10.1155/2011/786759.
- [2] M. Carrier, N. Perol, J.-M. Herrmann, C. Bordes, S. Horikoshi, J.O. Paise, R. Baudot, C. Guillard, Kinetics and reactional pathway of Imazapyr photocatalytic degradation Influence of pH and metallic ions, *Appl. Catal. B Environ.* 65 (2006) 11–20. doi:10.1016/j.apcatb.2005.11.014.
- [3] E. Tauchert, Interactions and Photocatalytic Reactions of Organochlorine Compounds at the Nanoparticulate TiO<sub>2</sub> Surface: A FTIR Study, 2012. <http://edok01.tib.uni-hannover.de/edoks/e01dh12/688549365.pdf>.
- [4] C.B. Mendive, Effects of the UV(A) light on chemical reactions at the interface metal oxide / aqueous solution, Universidad Nacional de San Martin, 2007.
- [5] A. Mills, S. Morris, Photomineralization of 4-chlorophenol sensitized by titanium dioxide: a study of the initial kinetics of carbon dioxide photogeneration, *J. Photochem. Photobiol. A Chem.* 71 (1993) 75–83. doi:10.1016/1010-6030(93)87012-C.
- [6] F. Zhang, J. Zhao, T. Shen, H. Hidaka, E. Pelizzetti, N. Serpone, TiO<sub>2</sub>-assisted photodegradation of dye pollutants II. Adsorption and degradation kinetics of eosin in TiO<sub>2</sub> dispersions under visible light irradiation, *Appl. Catal. B Environ.* 15 (1998) 147–156.

## Chapter 6

### Conclusion and Outlook

The approach to correlate surface interactions, photocatalytic degradation, and adsorption phenomena, taking both the adsorption equilibrium and the adsorption kinetics into consideration has improved the fundamental understanding of the basic mechanisms involved in the adsorption as well as in the photocatalytic oxidation of imazapyr in the presence  $\text{TiO}_2$ .

The ATR-FTIR technique providing the opportunity to obtain novel information concerning interfacial processes in situ has been used to identify several surface complexes of imazapyr on the  $\text{TiO}_2$  surface elucidating possible surface reaction mechanisms. Furthermore, the results can be taken as a key for a deeper understanding of the mechanisms occurring in the photocatalytic degradation process of imazapyr resulting in a newly proposed mechanistic pathway involving the participation of the  $\text{TiO}_2$  surface lattice oxygen as hole traps.

Depending on the type and degree of interaction, organic species are photocatalytically oxidized either via the direct hole transfer mechanism, the indirect mechanism via  $\bullet\text{OH}$  radical intermediates, or a combination of both mechanisms. The ATR-FTIR study revealed that imazapyr is strongly adsorbed at the  $\text{TiO}_2$  surface forming bridging carboxylate complexes and other surface complexes involving the heterocyclic rings of this probe molecule. The adsorption of imazapyr has been successfully described by the Langmuir isotherm. This implies that the  $\text{TiO}_2$  and the imazapyr are strongly interacting. However, the investigation of the adsorption kinetics of imazapyr has shown that the adsorption of imazapyr is slow, and reaches the equilibrium concentration in the liquid phase after about 120 min.

the comparison of the initial rate of adsorption obtained in the dark with the initial rate of the photocatalytic imazapyr degradation revealed that the photocatalytic reaction of imazapyr is always faster than the dark adsorption rate obtained in the dark.

The determined degradation rates can be explained by two different concepts:

- a) The photocatalytic degradation is a surface reaction of adsorbed imazapyr but the UV irradiation is not only initiating the degradation reaction but also

changing the structure of the photocatalyst, thus, significantly affecting the adsorption kinetics of the probe molecule.

- b) The photocatalytic reaction of imazapyr occurs not only at the TiO<sub>2</sub> surface involving adsorbed species, but also in the aqueous suspension involving freely diffusing •OH radicals and the dissolved organic reactant.

In this respect, it is pertinent to mention here that the efficiency of the charge transfer mechanism could also be improved via the synthesis of TiO<sub>2</sub> materials. In this work, it has been shown that the mesoporous structure, the morphology, the crystal growth, the phase transformation, and the surface area of the material determine the mechanism as well as the kinetics of the photocatalytic reaction of imazapyr.

The experimental procedure and methodological analysis presented here can be applied to the study of almost any photocatalytic reaction, allowing the illustration of the type of adsorption as well as the photooxidation mechanisms involved in this reaction. However one important point for future studies is to investigate the adsorption under light irradiation using an adequate substrate, in order to reveal light-induced changes of the photocatalyst that affect the adsorption process.

## List of Publications

- **M. Faycal Atitar**, Asmae Bouziani, Ralf Dillert, Mohamed El Azzouzi, Detlef W. Bahnemann, Photocatalytic degradation of the herbicide imazapyr: Do the initial degradation rates correlate with the adsorption kinetics and isotherms?, *Catal. Sci. Technol.*, 2018, 8, pp 985-995.
- **M. F. Atitar**, R. Dillert, D. W. Bahnemann, Surface interactions between imazapyr and the TiO<sub>2</sub> surface: An *in situ* ATR-FTIR study, *J. Phys Chem C*, 2017, 121(8), pp 4293-4303.
- A. Ismail, I. Abdelfattah, **M. F. Atitar**, L. Robben, H. Bouzid, S. A. Al-Sayari, D. W. Bahnemann, Photocatalytic degradation of imazapyr using mesoporous Al<sub>2</sub>O<sub>3</sub>-TiO<sub>2</sub> nanocomposites, *Separation and Purification Technology*, 2015, 145, pp 147-153.
- **M. F. Atitar**, H. Belhadj, R. Dillert, D. W. Bahnemann, The relevance of ATR-FTIR spectroscopy in semiconductor photocatalysis, *Intech*, 2015.
- E. S. Artemyeva, D. S. Barinov, **M. F. Atitar**, A. A. Murashkina, A. V. Emeline, N. Serpone, Luminescence of photoactivated pristine and Cr doped MgAl<sub>2</sub>O<sub>4</sub> spinel, *Chemical Physics Letters*, 2015, 626, p. 6-10.
- **M. F. Atitar**, A. A. Ismail, S. A. Al-Sayari, D. W. Bahnemann, D. Afanasev, A. V. Emeline, Mesoporous TiO<sub>2</sub> nanocrystals as efficient photocatalysts: impact of calcination temperature and phase transformation on photocatalytic performance, *Chem Eng J.* 2015, 264, p. 417-424.
- J. F. Montoya, **M. F. Atitar**, D. W. Bahnemann, J. Peral, P. Salvador, Comprehensive kinetic and mechanistic analysis of TiO<sub>2</sub> photocatalytic reactions according to the direct-indirect model: (II) experimental validation, *J. Phys Chem C*, 2014, 118, p. 14276-14290.
- **M. F. Atitar**, R. Dillert, M. El Azzouzi, D. W. Bahnemann, Photocatalytic degradation of the herbicide imazapyr in aqueous titania suspension: effect of the adsorption, and the formation of surface complexes on the degradation mechanism, Conference on Oxidation Technologies for Water and Wastewater Treatment -AOP6-, Goslar Germany, May 07-09. 2012, Proceeding.
- M. El Madani, **M. F. Atitar**, M. Mekkaoui, A. El Hourch, M. El Azzouzi, The removal of imazethapyr herbicide from water using titanium dioxide coupled to

UV light, Fourteenth International Water Technology Conference -14IWTC-,  
Cairo Egypt, March 21-23. 2010, Proceeding.

- **M. F. Atitar**, L. Fariane, S. Kitane, M. A. El Belghiti, O. K. Bouhelal, A. G. Didi, Biodiesel production from waste chicken fat, First National Workshop On Biofuels - Carburez Vert l'Avenir, Oujda Morocco, Nov 19-22. 2008, Proceeding.



# Curriculum vitae

## Personal data

---

### **Mohamed Faycal Atitar**

born February, 15<sup>th</sup> 1985 in Rabat - Morocco.

## Education

---

- |                   |   |
|-------------------|---|
| Since 02.2013     | <b>PhD Study in Chemistry</b> , Institute for Technical Chemistry - Leibniz Universität Hannover. Photocatalysis and Nanotechnology.<br>Supervisor: Prof. Dr. Detlef Bahnemann. |
| 02.2007 – 04.2009 | <b>D.E.S.A., Chemistry Environment and Analysis</b> , University Mohamed V Rabat – Morocco  |
| 09.2001 – 07.2006 | <b>Bachelor of Science in Chemistry</b> , University Mohamed V Rabat – Morocco  |
| 09.1998 – 06.2001 | <b>High School Degree</b> , Lycée El Maghrib El Arabi -Rabat- Morocco   |